AFOSR-TR- 93 0499

GA-C21284
5/93

# CERAMIC FIBER COATINGS DEVELOPMENT AND DEMONSTRATION

## FINAL TECHNICAL REPORT



For Period:
July 1, 1989 - May 31, 1993

Prepared by
H. Streckert, Program Manager
D. Hazlebeck, F. Montgomery, K. Norton,
I. Schneir, T. Moore, J. Kaae, I. Tzartzas

Approved by: T. D. Gulden
T. D. Gulden, Director
Advanced Materials Technology Div.

Sponsored by
Defense Advanced Research Projects Agency
ARPA Order No. 6808
Monitored by AFOSR Under
Contract No. F49620-89-C-0078

GA PROJECT 3858



GENERAL ATOMICS

# REPORT DOCUMENTATION PAGE

Form Approved
OMB No. 0704-0188



| 1. AGENCY USE ONLY (Leave blank) | 2. REPORT DATE | 3. REPORT TYPE AND DATES COVERED |
|---|---|---|
| | May 28, 1993 | FINAL REPORT 7-1-89 to 5-31-93 |

**4. TITLE AND SUBTITLE**
Ceramic Fiber Coating Development and Demonstration
Final Report

**5. FUNDING NUMBERS**
F49620-89-C-0078

**6. AUTHOR(S)**
H.Streckert, D. Hazlebeck, K. Norton, I. Schneir,
I.Tzartzas, F. Montgomery, T. Moore, J. Kaae

**7. PERFORMING ORGANIZATION NAME(S) AND ADDRESS(ES)**
General Atomics
P.O.Box 85608
San Diego, CA 92186-9784

**8. PERFORMING ORGANIZATION REPORT NUMBER**
GA-C21284

**9. SPONSORING/MONITORING AGENCY NAME(S) AND ADDRESS(ES)**
Lt. Col. Larry Burggraf
Air Force Office of Scientific Research
Bolling Air Force Base
Washington, D.C. 20332

**10. SPONSORING/MONITORING AGENCY REPORT NUMBER**

**11. SUPPLEMENTARY NOTES**

**12a. DISTRIBUTION/AVAILABILITY STATEMENT**
Unlimited
Approved for public release;
distribution unlimited.

**12b. DISTRIBUTION CODE**

**13. ABSTRACT (Maximum 200 words)**
The objective of this program was to develop fiber coating techniques by gas phase and liquid phase processes for interface control in ceramic matrix and metal matrix composites. Thermochemical evaluations of fiber/coating/matrix systems were performed theoretically and experimentally. Liquid phase processes were developed mainly for oxide coatings. Gas phase processes were developed for carbide, nitride and boride coatings. Coatings were produced on continuous fiber tows and woven fabric. A small scale continuous fabric coater was designed and constructed. Coated fiber tows were infiltrated with silicon nitride matrix by chemical vapor deposition in order to study fiber matrix interactions. Composite coupons were made from Nicalon cloth and infiltrated with silicon nitride. Samples coated with high temperature BN showed flexural strengths up to 350 MPa.

**14. SUBJECT TERMS**
Ceramic Fiber Coating, Chemical Vapor Deposition, Sol-Gel
Ceramic Matrix Composites, Metal Matrix Composites

**15. NUMBER OF PAGES**
188

**16. PRICE CODE**

| 17. SECURITY CLASSIFICATION OF REPORT | 18. SECURITY CLASSIFICATION OF THIS PAGE | 19. SECURITY CLASSIFICATION OF ABSTRACT | 20. LIMITATION OF ABSTRACT |
|---|---|---|---|
| Unclassified | Unclassified | Unclassified | Unclassified |

## EXECUTIVE SUMMARY

Ceramic matrix composites and metal matrix composites offer the potential for dramatic performance improvements in a wide variety of commercial and defense systems. The successful commercialization of advanced ceramics depends on providing high quality components at prices comparable to their metallic counterparts. One of the critical variables guiding the process economics of high temperature, structural composites is the nature of the fiber/matrix interface, which controls load transfer from matrix to fiber and which largely determines the mode of crack propagation in brittle matrix composites. A number of methods exist to modify the fiber surface, including in-situ reactions of the fiber surface, matrix additions to alter the matrix chemistry near the fiber and direct chemical modification of the fiber surface via fiber coating. Fiber coating remains the easiest and therefore the most economical method for controlling the chemistry of the fiber/matrix interface.

During the period from July 1989 through May 1993, ARPA (formerly DARPA) sponsored a broad-based, ceramic fiber coating program involving several contractors. Although fiber coatings were long viewed as a key technology in developing strong, tough composites, the technique was limited by available coating chemistries, reliable coating techniques and low coating rates. Other unknown variables included optimum coating chemistries, required thicknesses and debond mechanisms, as well as the process variables required to uniformly coat multifilament tows. The general goals of the program were to (1) develop fiber coating techniques and novel fiber coatings for multifilament ceramic tows, (2) evaluate coated fibers in CMC's and MMC's to improve strength and toughness, (3) develop better control of the interfacial bond strength to optimize toughening.

General Atomics evaluated gas phase and liquid phase methods to develop improved fiber coatings. A low pressure chemical vapor deposition apparatus, Figure I, was implemented to achieve these goals for carbide, nitride and boride coatings.

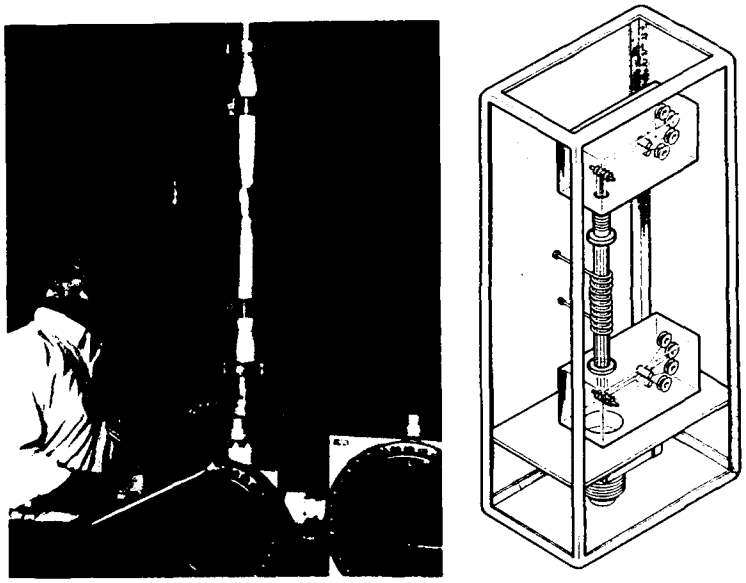

Figure I. Continuous CVD Fiber Coater Operated by GA

Liquid phase methods, based on solution chemistry and preceramic polymers yielded improvements mainly for oxide coatings and proved particularly promising for low cost processing. A schematic for this equipment is shown in Figure II.

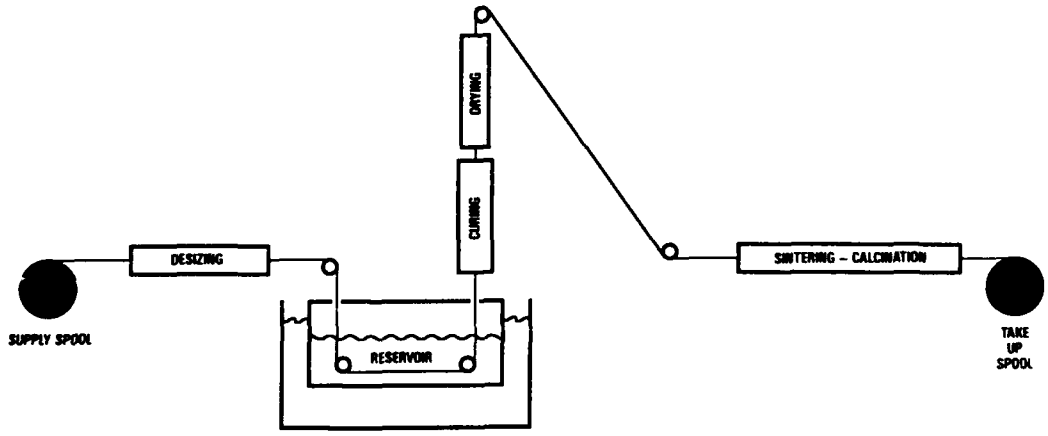


Figure II. Schematic of Liquid-Phase Coating Process

A large number of high-quality coatings was developed in this program. These are summarized in the table. Multiple coatings, for example, BN/SiC and SiC/BN/SiC have also been produced. The importance of an effective fiber coating is demonstrated in Figure III. As a propagating crack in a strained composite encounters a coated fiber, it is deflected by the coating, leaving the reinforcing fiber and therefore the load carrying capability of the component intact.

**COATINGS FOR CERAMIC FIBERS**

| COATING | COATING METHOD |
|---|---|
| $Al_2O_3$ | sol-gel |
| $Y_2O_3$ | sol-gel |
| MgO | sol-gel |
| YAG | sol-gel |
| $HfO_2$ | sol-gel |
| $SiO_2$ | sol-gel |
| $ZrO_2$ | sol-gel |
| $LaNiO_3$ | sol-gel |
| $La_2NiO_4$ | sol-gel |
| $MgAl_2O_4$ | sol-gel |
| SiC | sol-gel, CVD |
| ZrC | CVD |
| $Si_3N_4$ | sol-gel, CVD |
| BN | sol-gel, CVD |
| $TiB_2$ | CVD |
| Si | CVD |
| C | CVD |

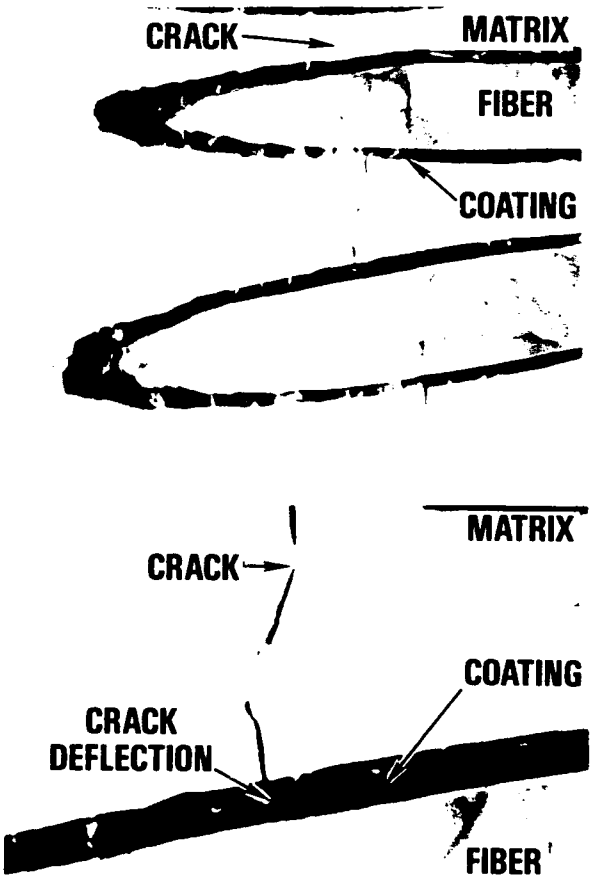


Figure III. BN Coated Nicalon Exhibit Crack Deflection at Interface

The optimum coating thickness is a critical variable that had received little attention prior to this program. We performed experiments on composite strength as a function of coating thickness. The experiments yielded an optimum thickness of 0.3 to 0.4 μm. Such a coating of BN on HPZ fiber is shown in Figure IV. This important result has become a baseline for the composite fabrication industry.

Figure IV. CVD BN Coating on HPZ Fiber

A number of technical improvements led to new inventions. Patent application #553904 "Preparing Refractory Fiber-Reinforced Composites" was filed early in the program. This work was considered potentially sensitive by the Air Force, hence a secrecy order was attached. The secrecy order was rescinded a year later and we could proceed with the patent. A notice of allowance was received late in 1992 for Patent application #822012 "Liquid Phase Coating of Refractory Fiber Tows with Oxides." The patent should issue in July 1993. Patent application #694137 "Method of Fabrication of Composites" is under examination by the patent office. The significant claims of these inventions are the economical preparation of oxide coatings by a variety of precursors on multifilament tows and a simplified method for fabricating complex shaped components. A wide range of coatings and improvements in coating methods integrated with composite fabrication were developed in this program. Combined, these innovations provide novel processes which greatly advanced the state-of-the-art of fiber coating for composite fabrication.

Cost effective composites depend on low cost manufacture of reinforcements, fiber coatings and matrix densification. The fiber coatings developed in this program are based on inexpensive precursors, minimizing the materials costs. The processes and equipment have been simplified to reduce labor and capital costs. The deposition rates were optimized and the proper coating thickness identified to maximize the throughput of coated fiber. A further increase in throughput from the current 50 m/hr could be achieved by increasing the coating zones of the present equipment. Combining all these factors demonstrates that fiber coatings can be applied economically to provide cost-effective composites for commerical and military applications. To obtain a further increase in throughput and a concommitant decrease in cost, the coating of woven fiber in the form of fabric, particularly in continuous form should be further investigated. A small scale coater was designed and built as part of this program to demonstrate the principles of continuous fabric coating with promising results.

This final report documents all the work performed between July 1, 1989 and May 31, 1993 on DARPA/AFOSR Contract F49620-89-C-0078 entitled "Ceramic Fiber Coating Development and Demonstration." The data are presented in chronological order to best reflect our understanding at the time the work was performed. The various areas of study are summarized below.

## CHEMICAL COMPATIBILITY AND INTERFACE MECHANICS

Theoretical studies of the chemical compatibility between candidate coating, fiber, and matrix materials were performed. Evaluation of Nicalon, HPZ and Nextel fibers and associated coating and matrix candidates for potential application in the aircraft turbine engine exhaust gas environment at temperatures up to 1600K was performed. This evaluation revealed several stable fiber/coating/matrix systems.

Experimental compatibility studies were performed by CVD coating dense ceramic disks that simulate fibers used in this program. Coated substrates were heated to various temperatures up to 1400°C. No reaction zones were apparent by scanning electron microscopy.

## LIQUID PHASE PROCESS DEVELOPMENT

Fiber coating by liquid-phase processes can be accomplished by gelation of three basic types of solutions: metallic salts, colloidal sols, and polymerized organometallic species. General Atomics developed conditions by each of these methods for preparing oxide, nitride and carbide coatings on ceramic fibers. A continuous fiber coater was designed and built and coating of full size fiber spools was performed.

## GAS PHASE PROCESS DEVELOPMENT

Fiber coating experiments by gas phase processes were performed by plasma assisted chemical vapor deposition and low pressure chemical vapor deposition on continuous fiber tow.

A wide variety of coatings for fiber/matrix interface control including borides, carbides and nitrides were explored. Conditions for these coatings were firmly established relating coating characteristics to processing parameters. Dual and triple coatings were prepared as well as batch coating of fabric by conventional chemical vapor deposition.

## COMPOSITE FABRICATION AND EVALUATION

Coated fiber tows were infiltrated with $Si_3N_4$ matrix by chemical vapor deposition in order to study fiber matrix interactions. Some fiber coating combinations showed considerable strength and fiber pull out, while others failed in a brittle manner with little strength, in some cases

verifying present models on fiber/matrix bonding. Interfacial properties of the composites were examined by transmission electron microscopy where mechanistic data on toughening were obtained from interfacial chemistry measurements. Strong, tough composites were prepared with proper fiber matrix interface coatings and an optimized coating thickness. These studies contributed to the fundamental understanding of the fabrication of ceramic matrix composites

# TABLE OF CONTENTS

LIST OF FIGURES

LIST OF FIGURES

LIST OF FIGURES

LIST OF FIGURES

LIST OF FIGURES

LIST OF FIGURES

LIST OF FIGURES

LIST OF TABLES

No.

## PROGRAM ACTIVITY

### INTRODUCTION

General Atomics has worked on the development of fiber-reinforced composites for over 10 years. Early work on continuous fiber reinforced ceramic matrix composites identified the need for proper fiber-matrix interface control. Various methods of interface control can be used including in-situ modification of the fiber surface, matrix additions that yield an interphase layer or chemical modification of the fiber surface, i.e., fiber coating. These methods all have advantages and disadvantages, but fiber coating remains the easiest and most versatile method with the widest range of applications. In the course of developing high-quality ceramic matrix composite at GA, fiber coating methods were successfully employed.

The work on fiber coatings and fiber coating technology was developed further in this program. The program was divided into two phases. Phase I consisted of four main tasks: Task 1-1, Chemical Compatibility and Interface Mechanics, Task 1-2, Liquid Phase Process Development, Task 1-3, Gas Phase Process Development and Task 1-4, Coated Fiber Evaluation and Screening. Phase II consisted of three main tasks: Task 2-1, Coating Process Scale Up; Task 2-2, Coated Fiber Production; and Task 2-3, Composite Fabrication and Evaluation. This report summarizes the progress made under all seven tasks between July 1, 1989 and May 31, 1993.

## TASK 1-1 CHEMICAL COMPATIBILITY AND INTERFACE MECHANICS

### Theoretical Analysis

The support work on theoretical studies of the chemical compatibility between candidate coating, fiber, and matrix materials was performed at MSNW. Initially, the chemical compositions and constituents of relevant fibers were determined. The chemical compatibility of these constituents with candidate fiber coatings was evaluated via equilibrium calculations based on potential reaction products. The chemical compatibility of coatings with candidate matrices was calculated. Finally, the compatibility of candidate coatings with aircraft gas turbine exhaust environment was assessed.

### FIBER COMPOSITIONS

For this evaluation a SiC, a $Si_3N_4$ and an oxide substrate were of interest. Commercial fibers, which resemble these substrates, are Nicalon, HPZ and Nextel.

Nicalon, a product of Nippon Carbon Company of Japan, is a silicon carbide type fiber produced from polycar- bosilane polymer. The fiber is mostly amorphous with some microcrystalline beta-SiC. A typical elemental composition (wt %) is 57% silicon, 31% carbon, and 11% oxygen (Ref. 1).

HPZ, a product of Dow Corning, is a silicon nitride type fiber prepared from the polymer hydridopolysilazane by a pyrolytic process. The fiber is amorphous with a typical elemental composition (wt %) of 57% silicon, 28%

nitrogen, 10% carbon, and 4% oxygen. The stable (equilibrium) constituents of the fiber would be $Si_3N_4$, $Si_2N_2O$, $SiO_2$, SiC, and free carbon (Refs. 2,3).

Nextel 440 and Nextel 480 are continuous filament fibers manufactured by the 3M Company. The fibers consist of boria-modified alumina-silica (mullite). The nominal composition of the two fibers (wt %) is 70% $Al_2O_3$, 28% $SiO_2$, and 2% $B_2O_3$. Published phase analysis results indicate that the 480 fiber consists of mullite and a minor amount of amorphous phase and that the 440 fiber consists of mullite, an amorphous phase, and eta-$Al_2O_3$. Reported physical property studies found that the 480 fiber is preferable for use as a high temperature reinforcing material (Refs. 4, 5).

## FIBER STRUCTURE, STRENGTH, AND THERMAL STABILITY

The results of our thermochemical assessments of the thermal stability of the three candidate fibers and the results of published studies (Refs. 6-13) of the structure, strength, and thermal stability of the candidate fibers led to the following conclusions:

- Nicalon and HPZ fibers, as well as other fibers prepared from polymer precursors, are predominantly amorphous in structure. Only Nicalon shows crystallinity, other than microcrystalline graphite in all the fibers studied. The amorphous structure appears to be the continuous phase in the fiber.

- Nicalon and HPZ fibers show similar strength and fracture behavior over the temperature range studied (up to 1400°C). The strength of each fiber is apparently controlled by the amorphous (glassy) phase.

- Nicalon and HPZ fibers are thermodynamically unstable and degrade (lose strength) at temperatures above about 1000°C as a result of (1) chemical reactions (with evolution of CO, $N_2$, and SiO) and (2) crystallite growth.

- Nextel fibers, as well as other oxide fibers studied, are relatively stable chemically, but softening of the glassy phase leads to large strength reduction at 1200°C and to almost complete loss of strength at 1300°C.

- Nicalon and HPZ fibers are stronger than Nextel fibers at room temperature and retain more of their strength at high temperature.

Based on these conclusions, we rank the fibers as follows with regard to strength and thermal stability characteristics:

Nicalon > HPZ > Nextel

Actually, these characteristics are similar for all three fibers, although their chemical compositions differ. They start to degrade (lose strength) at temperatures above about 1000°C as a result of built-in instability, and this instability must be taken into account when fixing processing and service conditions.

## FIBER DEGRADATION MECHANISMS

Consideration of degradation mechanisms is important. If a fiber, for example, Nicalon or HPZ, degrades by a gas-producing chemical reaction, a sound (gas-tight) coating will likely improve the thermal stability of the fiber. On the other hand, if the fiber

degrades by crystallite growth or softening of the predominant phase, a coating will probably not improve the thermal stability of the fiber. The effect of the coating application process on the integrity of the fiber must, of course, be taken into account.

We found more information in the literature on degradation mechanisms for Nicalon than for the other two fibers. Mah et al. (Ref. 6) found severe degradation in the strength of Nicalon fiber after heat treatment in argon and under vacuum at 1200°, 1300°, and 1400°C. Their results indicated the degradation was associated with the evaporation of CO from the fiber.

Our equilibrium thermochemical calculations and those of Luthra (Ref. 11) are in accord with the experimental results of Mah et al. These calculations predicted that at high temperature (1000K - 1600K), the predominant gas species over SiC plus $SiO_2$ and excess carbon would be CO, with an SiO partial pressure about two orders of magnitude below that of CO.

Johnson et al (Ref. 12) performed vaporization studies on Nicalon fiber at 800° to 1400°C using a Knudsen-cell, mass-spectrometric method. The major gaseous species observed were SiO, CO, Al, and $Al_2O$. Clearly, SiO was the predominant species. The Al and $Al_2O$ gaseous species were accounted for by the Al content of the fiber (0.44 wt %, by chemical analysis). The CO pressure decreased with time, indicating depletion of excess carbon readily available for volatilization as CO. The results suggest that the thermal degradation of Nicalon fiber may be primarily due to the loss of structurally bound silicon as SiO and not to reactions

involving excess carbon. Johnson, et al. explained the difference between their observations and those of Mah et al. by the fact that the analysis technique of Mah et al. was unable to detect condensable species.

Clearly, additional studies of fiber degradation mechanisms are needed. Light coatings may prevent chemical interactions; but since the fibers of interest are crystallographically metastable, they might degrade (lose strength) at high temperature anyway as a result of crystallite growth.

An experimental suggestion would be to evaluate fiber property loss after heating in CO, in the case of Nicalon fiber, and CO + $N_2$, in the case of HPZ fiber. The gases would be at sufficient pressure to hold the chemical degradation reactions which produce these gases. Observed loss would be attributable to other chemical reactions or structural changes, such as crystallite growth.

Jaskowiak and DiCarlo (Ref. 13) demonstrated that application of high external gas pressure (argon at 138 MPa) can temporarily inhibit the reactions which lead to high temperature degradation of Nicalon fibers. High pressure treatment delayed the onset of fiber weight loss to temperatures above 1500°C. Strength degradation and grain growth were correlated with weight loss and were thus also inhibited by high pressure treatment.

## COMPATIBILITY OF NICALON FIBER WITH COATING CANDIDATES

Nicalon fiber is inherently unstable. The fiber starts to degrade at temperatures above about 1000°C,

probably owing to chemical reactions between fiber constituents producing CO and SiO (see above). A gas retentive (crack-free) coating may restrict the chemical reactions enough to make the fiber serviceable above 1000°C.

Nicalon/Alumina

We evaluated the compatibility of $Al_2O_3$ and Nicalon fiber by considering several potential reactions involving $Al_2O_3$ and five constituents. The key (most important) reaction is:

$$Al_2O_3(s) + 9/2C(s) \rightarrow 1/2\ Al_4C_3(s) + 3CO(g) \qquad (1)$$

The calculated equilibrium partial pressure of CO is $1.9 \times 10^{-4}$ atm at 1600K. This partial pressure value is not high enough to be of concern since a tight coating is required to restrict gas-producing fiber degradation reactions.

Standard free energy ($\Delta G°$) values for reactions between $Al_2O_3$ and the $SiO_2$ fiber constituent to form aluminosilicates are small negative values, indicating little driving force for the formation of aluminosilicates. However, a tight bond between $Al_2O_3$ coating and fiber will likely occur due to some reaction or solution between $Al_2O_3$ and the $SiO_2$ constituent of the fiber.

Nicalon/Yttria

Since (1) a reaction involving $Y_2O_3$ and carbon appears to be the only potential gas-producing reaction

between $Y_2O_3$ and fiber constituents and (2) $YC_2$ appears to be the most stable carbide phase in the Y-C system, we evaluated the reaction

$$Y_2O_3(s) + 7C(s) \rightarrow 2YC_2(s) + 3CO(g) \qquad (2)$$

and found that the equilibrium partial pressure of CO is less than $10^{-4}$ atm at temperature below 1600K. Therefore, the reaction is not of concern.

The phase diagram for the $Y_2O_3$-$SiO_2$ system shows that the two oxides react to form several compounds (see Fig. 2388 in Ref. 19). Therefore, a tight bond between $Y_2O_3$ coating and fiber will likely occur due to some reaction or solution between $Y_2O_3$ and the $SiO_2$ constituent of the fiber.

Nicalon/YAG

We expect YAG ($3Y_2O_3 \cdot 5Al_2O_3$), like $Al_2O_3$ and $Y_2O_3$, to form a tight bond with Nicalon fiber due to some reaction or solution with the $SiO_2$ constituent of the fiber.

Nicalon/Silicon Carbide

Silicon carbide seems to be a viable coating candidate for Nicalon fiber. Since silicon carbide is the major component in the fiber, using silicon carbide as a coating would introduce no new component.

## Nicalon/Boron Nitride

Our thermochemical analyses show that reactions involving boron nitride and fiber constituents yield product gases at relatively high partial pressures. For example, for the reaction

$$3SiO_2(s) + 2BN(s) \rightarrow B_2O_3(l) + 3SiO(g) + N_2(g) \qquad (3)$$

calculated equilibrium partial pressures of SiO are $7.1 \times 10^{-13}$ atm at 1000K and $7.9 \times 10^{-5}$ atm at 1600K. However, these partial pressure values are appreciably lower than calculated partial pressure values resulting from fiber degradation reactions involving the fiber components free carbon and $SiO_2$. Therefore, if a boron nitride coating can be made sound (gas retentive) enough to control the fiber degradation reactions, it will also control the coating-fiber constituent reactions.

A particular concern, if reaction (3) proceeds, is the formation and release of liquid $B_2O_3$. It has a relatively high vapor pressure ($1.5 \times 10^{-4}$ atm at 1600K). The oxide reacts readily with water vapor to form volatile $HBO_2(g)$, and it dissolves most metal oxides and thus is very corrosive to metals in the presence of oxygen.

## Nicalon/Boron

For this system, we evaluated reactions between boron and fiber constituents $SiO_2$, free carbon, and SiC. For the reaction between boron and $SiO_2$ to yield $B_2O_3$ and SiO(g), $\Delta G° = 34$ kcal/mol boron ($p_{sio} = 7.9 \times 10^{-4}$ atm at 1600K). For the reaction between boron and $SiO_2$ to yield

$B_2O_3$ and silicon, $\Delta G^\circ$ = 6 kcal/mol boron at 1600K. For the reaction between boron and free carbon to yield $B_4C$, $\Delta G^\circ$ = -3 kcal/mol boron at 1600K. For the reaction between boron and SiC to yield $B_4C$ and silicon, $\Delta G^\circ$ = -0.3 kcal/mol boron at 1600K. None of these reactions has a large driving force; however, occurrence of one or more of the reactions could degrade a thin coating. This partial pressure of product gas SiO ($7.9 \times 10^{-4}$ atm at 1600K is not of particular concern, since it is lower than the calculated partial pressures of product gases resulting from fiber degradation reactions).

Nicalon/Silicon

The main concern with this system is the potential reaction between silicon and free carbon in the fiber to form silicon carbide. This reaction has a relatively large driving force ($\Delta G^\circ \approx$ -15 kcal/mol silicon at 1000K to 1600K). Since the fiber has 30 mol % free carbon, this reaction could seriously degrade, or consume, the coating. On the other hand, the reaction may convert, in-situ , the silicon coating to a more serviceable silicon carbide coating. Another consideration is that a silicon coating would probably not be serviceable above about 1270K [0.75 x silicon melting point, 1693K, (Ref. 14)].

Nicalon/Silicon Nitride

The reaction of concern for this system is between $Si_3N_4$ and free carbon in the fiber:

$$3C(s) + Si_3N_4 \rightarrow 3SiC(s) + 2N_2(g) \qquad (4)$$

Calculated equilibrium partial pressure values for this

reaction are $2.0 \times 10^{-6}$ atm at 1000K and 0.27 atm at 1600K (Ref. 5). These partial pressure values are even higher than calculated partial pressure values for product gases resulting from Nicalon fiber degradation reactions. (The calculated partial pressure of CO formed by the reaction between fiber constituents carbon and $SiO_2$ is 0.1 atm at 1600K). We conclude that $Si_3N_4$ would not be suitable as a coating for high temperature service (up to 1600K) unless the coating can be made gas retentive.

## COMPATIBILITY OF HPZ FIBER WITH COATING CANDIDATES

Boron nitride and silicon carbide with excess carbon were selected as coating candidates for HPZ fiber. As indicated above, the HPZ fiber degrades above about 1000°C probably as a result of chemical reaction (with evolution of CO, $N_2$, and SiO). Therefore, for service above this temperature, a sound (gas-tight) coating is required.

### HPZ/Boron Nitride

Published information indicates that boron nitride is compatible with the $Si_3N_4$ and $Si_2N_2O$ constituents of HPZ fiber at temperatures up to 1600K. However, potential reactions involving boron nitride and fiber constituents $SiO_2$, SiC, and carbon are of concern. Of the reactions that we considered, the reaction yielding the highest partial pressure of product gases is

$$2BN(s) + 3SiO_2(s) \rightarrow B_2O_3(l) \quad 3SiO(g) + N_2(g) \qquad (5)$$

Calculated equilibrium partial pressures of SiO and $N_2$ are $7.1 \times 10^{-13}$ atm at 1000K and $7.9 \times 10^{-4}$ atm at 1600K.

These values are much lower than partial pressure values resulting from fiber degradation reactions and therefore are not of concern. If gas retention by the coating is adequate to prevent occurrence of the degradation reactions, it will prevent occurrence of reaction (5).

HPZ/SiC-C

A SiC-C coating would provide additional carbon for potential fiber, degradation reactions involving fiber constituents. (The fiber, as fabricated, contains free carbon.) Of the degradation reactions considered, the reaction

$$3C(s) + Si_3N_4 \rightarrow 3SiC(s) + 2N_2(g) \qquad (6)$$

is of most concern. Calculated partial pressures of $N_2$ for this reaction are $2.0 \times 10^{-6}$ atm at 1000K and 0.27 atm at 1600K. Therefore, gas retention is required to prevent occurrence of this and other HPZ degradation reactions.

## COMPATIBILITY OF NEXTEL FIBERS WITH COATING AND/OR MATRIX CANDIDATES

The materials alumina, yttria, YAG, mullite, CAS, boron nitride, silicon carbide, and silicon nitride were selected for compatibility assessments of Nextel 440 and 480 fibers. It was assumed that each material could be in contact with the fiber, either as coating or matrix.

Nextel Fibers/Alumina

Phase diagrams indicate that alumina is compatible

(can co-exist) with Nextel fiber constituents. However, the phase behavior of mullite (the primary constituent of Nextel fiber) suggests that alumina and fiber will form a strong bond at elevated temperature process and service conditions. The change in chemical composition (solid solution boundaries) of mullite with temperature is especially conducive to bond formation. The presence of boria ($B_2O_3$) in the fibers will likely increase the rate at which bonding occurs and may even increase the bond strength.

Nextel Fibers/Mullite

Since Nextel fibers are mullite-based, mullite and fiber should be compatible. However, mullite will likely bond strongly to the fibers at elevated process and service temperatures.

Nextel Fibers/Anorthite (CAS)

The phase diagram for the $CaO-Al_2O_3-SiO_2$ system (Fig. 2493, Ref. 15) indicates that mullite and CAS can coexist. Therefore, Nextel fibers and CAS are considered to be compatible. However, because of solubility among oxides, it is likely that the fibers and CAS would bond strongly at an interface.

Nextel Fibers/Silicon Carbide

We consider the reaction between mullite and silicon carbide to be the key reaction for assessing the compatibility of Nextel fibers and silicon carbide. Product gases are SiO and CO. Calculated equilibrium partial pressures for the two gases at 1600K are 9.8 x

$10^{-4}$ and $3.3 \times 10^{-4}$ atm, respectively. These relatively high partial pressure values indicate that Nextel fibers and silicon carbide are not compatible at 1600K unless the product gases are retained.

Nextel Fibers/Yttria

Phase diagrams of the $Al_2O_3$-SiO-$Y_2O_3$ system (Refs. 16, 17), measured at temperatures around 1500°C, show no tie-line between mullite and yttria, indicating that the two compounds cannot coexist in chemical equilibrium with each other. Thus, at high temperature, Nextel fibers and yttria would tend to react at an interface (see below). Also, yttria would tend to react with the boria constituent of Nextel fibers to form $YBO_3$ (see Fig. 4390, Ref. 15). It is concluded that for high temperature service, Nextel fibers and yttria are not compatible.

Nextel Fibers/YAG

The published phase diagrams of the $Al_2O_3$-$SiO_2$-$Y_2O_3$ system (Refs. 20, 21) indicate that mullite and YAG cannot coexist in chemical equilibrium. It is therefore concluded that Nextel fiber and YAG are not compatible. If the phase diagrams are correct, either yttria or YAG would, at equilibrium with mullite in the Nextel fiber, result in a $Y_2O_3 \cdot 2SiO_2$ + $Al_2O_3$ conversion layer, which could provide some control on bonding at the interface. $Y^{+3}$ and $Al^{+3}$ are moderately diverse in radius, 0.93 and 0.46 Å, respectively.

Nextel Fibers/Silicon Nitride

For evaluating the compatibility of Nextel fibers

and silicon nitride, we consider the reaction between mullite and silicon nitride to form alumina and silicon oxynitride ($Si_2N_2O$) to be relevant. Calculated $\Delta G°$ values for the reaction are -42.97 kcal/mol $Si_3N_4$ at 1000K and -34.20 kcal/mol $Si_3N_4$ at 1600K. These negative $\Delta G°$values indicate that the reaction is favorable. Mullite and silicon nitride can also react to form sialon-type compounds. [Sialons are phases in the Si-Al-O-N system (Ref. 18).] These results indicate that Nextel fibers and silicon nitride are not compatible at elevated temperatures.

### Nextel Fibers/Boron Nitride

We consider the reaction between mullite and boron nitride to be the key reaction for assessing the compatibility of Nextel fibers and boron nitride. Product gases are SiO and $N_2$. Calculated equilibrium partial pressures for the two gases at 1600K are $2.6 \times 10^{-4}$ and $8.9 \times 10^{-5}$ atm, respectively. These relatively high partial pressure values indicate that Nextel fibers and boron nitride are not compatible at 1600K unless product gases are retained.

## COMPATIBILITY OF COATING AND MATRIX CANDIDATES

This section presents thermochemical assessments of the compatibility of coating and matrix candidates. Where coating and matrix materials react to product gaseous species, the maximum service temperature is assumed to be the temperature at which the calculated partial pressure of the product gaseous species reaches $10^{-4}$ atm.

In evaluating the compatibility of coating and matrix candidates, we assume an inert environment (i.e., no interaction with exhaust gas).

## Compatibility of Boron Nitride with Matrix Candidates

### Boron Nitride Coating/Silicon Nitride Matrix

No indication has been found in the literature or in our thermochemical analyses that significant reaction or solution would occur in the $BN/Si_3N_4$ system. It is concluded that boron nitride and silicon nitride are compatible at temperatures up to 1600K.

### Boron Nitride Coating/Spodumeme (LAS) Matrix

Our thermochemical analyses indicate that (1) within the accuracy of the data, the activity of $SiO_2$ in spodumene is equal to that of pure $SiO_2$ and (2) the key reaction for assessing the compatibility of spodumene and boron nitride is

$$2/3BN(s) + SiO_2(s) \rightarrow SiO(g) + 1/3B_2O_3(s \text{ or } 1) + 1/3N_2(g) \quad (7)$$

Calculated equilibrium partial pressures at 1600K for the product gases SiO and $N_2$ are $1.0 \times 10^{-4}$ and $3.5 \times 10^{-5}$ atm, respectively. These partial pressure values are not high enough to be of serious concern. Therefore, boron nitride and spodumene are considered to be compatible up to 1600K.

### Boron Nitride Coating/Cordierite (MAS) Matrix

Our thermochemical analyses indicate that (1) within

the accuracy of the data, the activity of $SiO_2$ in cordierite is equal to that of pure $SiO_2$ and (2) reaction (7) is the key reaction for assessing the compatibility of cordierite and boron nitride. Since the calculated partial pressures of the product gases are not high enough to be of serious concern, boron nitride and cordierite are considered to be compatible up to 1600K.

## Compatibility of Silicon Carbide with Matrix Candidates

### Silicon Carbide Coating/Silicon Nitride Matrix

Our thermochemical analyses indicate that no significant reaction would occur in the $SiC/Si_3N_4$ system at temperatures up to 1600K. Also, we have found no indication in the literature that reaction or solution would occur. Therefore, good compatibility is expected for the two materials.

### Silicon Carbide Coating/Spodumene (LAS) Matrix

Our analyses indicate that for evaluating the compatibility of silicon carbide and spodumene, the key reaction is

$$SiC(s) + 2SiO_2(s) \rightarrow 3SiO(g) + CO(g) \qquad (8)$$

(As noted above, the activity of $SiO_2$ in spodumene is essentially unity). Calculated equilibrium partial pressures for the respective product gases SiO and CO are $1.7 \times 10^{-10}$ and $5.8 \times 10^{-11}$ atm at 1000K and $1.7 \times 10^{-3}$ and $5.7 \times 10^{-4}$ atm at 1600K. The values at 1600K exceed the criterion of $1.0 \times 10^{-4}$ atm (see above). By interpolation, on a plot of log $p_{SiO}$ vs 1/T, we find that

the SiO partial pressure is $1.0 \times 10^{-4}$ atm at about 1460K. Thus, the maximum service temperature for a silicon carbide coating/spodumene matrix system is indicated to be 1460K.

### Silicon Carbide Coating/Cordiertie (MAS) Matrix

The key reaction for the silicon carbide-cordierite system, as for the silicon carbide spodumene system, is reaction (8). Therefore, the maximum service temperature for a silicon carbide coating/cordierite matrix system is indicated to be 1460K.

## Compatibility of SiC-C with Matrix Candidates

The phase diagram of the Si-C system shows SiC to be essentially a line compound. Therefore, excess carbon will exist as a separate phase, and reactions between free carbon and matrix candidates must be considered.

### SiC-C Coating/Spodumene (LAS) and Cordierite (MAS) Matrices

The key reaction for evaluating the interaction of free carbon with spodumene and cordierite is

$$3/2C(s) + 1/2SiO_2(s) \rightarrow 1/2SiC(s) + CO(g) \qquad (9)$$

(As noted above, the activity of $SiO_2$ in spodumene and cordierite is essentially unity.) Calculated equilibrium partial pressures of CO for the reaction are $1.3 \times 10^{-7}$ atm at 1000K and $9.4 \times 10^{-2}$ atm at 1600K. Interpolating, we find the partial pressure of CO is $1 \times 10^{-4}$ atm at 1230K. Therefore, the maximum service temperature for the two systems is indicated to be 1230K.

SiC-C Coating/Silicon Nitride Matrix

The key reaction for evaluating the interaction of free carbon with silicon nitride is

$$3C(s) + Si_3N_4(s) \rightarrow 3SiC(s) + 2N_2 \qquad (10)$$

Calculated equilibrium partial pressures of $N_2$ are $2.0 \times 10^{-6}$ atm at 1000K and $2.7 \times 10^{-1}$ at 1600K. The maximum service temperature is indicated to be 1140K, which is the temperature at which the calculated pressure of $N_2$ is $1.0 \times 10^{-4}$ atm.

Compatibility of Boron with Matrix Candidates

Boron Coating/Silicon Carbide Matrix

The pertinent reaction for evaluating the compatibility of a boron coating and a silicon carbide matrix is

$$4B(s) + SiC(s) \rightarrow B_4C(s) + Si(s) \qquad (11)$$

$\Delta G^\circ$ values are close to zero at high temperature (1000K to 1600K), indicating little driving force for the reaction. However, formation of boron silicides ($SiB_3$, $SiB_6$, and $SiB_{14}$), which are known to exist, and/or changes in activities, for example by solution or mixed carbide formation, could cause the reaction to proceed enough to degrade the coating. Accordingly, the compatibility of a boron coating and a silicon carbide matrix is doubtful.

Boron Coating/Silicon Nitride Matrix

The key reaction for this system is

$$4B(s) + Si_3N_4(s) \rightarrow 4BN(s) + 3Si(s) \qquad (12)$$

Calculated $\Delta G^\circ$ values for the reaction are -56.7 and -53.4 kcal/mol at 1000K and 1600K, respectively (Ref. 14). The high negative values indicate that the reaction is very favorable. Accordingly, a boron coating and a $Si_3N_4$ matrix are not compatible for high temperature service.

## Compatibility of Alumina with Matrix Candidates

### Alumina Coating/Mixed Oxide Matrices

The accuracy of phase diagrams and thermochemical data is, in general, not adequate for predicting the potential for chemical reactions (new phase formation reactions) between alumina and the mixed oxide matrix candidates mullite, spodumene (LAS), cordierite (MAS), and anorthite (CAS) in the temperature range of interest (up to 1600K). However, it is likely that an alumina coating will bond strongly, either by reaction or solution, with a mixed oxide matrix.

### Alumina Coating/Silicon Carbide Matrix

The reaction to consider for evaluating this system is

$$Al_2O_3(s) + 3/2SiC(s) \rightarrow 1/2Al_4C_3(s) + 3/2SiO_2(s) \qquad (13)$$

Calculated $\Delta G^\circ$ values for the reaction are +66 kcal/mol at 1000K and +59 kcal/mol at 1600K. These relatively large positive $\Delta G^\circ$ values indicate that the reaction is not favorable. Taking account of interactions of $Al_4C_3$ and SiC to form $Al_4SiC_4$, $Al_4C_3$ and $Al_2O_3$ to form $Al_4O_4C$, and $SiO_2$ and $Al_2O_3$ to form $3Al_2O_3 \cdot 2SiO_2$ (mullite) does not significantly reduce the $\Delta G^\circ$ values. Therefore, we conclude that an alumina

coating and a silicon carbide matrix are compatible.

### Alumina Coating/Silicon Nitride Matrix

The compatibility of an $Al_2O_3$ coating and a $Si_3N_4$ matrix is doubtful because of the potential formation of sialons (Ref. 18).

## COMPATIBILITY OF COATING CANDIDATE WITH EXHAUST GAS ENVIRONMENT

This section presents thermochemical evaluations of the compatibility of coating candidates with the exhaust gas environment in the temperature range 1000K to 1600K. The matrix is assumed to be porous, allowing the exhaust gas to reach the coating. The reference partial pressures of $N_2$, $O_2$, $H_2O$, and CO in the exhaust gas are assumed to be 6.0, 0.92, 0.50, and $9 \times 10^{-6}$ atm, respectively.

The calculated exhaust gas compositions and operating conditions for three engine operating conditions are given in Table 1. The calculations were performed assuming an adiabatic (no heat loss) constant pressure process. It was assumed that liquid n-octane ($C_8H_{18}$) is supplied at temperature $T_1$ and that the compressor discharge is dry air at temperature $T_2$. The total pressure of gases in the flame was assumed to be 8 atm. $T_3$ is the assumed combustion chamber or afterburner gas discharge temperature. Flame temperatures of 1200 and 1600K were selected for Cases 1 and 2, respectively. The afterburner (augmented) flame temperature was selected to be 2300K for Case 3. Gas tables (Refs. 14 and 19) were utilized. The gas table data are at 1 atm, and no correction was made for adjusting the total gas pressure to 8 atm.

Table 1

CALCULATED COMBUSTION GAS COMPOSITIONS FOR THREE ASSUMED AIRCRAFT GAS TURBINE CONDITIONS[a]

| | Case 1[b] | Case 2[c] | Case 3[d] |
|---|---|---|---|
| $T_1$ (K) | 298 | 298 | 298 |
| $T_2$ (K) | 600 | 600 | 600 |
| $T_3$ (K) | 1200 | 1600 | 2300 |
| Fuel/air (by weight) | 0.0160 | 0.0284 | 0.0538 |
| Excess air (%) | 245 | 132 | 22.5 |
| Combustion Gas Partial Pressures (atm)[e] | | | |
| $N_2$ | 6.13 | 6.04 | 5.86 |
| $O_2$ | 1.25 | 0.92 | 0.28 |
| $H_2O$ | 0.29 | 0.50 | 0.91 |
| $CO_2$ | 0.25 | 0.45 | 0.80 |
| Ar | 0.08 | 0.08 | 0.07 |
| CO | $<10^{-6}$ | $9 \times 10^{-6}$ | 0.018 |
| $H_2$ | $<10^{-6}$ | $3 \times 10^{-6}$ | $3.5 \times 10^{-3}$ |
| NO | $2.2 \times 10^{-3}$ | $1.2 \times 10^{-2}$ | 0.053 |
| $CH_x$ | $\sim 10^{-5}$ | $\sim 10^{-5}$ | $\sim 10^{-5}$ |

[a] $T_1$ = assumed fuel ($C_8H_{18}$) supply temperature,
$T_2$ = assumed compressor air supply temperature,
$T_3$ = assumed combustion chamber or afterburner gas discharge temperature (adiabatic flame temperature). Temperatures are in degrees Kelvin.

[b] Case 1 is typical of maximum temperature operating conditions for presently used materials.

[c] Case 2 is typical of design goal operating conditions.

[d] Case 3 is typical of augmented (afterburner) conditions.

[e] Assumed combustion chamber total pressure = 8 atm.

The calculated gas compositions are consistent with measured gaseous emissions provided independently by Pratt & Whitney Aircraft Division, United Technologies Corporation.

The gas compositions for Case 2 is of particular interest since 1600K was selected as the reference service temperature for evaluating fiber/coating/matrix composites. Cases 1 and 3 were calculated to provide insight on how the gas composition changes with engine operating conditions. Case 1 is typical of maximum temperature operating conditions for materials such as Ni- or Co- base superalloys presently utilized in the exhaust gas environment. Case 3 is typical of conditions and gas compositions in the afterburner downstream of the turbine.

These are calculated values for the reference combustion chamber temperature of 1000K (see Table 1, case 2, in Ref. 6). [For comparison, calculated values at 1200K (case 1) are 6.1, 1.2, 0.29, and $<10^{-6}$, respectively.]

Where the coating and the exhaust gas react to produce gaseous components, the maximum service temperature is assumed to be the temperature at which the calculated partial pressure of the product gaseous species reaches $10^{-4}$ atm. We assume no hot corrosion. (See below for brief description of hot corrosion.)

Alumina Coating/Exhaust Gas

From the thermochemical standpoint, alumina is stable in an oxidizing atmosphere, except for small changes in composition with temperature. Therefore, an alumina coating is expected to be compatible with the exhaust gas.

## Mixed Oxide Coatings Exhaust Gas

Mixed oxides are generally stable in an oxidizing atmosphere. Therefore, the mixed oxides mullite, anorthite (CAS), and cordierite (MAS), as coatings, are expected to be compatible with the exhaust gas (assuming no hot corrosion).

## Spodumene Coating/Exhaust Gas

A drawback for the application of spodumene in the exhaust gas environment is the potential volatility of $Li_2O$ in the presence of water vapor at high temperature. The vaporization reaction is

$$1/2Li_2O(\text{in LAS}) + 1/2H_2O(g) \rightarrow LiOH(g) \qquad (14)$$

$\Delta G°$ values for the reaction are +44 kcal/mol at 1000K and +34 kcal/mol at 1600K. Taking the water pressure to be 0.50 atm, we find that $p_{LiOH}$ is $1.4 \times 10^{-5}$ at 1600K. This is below the criterion value of $10^{-4}$ atm (see above). Therefore, from the thermochemical standpoint, a spodumene coating is expected to be compatible with the exhaust gas at temperatures up to 1600K.

## Silicon Carbide Coating/Exhaust Gas

The key reaction for evaluating the compatibility of silicon carbide with the exhaust gas environment is the oxidation reaction

$$2/3SiC(s) + O_2(g) \rightarrow 2/3SiO_2(s) + 2/3CO(g) \qquad (15)$$

$\Delta G°$ values for the reaction are -138 kcal/mol at 1000K and -130 kcal/mol at 1600K. Using $p_{O2} = 0.92$ atm and $p_{CO} = 9 \times 10^{-6}$

atm, we find $\Delta G$ = -153 kcal/mol at 1000K and $\Delta G$ = -155 kcal/mol at 1600K. These large negative values for $\Delta G°$ and $\Delta G$ indicate that the reaction is very favorable (Ref. 14).

In spite of the high negative $\Delta G°$ values, silicon carbide normally has good resistance to high temperature oxidation owing to formation of a protective $SiO_2$ film. The oxidation is diffusion controlled and follows a parabolic rate law. A study (Ref. 20) found that water vapor slightly increases the oxidation rate. Also, the presence of additives and impurity elements tends to increase the oxidation rate.

Of serious concern are the results of oxidation studies which indicate that the oxidation of silicon carbide in a SiC-reinforced composite is affected by the matrix constituent. These studies (Refs. 21, 22) conducted at 1000° to 1575°C on $Al_2O_3$-SiC and mullite-SiC composites found parabolic rate constants three to four orders of magnitude higher than those expected for silicon carbide. Accordingly, the compatibility of silicon carbide and the exhaust gas at temperatures up to 1600K is doubtful.

Silicon Nitride Coating/Exhaust Gas

Silicon nitride, like silicon carbide, normally has good resistance to high temperature oxidation owing to formation of a protective oxide film. The overall oxidation reaction for $Si_3N_4$ (neglecting the intermediate compound $Si_2N_2O$) is

$$1/3Si_3N_4(s) + O_2(g) \rightarrow SiO_2(s) + 2/3N_2(g) \qquad (16)$$

$\Delta G°$ values for the reaction are -141 kcal/mol at 1000K and -132 kcal/mol at 1600K. Using $p_{O2}$ = 0.92 atm and $p_{N2}$ = 6.0 atm, we find $\Delta G$ = -139 kcal/mol at 1000K and -128 kcal/mol at

1600K. These high negative $\Delta G$ values indicate that the reaction is very favorable (Refs. 14).

Like silicon carbide, the suitability of $Si_3N_4$ as a coating exposed to exhaust gas depends on the rate (extent) of oxidation. Although the intermediate compound $Si_2N_2O$ forms in the case of $Si_3N_4$ oxidation, measured oxidation rates for SiC and $Si_3N_4$ are similar (Ref. 23). The oxidation rate of $Si_3N_4$, as well as that of silicon carbide, increases with (1) water vapor and (2) additives and impurities in the material (Refs. 23, 24). In view of the similar oxidation behavior of $Si_3N_4$ and silicon carbide and the finding of much higher oxidation rates for silicon carbide in a SiC-reinforced matrix (see above), we conclude that the compatibility of a $Si_3N_4$ coating with the exhaust gas is doubtful.

Boron Nitride/Exhaust Gas

The key reaction for evaluating the stability of boron nitride in the exhaust gas environment is

$$2BN(s) + 3/2O_2(g) \rightarrow B_2O_3(l) + N_2(g) \qquad (17)$$

The standard free energy change ($\Delta G°$) for this reaction is -165 kcal/mol at 1000K and -160 kcal/mol at 1600K. With $p_{N2}$ = 6.0 atm and $p_{O2}$ = 0.92 atm, $\Delta G$ is -162 kcal/mol at 1000K and -154 kcal/mol at 1600K, where $\Delta G$ is a measure of the driving force of the reaction at the existing oxygen and nitrogen partial pressures. These large negative $\Delta G$ values indicate that the reaction is very favorable. Kinetics cannot be counted on to limit the reaction; boron nitride oxidation in air commences at about 900°C. Another problem as the reaction proceeds is the reaction of $B_2O_3$ with water vapor to form gaseous boric acids. It is concluded that boron nitride is

not a suitable coating unless exposure to the exhaust gas can be restricted (Ref. 14).

## COMPATIBILITY OF MATRIX CANDIDATES WITH EXHAUST GAS ENVIRONMENT

This section summarizes our thermochemical assessments of the compatibility of matrix candidates with the exhaust gas environment at temperatures up to 1600K. The reference partial pressures of $N_2$, $O_2$, $H_2O$, and CO in the exhaust gas are assumed to be 6.0, 0.92, 0.50, and $6 \times 10^{-6}$ atm, respectively.

Where matrix and exhaust gas components react to produce gaseous species, the maximum service temperature is assumed to be the temperature at which the calculated partial pressure of the predominant gaseous species reaches $10^{-6}$ atm. (This follows the example of Luthra and Park, Ref. 25, p. 35.)

We assume no hot corrosion. Ceramics containing the component $SiO_2$ are especially susceptible to a type of hot corrosion which occurs when sodium compounds, present in the exhaust gas as the result of fuel impurities or airborne contaminates, condense on the ceramic surface and react with $SiO_2$ to form the silicate $Na_2O \cdot x(SiO_2)$. The resulting scale grows at high temperature because the silicate is liquid above about 1000°C. Accordingly, if hot corrosion occurs, the maximum service temperature for the matrix material is about 1000°C (1273K).

### Alumina Matrix/Exhaust Gas

From the thermochemical standpoint, alumina is stable in an oxidizing atmosphere. Therefore, an alumina matrix is expected to be compatible with the exhaust gas environment at

temperatures up to 1600K (assuming no hot corrosion).

Mixed Oxide Matrices/Exhaust Gas

From the thermochemical standpoint, the mixed oxide matrix candidates, mullite, cordierite, and anorthite, appear to be compatible with the exhaust gas environment at temperatures up to 1600K (assuming no hot corrosion).

$Y_2O_3$ AND YAG Matrices/Exhaust Gas

From the thermochemical standpoint, $Y_2O_3$ and YAG appear to be compatible with the exhaust gas environment at temperatures up to 1600K.

Silicon Carbide and $Si_3N_4$ Matrices/Exhaust Gas

As described above, the oxidation of silicon carbide and $Si_3N_4$ is thermodynamically very favorable. Therefore, the serviceability of the two materials in the exhaust gas environment depends on the ability of a protective silica film to reduce the oxidation rate to acceptable levels. One concern is that contaminants might affect the silica film properties such that oxidation rates become intolerably high. Accordingly, the suitability of silicon carbide and $Si_3N_4$ for high temperature service in the exhaust gas is doubtful.

Spodumene (LAS) Matrix/Exhaust Gas

As described above, a drawback for the application of spodumene in the exhaust gas environment is the potential volatility of $Li_2O$ in the presence of water vapor at high temperature. Using the $\Delta G°$ values cited above for reaction (14) and taking the water pressure as 0.50 atm, we find that

$p_{LiOH}$ is $10^{-6}$ atm at 1390K (note the $10^{-6}$ atm criterion stated above). Accordingly, from the thermochemical standpoint, the maximum service temperature is 1390K.

## SUMMARY AND CONCLUSIONS

This section summarizes the results and conclusions from the evaluation of Nicalon, HPZ, and Nextel fibers and associated coating and matrix candidates for potential application in the aircraft turbine engine exhaust gas environment at temperatures up to 1600K (2420°F).

Nicalon (SiC-based) and HPZ ($Si_3N_4$-based) fibers, as well as other fibers prepared from polymer precursors, are predominantly amorphous (glassy) in structure. The fibers are thermodynamically unstable and start to degrade (lose strength) above about 1000°C. Thus, their service life is limited above this temperature. Sound (gas-tight) coatings will likely extend the service life.

Nextel 440 and 480 (mullite-based) fibers are amorphous in structure and are relatively stable chemically, but they start to lose strength above about 1000°C owing to softening of the glass phase.

Nicalon and HPZ fibers are stronger than Nextel fibers at room temperature and retain more of their strength at high temperature.

The coating and matrix candidates which were assessed for chemical compatibility with each of the three candidate fibers are listed below in the approximate order of best to worst compatibility.

| NICALON | HPZ | NEXTEL |
|---|---|---|
| Alumina | BN | Alumina |
| Yttria | SiC-C | Mullite |
| YAG | | CAS |
| SiC | | SiC |
| BN | | Yttria |
| B | | YAG |
| Si | | $Si_3N_4$ |
| $Si_3N_4$ | | BN |

Oxides are more compatible with the fibers than non-oxides and are more likely to bond strongly to the fibers.

The results of cnemical compatibility assessments for candidate coating/matrix combinations are summarized below. An inert environment and $10^{-4}$ atm maximum partial pressure of the product gaseous species were assumed.

| | |
|---|---|
| $BN/Si_3N_4$ | Compatible at 1600K and below |
| BN/LAS | Compatible at 1600K and below |
| BN/MAS | Compatible at 1600K and below |
| $SiC/Si_3N_4$ | Compatible at 1600K and below |
| $Al_2O_3/SiC$ | Compatible at 1600K and below |
| SiC/LAS and MAS | Compatible up to 1460K |
| SiC-C/LAS and MAS | Compatible up to 1230K |
| $SiC-C/Si_3N_4$ | Compatible up to 1140K |
| B/SiC | Doubtful (could react to form $B_4C$) |
| $Al_2O_3$/mixed oxides | Doubtful (inadequate phase data) |
| $Al_2O_3/Si_3N_4$ | Doubtful (could form sialons) |
| $B/Si_3N_4$ | Not compatible (react to form BN) |

The results of chemical compatibility assessments for candidate coatings exposed to exhaust gas at temperatures up to 1600K are summarized below. We assumed no hot corrosion and $10^{-4}$ atm maximum partial pressure of product gaseous species.

| | |
|---|---|
| $Al_2O_3$ | Compatible |
| CAS and MAS | Compatible |
| Mullite | Compatible |
| LAS | Compatible ($p_{LiOH}$ below $10^{-4}$ atm) |

| | |
|---|---|
| SiC | Doubtful (oxidation rate may be too high) |
| $Si_3N_4$ | Doubtful (oxidation rate may be too high) |
| BN | Not compatible (reacts with $O_2$) |

The results of assessments of the chemical compatibility of candidate matrices and exhaust gas at temperatures up to 1600K are summarized below. We assumed no hot corrosion and $10^{-4}$ atm maximum partial pressure of gaseous species.

| | |
|---|---|
| $Al_2O_3$ | Compatible |
| CAS and MAS | Compatible |
| Mullite | Compatible |
| $Y_2O_3$ | Compatible |
| YAG | Compatible |
| SiC | Doubtful (oxidation rate may be too high) |
| $Si_3N_4$ | Doubtful (oxidation rate may be too high) |
| LAS | Compatible to 1390k, where $p_{LiOH} = 10^{-6}$ atm |

The overall conclusion, based on (1) the results of our thermochemical evaluations, (2) published results of fiber thermal stability tests, and (3) published results of oxidation and hot corrosion tests, is that several fiber and associated coating and matrix candidates would be suitable for service in the exhaust gas environment at temperatures up to 1600K for limited service life.

## EXPERIMENTAL RESULTS

Experimental studies of the chemical and mechanical interaction between coating and substrate materials were performed. Coatings were applied, using chemical vapor deposition, on dense ceramic disks that simulate the fibers used in this program. The experimental couples were then heat treated and characterized.

The substrate materials chosen were alumina, silicon carbide and silicon nitride. The alumina was purchased from

Alpha Ceramics and both the silicon carbide and silicon nitride were purchased from ESK ceramics. All three materials were in the form of high purity, high density ceramic rods. The ceramic rods were cut into 3 mm thick disks and polished. After polishing, the disks were cut into six smaller samples and then ultrasonically cleaned to remove any debris picked up during the initial stages of sample preparation.

Boron nitride, silicon carbide and silicon nitride coatings were applied to the substrates using chemical vapor deposition. BN was deposited onto all three substrate materials. SiC was deposited on $Si_3N_4$ and $Al_2O_3$; $Al_2O_3$ and SiC substrates were coated with $Si_3N_4$.

To promote chemical interaction between the coating and the substrate at various temperatures, the coated substrates were heat treated to 1000°, 1200° and 1400°C in a high purity helium atmosphere. The samples were held at temperature for two hours. The samples were re-polished for metallographic and SEM/EDAX analysis. A total of 18 samples were prepared and investigated.

Coating characteristics and any apparent reaction zones were determined by scanning electron microscopy (SEM). After heat treatment, the boron nitride coatings adhered only to the alumina and silicon carbide substrates. The BN coated $Al_2O_3$ substrates were studied only at 1000° and 1200°C but appeared to have adherent coatings at both temperatures with no evidence of any chemical interaction. The BN coated SiC couples maintained adherent coatings at 1000°, 1200° and 1400°C. The measured coating thickness was slightly larger in the 1200°C sample than in the other two samples, but Figure 1 shows no evidence of increased porosity. Therefore, this difference is probably due to variation in the initial coating

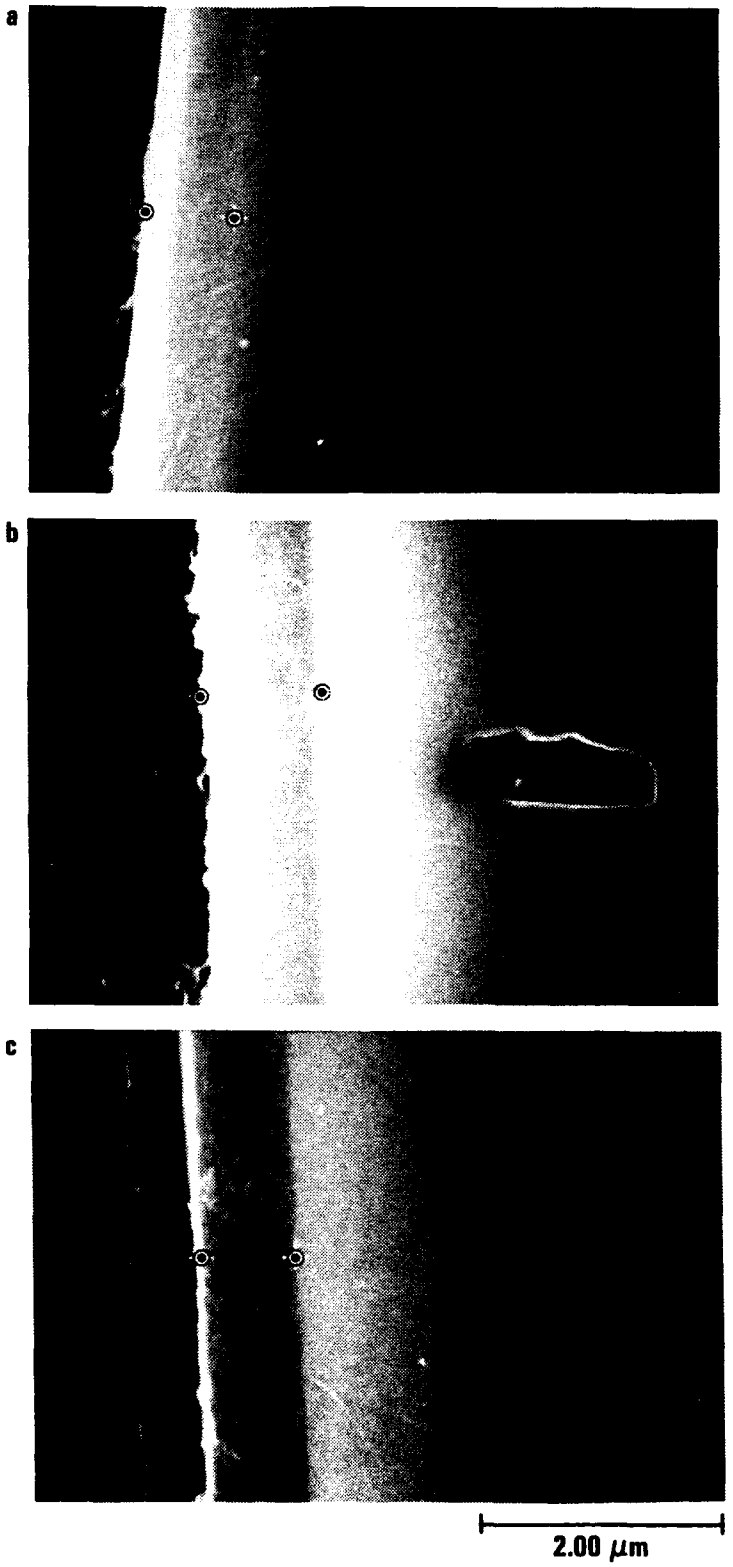


Figure 1. Scanning electron micrographs of BN coated SiC substrates after two hour heat treatment to (a) 1000°C (b) 1200°C (c) 1400°C. The distance between circles is given in bottom right corner of micrograph.

thicknesses rather than a result of the heat treatment. The BN coated $Si_3N_4$ samples only withstood the first heat treatment to 1000°C. At 1200°C, the coating was loosely attached to the substrate and at 1400°C, there was no evidence of a coating. It is possible but not probable that these two coatings were pulled from the substrates during metallographic preparation. Since these samples were prepared in the same mount with other samples that retained coatings, it suggests that the coating did not survive the heat treatment because of a weak interface between the coating and the substrate.

The silicon carbide coatings were not very adherent to the alumina or silicon nitride substrates. There was no SiC coating on the alumina samples, which was expected since the sample gained no weight after coating. The SiC did remain as a coating on the silicon nitride substrate heated to 1000°C; however, it was not very adherent as shown in Figure 2.

The alumina and silicon carbide substrates coated with silicon nitride remained coated after heat treatment to 1400°C. The coating thicknesses did not vary significantly from one heat treatment to the next and there was no evidence of chemical interaction between coating and substrate. This can be seen in the micrograph and elemental maps of an $Al_2O_3$ substrate coated with $Si_3N_4$ shown in Figure 3.

Along with the chemical interaction of substrates and coatings, a study was done to measure the strength of the interfaces by torsion tests.

The same silicon carbide and silicon nitride substrate materials used in the chemical interaction studies were coated and used for this mechanical testing study. Each substrate was three millimeters in thickness and 13.8 mm in diameter.

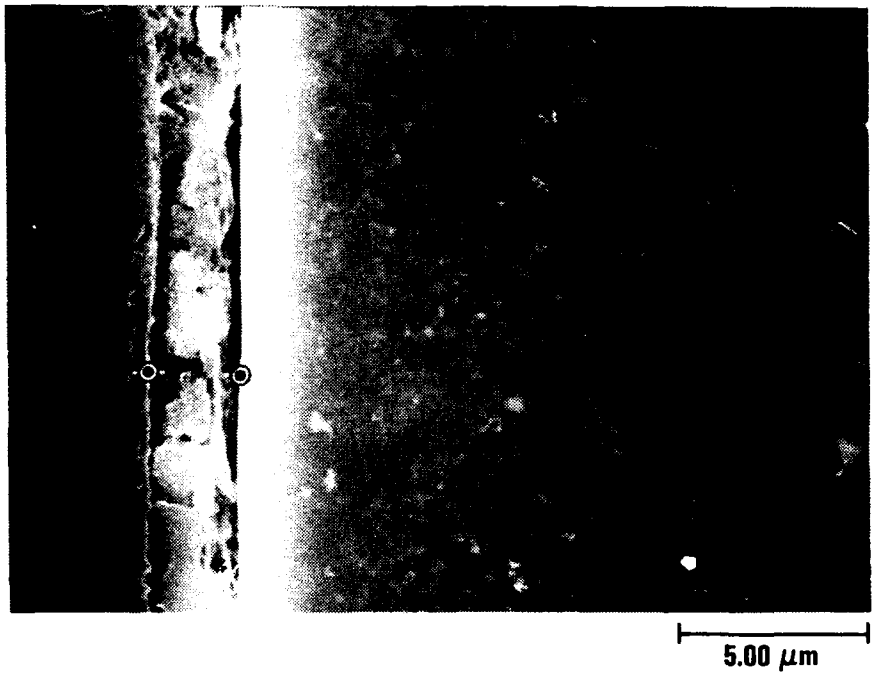


Figure 2. Scanning electron micrograph of SiC coated $Si_3N_4$ substrate after heat treatment to 1000°C for two hours. The distance between circles is given in bottom right corner of micrograph.

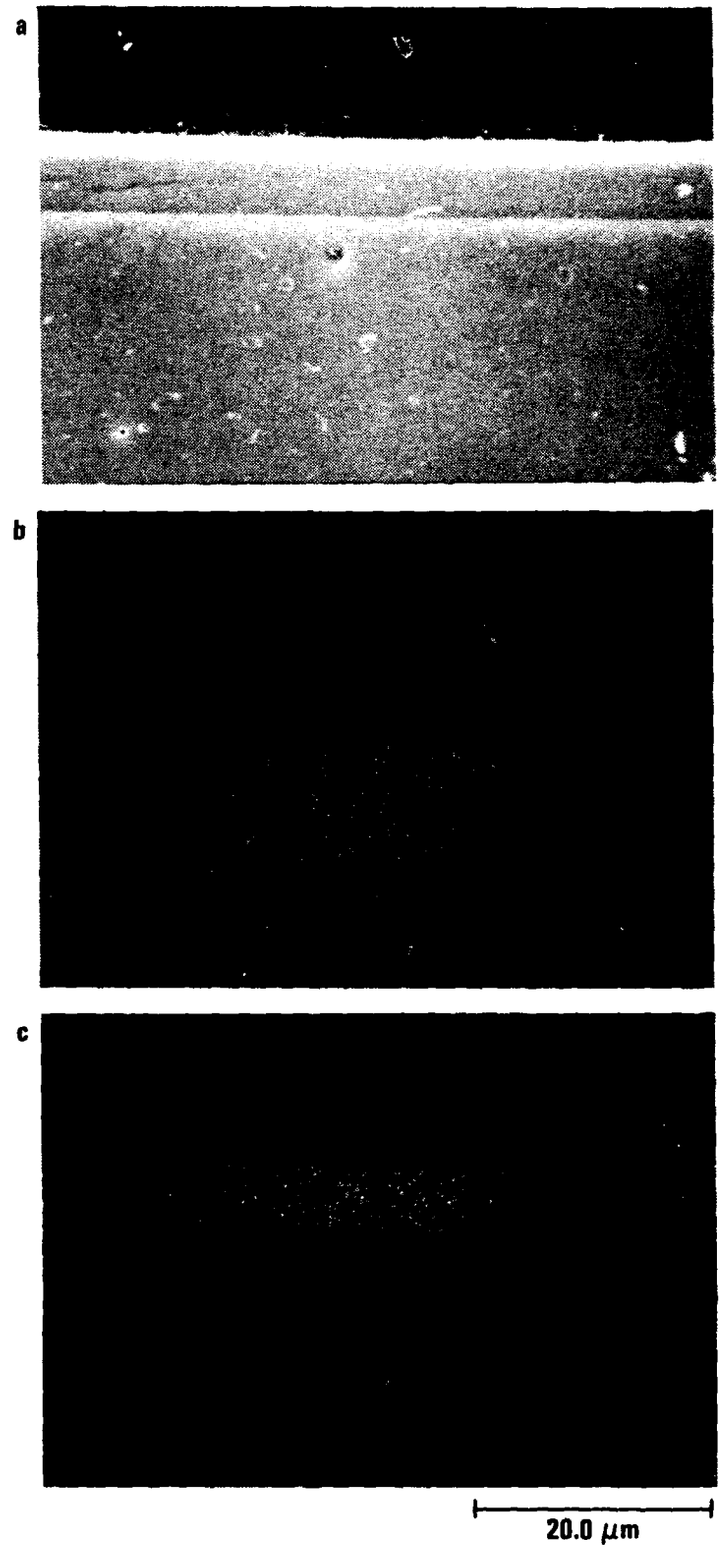


Figure 3. $Si_3N_4$ coated $Al_2O_3$ substrate after two hour treatment at 1200°C (a) SEM micrograph (b) Al X-ray map (c) Si X-ray map.

To study and compare the strengths of the coating/substrate interfaces, the coated substrates were heat treated to 1000°, 1200° or 1400°C. The samples were held at temperature for two hours.

The coated substrates were then individually mounted between two plates of aluminum metal using 3M Regular 1124 Epoxy and torsion applied until failure. It was important to note whether the failure occurred between the coating and the substrate, the coating and the epoxy or the epoxy and the metal plate.

The results of the torsion tests are shown in Table 2. The strengths of the interfaces ranged from 1.7 to 66 Mpa. The highest strength may have been limited by the strength of the epoxy. In most cases, the coating/substrate interface was strongest prior to heat treatment. The effect of the temperature on the strength of the interface was most evident for the samples heat treated to 1400°C.

Determination of the failure mode was complicated by the multilayer nature of the samples. Initial examination under an optical microscope revealed the failure point data in Table 2. Further study is required to confirm the failure mode for several of the samples.

Initial studies of the chemical compatibility and degree of chemical interaction between coating and substrate materials suggest that there is little substrate coating interaction during heat treatments up to 1400°C. No reaction zones were found in any of the coated couples. There were few problems with coating adherence at elevated temperatures. Mechanical strengths of the coating/substrate interfaces look promising.

Table 2

TORSION TEST RESULTS OF COATED SUBSTRATES

| SUBSTRATE | COATING | HEAT TREATMENT (°C) | FAILURE LOAD (kg-cm) | SHEAR STRESS Mpa | FAILURE POINT |
|---|---|---|---|---|---|
| SiC | BN | none | 427.3 | 66.51 | epoxy/coating |
| SiC | BN | 1000 | 362.8 | 56.11 | epoxy/coating |
| SiC | BN | 1200 | 345.5 | 53.71 | coating/substrate |
| SiC | BN | 1400 | 184.3 | 28.65 | epoxy/coating |
| $Si_3N_4$ | BN | none | 368.5 | 53.89 | epoxy/metal |
| $Si_3N_4$ | BN | 1000 | 374.3 | 55.29 | epoxy/metal |
| $Si_3N_4$ | BN | 1200 | 353.0 | 52.14 | epoxy/metal |
| $Si_3N_4$ | BN | 1400 | 57.6 | 8.51 | coating/substrate |
| $Si_3N_4$ | SiC | none | 23.0 | 3.35 | to be determined |
| $Si_3N_4$ | SiC | 1000 | 405.6 | 59.66 | coating/substrate |
| $Si_3N_4$ | SiC | 1200 | 394.4 | 57.97 | to be determined |
| $Si_3N_4$ | SiC | 1400 | 11.5 | 1.68 | coating/substrate |
| SiC | $Si_3N_4$ | none | 367.4 | 56.47 | epoxy/metal |
| SiC | $Si_3N_4$ | 1000 | 328.2 | 50.77 | substrate |
| SiC | $Si_3N_4$ | 1200 | 307.5 | 46.83 | epoxy/coating |
| SiC | $Si_3N_4$ | 1400 | 211.9 | 32.27 | epoxy/coating |

## TASK 1-2 LIQUID PHASE PROCESS DEVELOPMENT

The microstructure of sol-gel derived thin films can be controlled by the precursor structure prior to deposition. Thus, coatings can be prepared with unique properties. Oxide and non-oxide films can be prepared by gelation of three basic types of solutions: metallic salts, colloidal sols, and polymerized organometallic species. Each of these methods has advantages as well as disadvantages. Therefore, GA studied the possibility of using each of these methods for preparing oxide, nitride and carbide coatings on ceramic multifilament tows.

Processes to produce thin, smooth, continuous coatings on ceramic fibers from aqueous and nonaqueous solutions were developed. The processes involve six basic steps: (1) desizing, (2) sol/solution preparation, (3) dip coating, (4) curing, (5) drying, and (6) calcination.

A bench-scale continuous fiber coater was built and is operational. All of these steps can be controlled and performed with the continuous coater. A schematic of the coater is illustrated in Fig. 4. The fiber tow is first desized by pulling the as-received tow through a desizing furnace onto a take up spool. The fiber tow is level wound on an interchangeable take up spool. The spool can then be removed and used as the supply spool for coating. The tow is subsequently pulled through the coater by a motor on the level wind take up reel. The tow path is as follows: (1) over several rollers used to measure the tension, (2) vertically into the coating solution which is in a constant temperature ultrasonic bath, (3) out of the coating solution vertically and through a curing and two-zone drying chamber, (4) through a three-zone calcination furnace, and (5) level wound on the interchangeable take-up spool for storage and future use. The

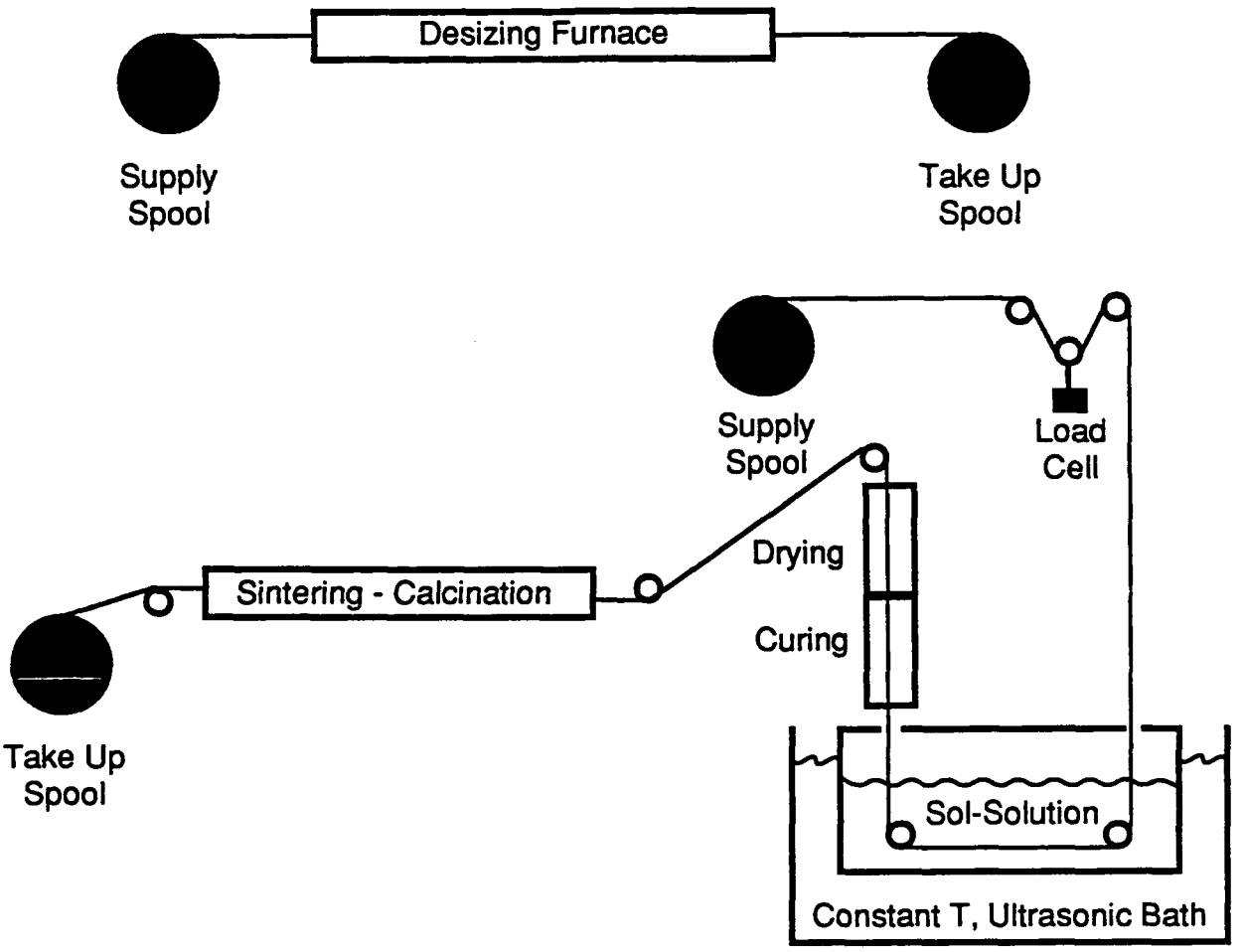


Fig. 4 Schematic of bench-scale continuous fiber coater

take-up reel motor, load cell, calcination furnace, and drying chamber have been calibrated.

Aqueous Sol Precursor

Coatings of $Y_2O_3$, $Al_2O_3$, $HfO_2$, $MgAl_2O_4$, $YAlO_3$, and MgO on Nicalon, Nextel 480, and FP-PRD-166 were produced by dip coating in nitrate sols. Continuous lengths of Nicalon up to 25 meters were coated with yttria and alumina. The critical parameters in the sol coating systems were extensively studied. The critical parameters include the type of sol, the sol production conditions and concentrations, the degree of fiber spreading during coating, the curing environment and time, and the drying rate and time.

The concentration of the sol, particle size in the sol, and use of fiber spreading techniques affect the degree of bridging and tracking. The adherence of the coating is controlled by the sol type and the curing environment. The smoothness of the coating is determined by the sol, the curing environment and the drying rate. An example of the effect of curing environment on the coating quality of $Y_2O_3$ on Nicalon is shown in Fig. 5. Panel A shows the coating after an anhydrous cure, while Panel B shows that a water saturated ammonia cure results in a smooth coating. The uniformity of infiltration within the tow is controlled by the drying rate and the gel point of the sol. Reaction of the coating with the fibers during calcination is controlled by the type of coating and fiber, the type of sol, and the curing environment. The calcination rate does not appear to significantly affect the coating adherence, smoothness, or continuity.

All the parameters which affect the appearance of the coating or the reaction of the coating with the fibers appear

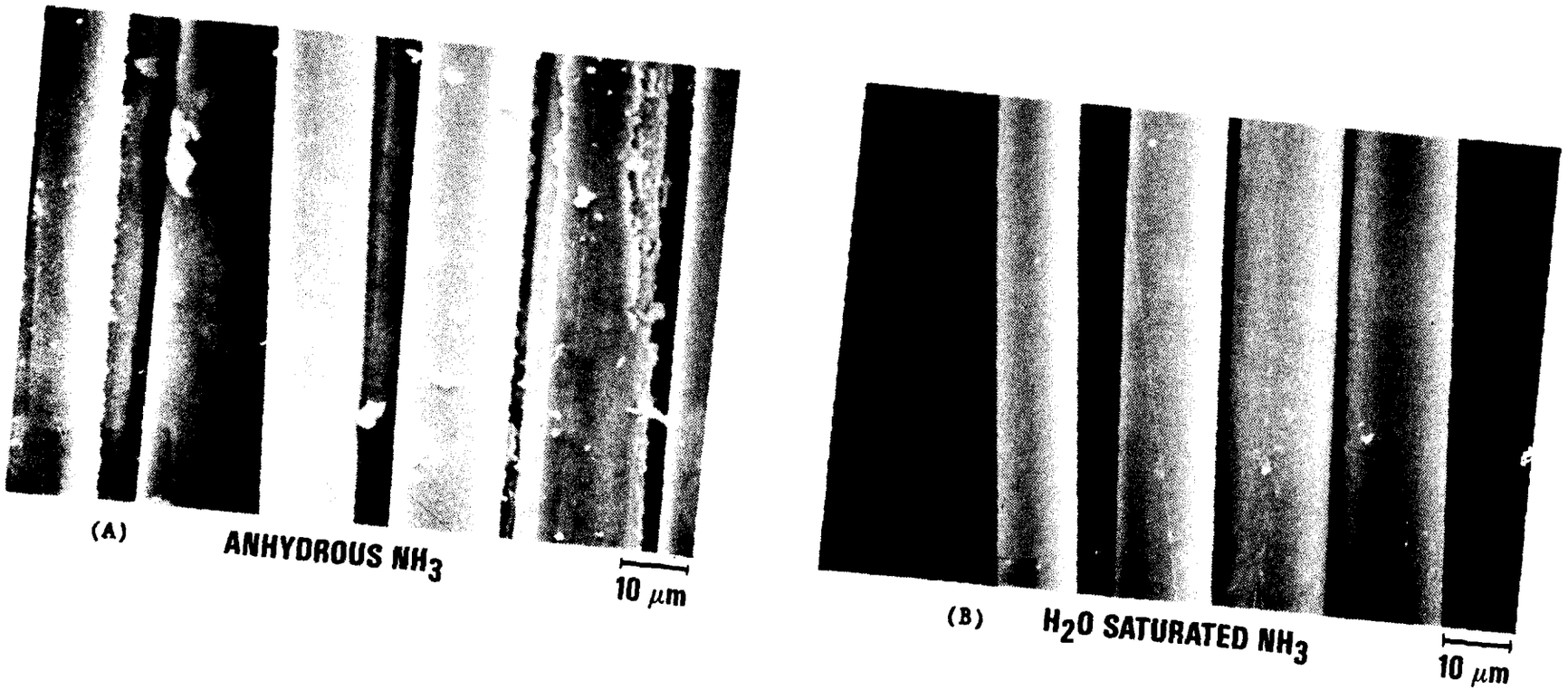


Fig. 5 Sol-gel yttria coating on Nicalon from a yttrium nitrate sol. The fibers in Panel A were cured in anhydrous ammonia. The fibers in panel B were cured in water saturated ammonia.

to affect the strength of the tow. In particular, smoother coatings result in stronger tows. Initial results indicate the tows are not significantly weakened by traveling over the rollers in the continuous coater although further analysis of the possible effect of the continuous coater on the strength of the tows was investigated (vide infra).

Particle size, concentration, and the degree of fiber spreading are important factors in determining the amount of bridging and tracking. For the small dip coater the concentration limit for coating Nicalon tows without bridging is approximately 0.10 M aluminum and 0.05 M yttrium. Lower molar concentrations of yttrium were used to account for the higher molecular weight to density ratio (cubic centimeters per mole) of yttria compared to alumina. However, this limit is dependent on the effectiveness of fiber spreading techniques and is substantially higher for the continuous coater because the rollers spread the tow apart. The effect of the degree of peptization, or particle size, is not as dramatic as the concentration, but it is an important factor. The withdrawal rate of the tow from the sol is not an important factor over the range studied because the sols wick into the fiber tows and are held there by the surface tension.

The curing environment is critical not only to the coating appearance and adherence, but also to the possible reaction of the coating with the substrate during calcination. The dip coating chamber of the continuous coater is kept under positive nitrogen pressure to keep the ammonia in the curing column from entering the coating chamber. The flow rate of water saturated ammonia into the curing column and the flow rate of water saturated nitrogen into the coating chamber significantly affect the final coating appearance. If the ammonia flow rate is too high, excessive tracking between the fibers occurs. For example, under otherwise equivalent

conditions, an ammonia flow rate of 50 cc/min resulted in a smooth coating, but a flow rate of 200 cc/min resulted in excessive tracking. If the ammonia flow rate is too low, or the nitrogen flow rate is too high, a continuous adherent coating of yttria is not obtained. Although smoother adherent coatings of alumina could be obtained without curing, Nicalon tows coated from an aluminum nitrate solution cured in the ambient atmosphere were significantly weaker after calcination than those cured in water saturated ammonia. This indicates the reaction of the coating with the fiber is dependent on the curing conditions.

The drying rate is also critical to the coating appearance and the strength of the fibers after calcination. The uniformity of infiltration of the tows is determined primarily by the drying rate of gel point of the sol. In addition to the sol that infiltrates the tow, there is a considerable amount of sol held outside of the tow. If the drying rate is too fast, the colloidal particles in the sol will drop out of solution quickly resulting in more deposition on the outer fibers than the inner fibers. If the drying rate is too slow, the particles will stay in solution until the outer areas of the tow are dry resulting in more deposition on the inner fibers. The drying rate also plays an important role in determining the final coating appearance. For Nicalon tows coated with yttria in the continuous coater, a drying temperature of 300°C for 3 min resulted in particulate formation on the fibers, but a drying temperature of 150°C for 3 min resulted in a smooth coating. The formation of particulates on the fibers significantly weakens the tow after calculation.

The calcination heating rate does not significantly affect the appearance of the coating, but the coating and fiber components often interdiffuse during calcination.

Silica from Nicalon fibers diffuses into the alumina coating. The yttria coated Nicalon tows exhibit very little interdiffusion of silica and yttria. The alumina from Nextel 480 fibers forms an yttrium aluminum garnet with the yttria coating after calcination, and the silicon in the Nextel 480 fibers diffuses into the alumina coatings resulting in nearly the same stoichiometry as the fiber. Further characterization of the final coating stoichiometry for various coating-fiber systems is required.

Typically the strengths of Nicalon tows coated with $Y_2O_3$ and $Al_2O_3$ were reduced to 40% to 50% of the strengths of the desized tows (which were 10% to 20% higher than the as-received strengths). Nicalon tows passed through the coater with distilled water in the coating chamber exhibited no reduction in strength. Therefore, the degradation in strength is not from any mechanical damage during the coating process. Nicalon fibers coated with yttria using multiple dips and heat treatment to 500°C showed no reduction in strength. However, heat treating the sample to 900°C resulted in a significant strength reduction. Thus, the weakening does not occur until strong bonding between the fiber and the coating at high temperatures occurs. The coating parameters for yttria coatings from the nitrate solutions were optimized to obtain the least reduction in strength of Nicalon fibers. A strength reduction of 10% to 20% was found in these cases. Thus, the as-received, sized Nicalon and Nicalon coated with yttria under optimal conditions had the same strength.

Continuous coating runs using zirconia and hafnia precursors with in-situ curing resulted in very nonuniform coatings. The reaction bonding process of hydroxide coating, alkoxide reaction, rinsing excess coating solution, and converting the bound alkoxide to the hydroxide was

applied to the zirconia system. This process is promising for producing smooth oxide coatings with a thickness of 1000 Å or more. Coatings produced by this process continue to be substantially free of bridging or tracking. The smoothness of the final coating is dependent to some extent on the smoothness of the initial thin hydroxide coating. Thus, producing the initial thin hydroxide film with a nonaqueous sol may be better than with aqueous systems. The coating systems will be evaluated below to determine which process produces the best coating of 1000 Å or greater thickness. The competing processes include: nonaqueous sols, aqueous sols, reaction bonding, and in-situ curing. The coating materials will be yttria, hafnia, and zirconia.

Coatings of yttria and hafnia that are approximately 0.1 μm thick were applied to SCS-6. However, a much thicker coating is preferred. Therefore, the viscosity of the sols for dip coating the monofilaments was increased to thicken the coating.

The continuous coater was modified to obtain a higher throughput by increasing the size of the curing and drying zones from 15cm each to 30cm each. The modifications enable coating of tows at a rate of 6 to 9 meters per hour with the present configuration. In addition, an insert was developed for the coating chamber to reduce the amount of solution needed for test runs. This insert reduces the solution requirements from 250 ml to 30 ml. Yttria coatings produced at the higher rate with the small coating chamber were not as smooth as previously obtained. The larger chamber was reinstalled to remedy this problem. The coater was used to obtain a 6 meter per hour continuous run of YAG coated Nicalon using a nitrate solution and in-situ curing.

Alkoxide reaction bonding was investigated further. This

process consists of the following steps:

1) A very thin coating of the hydroxide of the metal oxide to be coated is prepared by either dip coating or in-situ curing.
2) The precoated tow is dipped in an alkoxide solution and the alkoxide reacts with the free hydroxyl groups.
3) The excess solution is rinsed from the tow to avoid precipitation of unreacted alkoxide.
4) The bound alkoxide is converted to hydroxide by curing in a water vapor or an ammonia-water vapor atmosphere.
5) Steps 2 through 4 are repeated to build the required thickness.

Coatings prepared by this method exhibit almost no bridging or tracking. Also, the coatings are typically much smoother than the 'precipitation' processes of dip coating and in-situ curing. A SEM micrograph of yttria coated Nicalon produced by reaction bonding is shown in Figure 6. The initial coating was produced using in-situ curing of yttrium nitrate, and the reaction bonding was accomplished using yttrium isopropoxide and steam as the curing agent. The smoothness of this coating is typical of the coatings produced by reaction bonding. EDAX results indicate that smooth, continuous coatings of comparable thickness to those obtained by in-situ curing or dip coating can be obtained. This process could be used to overcome the uniformity, bridging, and tracking problems associated with coating of fibers in woven cloth.

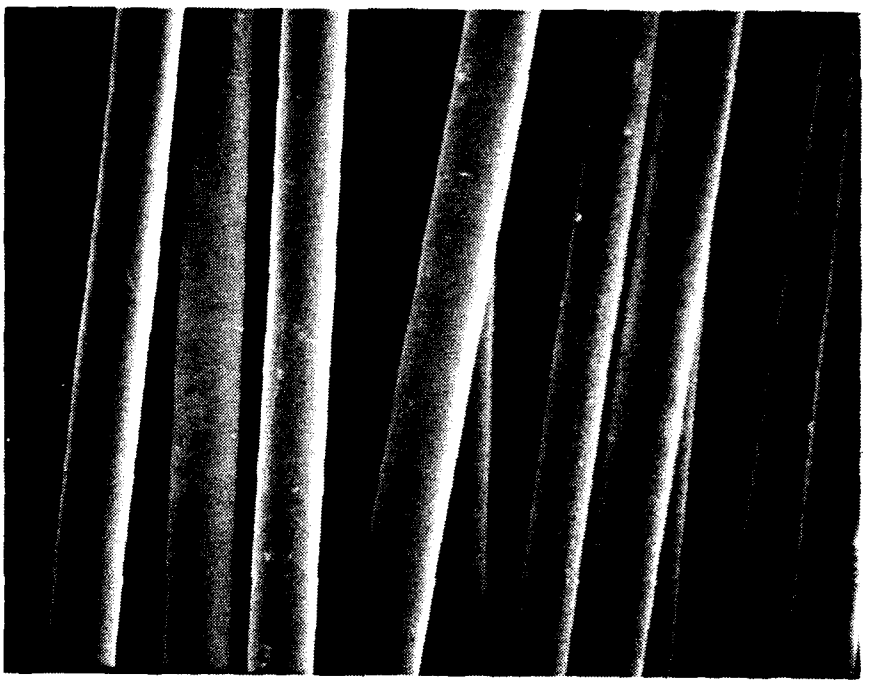

Fig. 6 Scanning electron micrograph of yttria coating on Nicalon prepared by reaction bonding process.

## Nonaqueous Sol Precursors

Several dip coating solutions were prepared using the procedures described in the following paragraphs.

### Alumina Coating Solution

Clear solutions of organoaluminum were prepared by the controlled hydrolysis of dilute solutions of aluminum sec-butoxide [$Al(OC_4H_9)_3$]. Initial experiments used sec-butanol and ethanol as the solvent, but it was found that the solutions were not stable and, after aging for several hours, formed a precipitate. Thus, the alkoxide was dissolved in 2-ethoxyethanol or 2-(2-ethoxyethoxy) ethanol which had been dried by distilling from barium metal. The solutions were hydrolyzed by dropwise addition of distilled water dissolved in a separate portion of alcohol. After the hydrolysis was complete, additional alcohol was added to give a concentration of 0.18 to 0.33 M alkoxide. The mixture was then heated for 1 to 15 h at 55°C to dissolve the precipitate.

### Yttria Coating Solution

Yttrium isopropoxide was prepared by reaction of yttrium metal with dry isopropanol following the procedure of Mazdiyasni (Ref. 26).

Yttrium 2-ethoxyethoxide and yttrium 2-(2-ethoxyethoxy) ethoxide were prepared from yttrium isopropoxide by alcohol exchange. Typically, 6.81 g (0.0256 mole) of the isopropoxide was reacted, while under a flow of nitrogen, in a round bottom flask with 30 ml of dry 2-ethoxyethanol (distilled from barium). The solution temperature was slowly increased from room temperature to 125°C, and the isopropanol, as it was

formed was swept from the vessel. After reacting for 3 to 5 h, the solution was cooled and filtered in a glove box to yield a clear, pale-yellow solution. The yttrium concentration was titrated with standard EDTA solution using Eriochrome black T indicator.

The coating solution was prepared from either alkoxide. Typically, 2.213 g of the stock yttrium 2-ethoxyethoxide (0.0005419 mole Y/g solution) was placed in a reaction vial under dry nitrogen. This was diluted with 6.015 g of dry 2-ethoxyethanol and the vial was sealed with a septum cap. The solution was heated in an oil bath at 57°C for 30 to 45 min. To this solution was added,dropwise, the hydrolysis solution consisting of 43 mg double distilled water in 1.00 ml dry 2-ethoxyethanol. The solution was heated for an additional 1 h, cooled and additional dry 2-ethoxyethanl was added to adjust the final concentration to 1 wt % equivalent $Y_2O_3$.

YAG Coating Solution

While under an inert atmosphere, the amounts of the stock aluminum and yttrium solutions (2-ethoxyethoxides) required to give stoichiometric YAG ($Y_2O_3 \cdot 5Al_2O_3$) were weighed into a reaction vial. The vial was sealed with a septum cap, and placed in an oil bath at 65°C. The solution was heated for 1.5 h and then water, dissolved in 2-ethoxyethanol, was added dropwise from a syringe. The solution was heated for an additional 16 h after the addition of water.

Hafnia Coating Solution

The synthesis of hafnium alkoxides from the tetrachloride was performed as described in the literature (Ref. 27). While working in a glove box under an anhydrous nitrogen atmosphere,

the anhydrous metal tetrachloride was added over 3 to 4 h to isopropyl alcohol and normal hexane saturated with anhydrous ammonia at 5°C. The solution was filtered through a fritted glass funnel to remove the ammonium chloride precipitate. The stock solution was stored in the glove box under nitrogen to prevent hydrolysis.

Hafnium 2-ethoxyethoxide was prepared from the isopropoxide by alcohol exchange using the procedure developed for yttrium 2-ethoxyethoxide described above.

Another solution used to deposit coatings of the hafnia precursor on the substrate fibers was prepared by controlled hydrolysis of hafnia 2-ethoxyethoxide. The alkoxide solution was placed into a reaction vial and sealed under an inert atmosphere with a septum cap. The solution was heated in an oil bath at 55°C for about 15 min and then alkoxide was hydrolyzed by injecting water, dissolved in 2-ethoxyethanol, into the reaction vial. The reaction was continued for 1 h at 55°C and then the solution was cooled to room temperature.

Dip Coating

The polyvinyl alcohol sizing was removed from continuous Nicalon fiber by heating in air at 700°C for 20 min. Approximately 4 cm long samples were cut from the desized yarn. Coating was accomplished by automated dipping into the hydrolyzed alkoxides solutions using an automated dip coater constructed at GA.

This instrument consists of a sample holding device attached to a Berg linear clutch assembly. The holder is contained in a pyrex glass enclosure, which also surrounds the vial with the coating solution. Inert, or reactive, gas can be purged through the enclosure during the dipping process.

Surrounding both ends of the enclosure are heaters, operated by separate omega temperature controllers, that function as a coating dryer and a coating solution heater. The linear clutch is driven at a variable speed by a Minarek reversible dc motor. The direction of travel of the linear assembly, the position of the assembly, and the number of dips is controlled by an LFE microprocessor based controller. The ramp-and-soak feature of the LFE allows the operator to change the length of time that the sample is held in the coating solution or in the heater zone. Samples were dipped into the coating solution for 20 s and removed at 2 mm/s. The coating was dried at 350°C to 500°C prior to repeating the dipping cycle for multiple dipped samples.

Calcining

After dip coating, the samples were heated at 10°C/min to 700°, 900°, 1100°, or 1300°C and held for 30 min. After the hold, the temperature was reduced at 20°C/min to about 700°C and then the furnace was turned off.

Figure 7 shows the relative thickness of the yttria and alumina coatings obtained when desized Nicalon fibers are dipped into the coating solutions. The relative coating thicknesses were determined by EDAX analyses of the coating compositions using the silicon peak as an internal standard. Increasing the number of dips increases the coating thickness. However, when the equivalent concentration of oxide exceeds 1 wt % , significant bridging between fibers can occur. This effect may be reduced by multiple dips into dilute coating solutions. The amount of water used in the hydrolysis has little effect on the thickness of alumina coatings when the concentration of metal oxide is below 0.5 wt %. When the wt % metal oxide exceeds this concentration, five dips in a solution hydrolyzed with two moles water per metal shows a

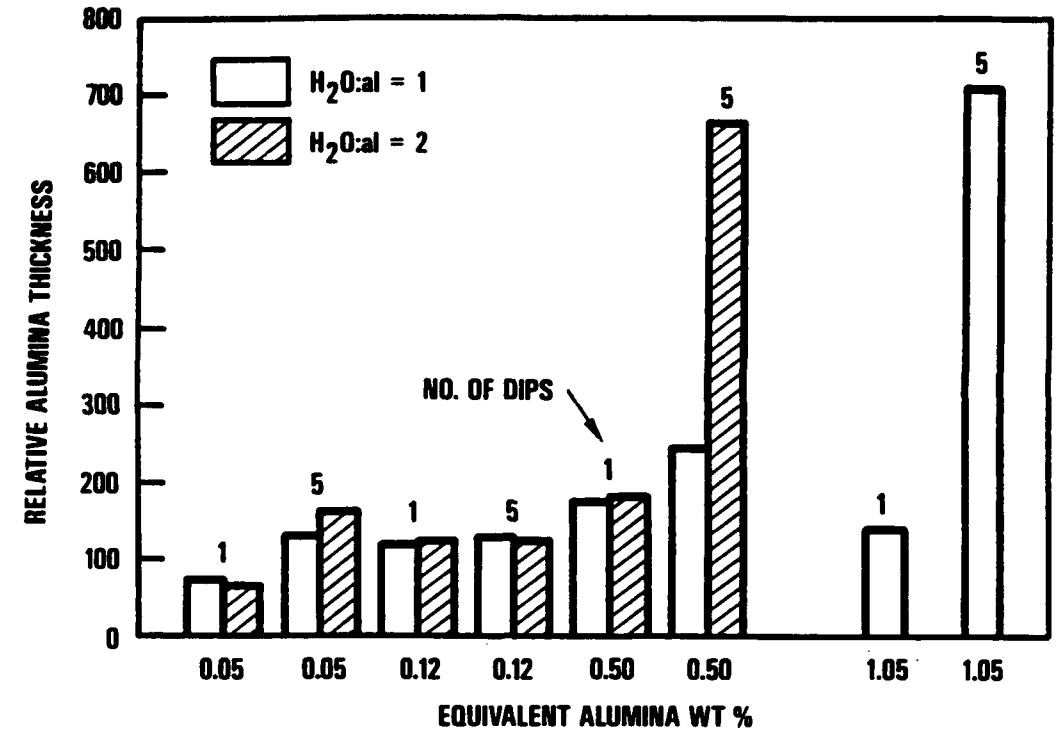


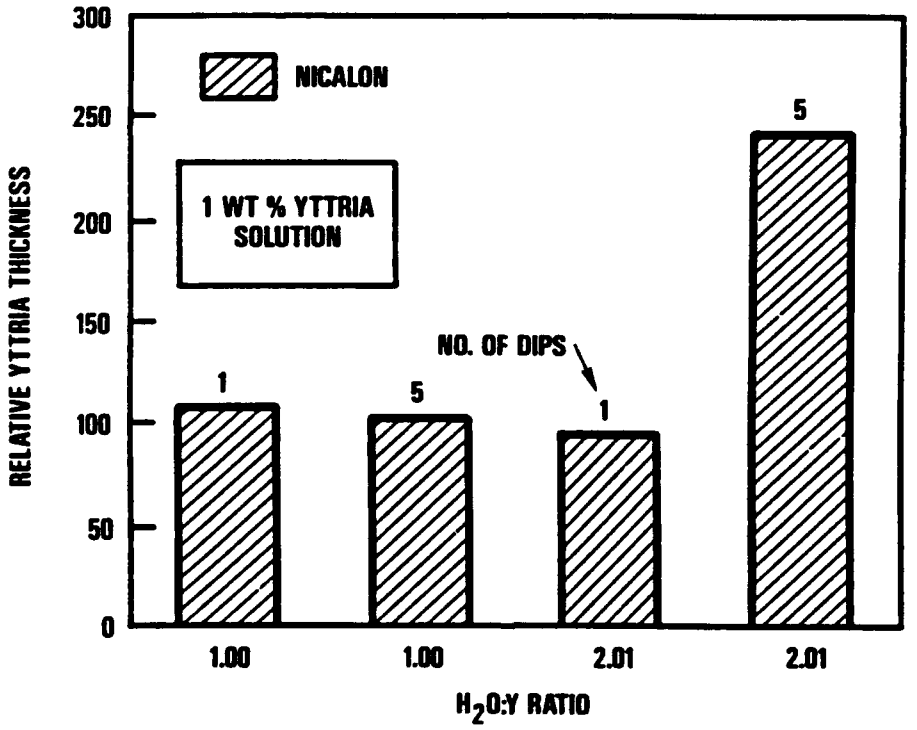


Fig. 7 Relative coating thickness as a function of process parameters. Top panel is for alumina coated Nicalon. Bottom panel is for yttria-coated Nicalon.

significant increase in the thickness of the coating. SEM observations show that the coatings appear similar with minor bridging.

The structure of the alkoxy moiety influences the coating, and the stability of the coating solution. The data in Fig. 7 were obtained using the 2-ethoxyethoxides in 2-ethoxyethanol. With one mole of water per mole of metal, the solutions were stable for several months. However, when the molar ratio is increased the solutions would continue to thicken and would gel in a few days. With the 2-(2-ethoxyethoxy) ethoxides, significant bridging was obtained at 1 wt % equivalent oxide. Furthermore, the solutions would gel within a few hours if the water:metal ratio was greater than one.

The tensile strength of the coated fibers was measured. All of the coatings tested to date degrade the fiber strength during 0.5 h anneals at temperatures greater than 700°C. Figure 8 compares the average failure load for individual fibers coated with alumina and yttria. YAG coated fibers were only tested after the 900°C anneal and were weaker than the alumina coated fibers. Presumably, the coating is reacting with the fiber creating flaws from which cracks propagate during tensile loading.

Non-Aqueous Alkoxide Precursor

Four meters of SCS-6 were coated continuously with zirconia using a small scale continuous process. Ten coats were applied from an alkoxide solution without curing. The final coating thickness was approximately one micron. The coating was predominantly monoclinic zirconia with a reaction layer of zirconium carbide at the carbon-zirconia interface. The coating was not strongly adherent, and was easily removed

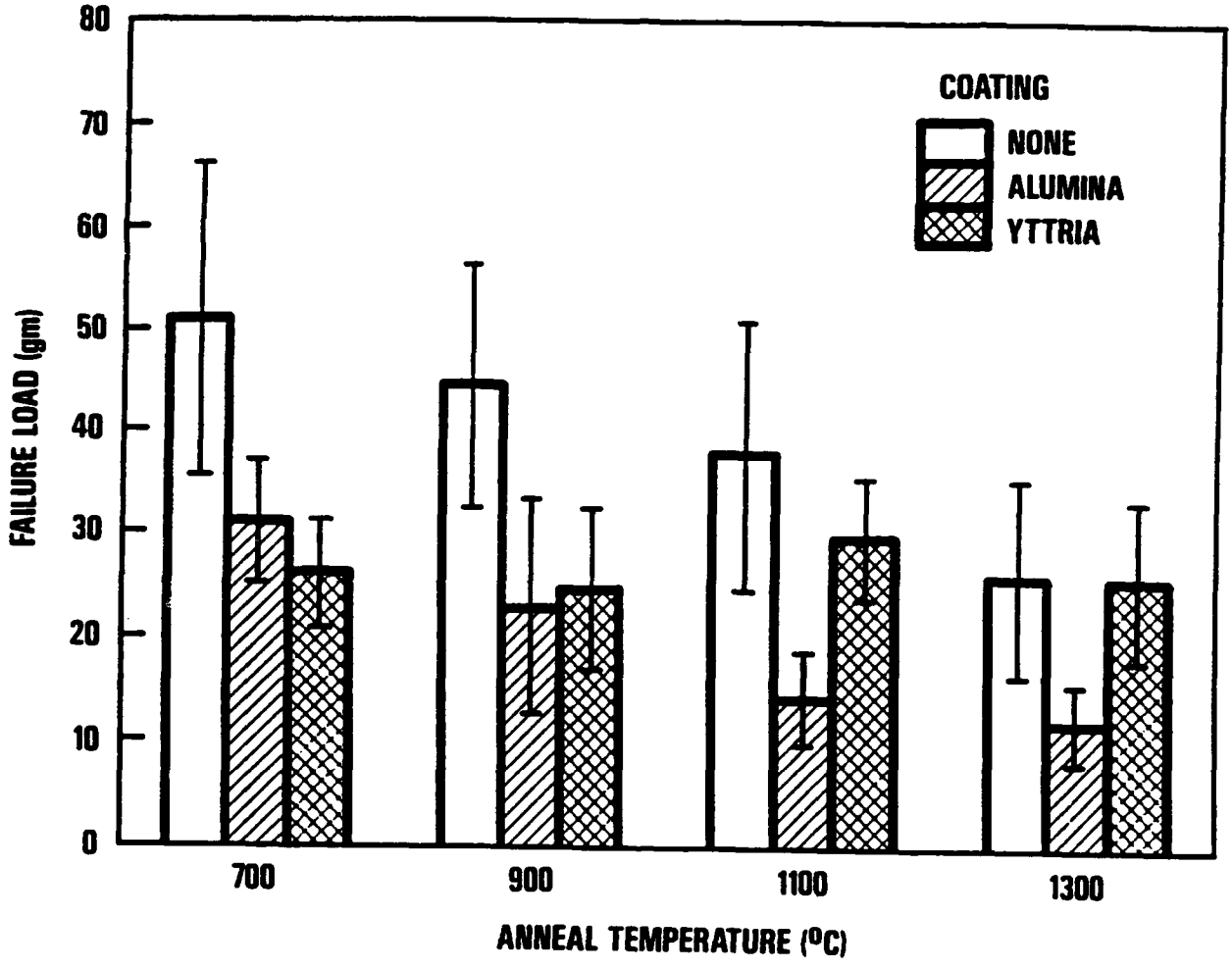


Fig. 8 Tensile strengths of coated and uncoated Nicalon as a function of anneal temperature

by excess bending of the filament. A more adherent coating will be necessary for practical use of filaments coated by this method.

A method for producing zirconia whiskers was discovered while developing the method for coating the SCS-6. If the monofilament is allowed to adsorb water before dip coating and is dried at 500°C, then whiskers grow out from the fiber perpendicular to the axis of the fiber. The water is probably acting as a catalyst and the reaction is probably from the gas phase with growth occurring on the end of the whiskers. Further investigation demonstrated that an alternative of humidifying the oxygen environment of the heating zone to 500°C also caused whisker growth. The whiskers varied in length from 1 to 10 mm and were on the order of 10 to 50 μm in diameter. This process is presently being developed further.

Polymer Precursors

Silicon carbide and silicon nitride coatings were produced from a polysilane polymer precursor. A polysilane resin was dissolved in xylene to produce solutions with polysilane weight percents of 0.1 to 10. The solutions were allowed to reach equilibrium conditions by storage for at least 48 h before use. The desized fiber tows were dipped in the solutions for 20 s and withdrawn at a rate of 1 mm/s. After dip coating, the tows were dried/cured for 5 min at 200°C in the ambient atmosphere. The tows were then calcined to 800°C in nitrogen (for silicon carbide coatings) or ammonia (for silicon nitride coatings). The heating rate was 10°C per minute.

Nicalon, Nextel 480, and FP-PRD-166 were coated with silicon carbide and silicon nitride. The coatings were verified by visual observation of the change in color of the

fibers, by EDAX, and by SEM observation. Figure 9 shows an SEM micrograph of silicon nitride and silicon carbide coatings on FP-PRD-166. The fiber has a grainy structure, making the coating appear rough. The EDAX results show a smooth variation in thickness of the coating with concentration of the solution. SEM analysis indicates the coatings are continuous, although the coating on Nextel was not uniform. The onset of bridging between fibers for tows coated in the small dip coater is ~10 wt % polysilane. The onset occurs at higher weight percents in the continuous coater. EDAX and SEM analyses indicate the coatings are on the order of 0.1 μm. The stoichiometry of the silicon carbide and silicon nitride is nominal based on the functional groups present in this polymer, but Auger analysis needs to be performed to better determine stoichiometry.

The silicon carbide and silicon nitride coatings from polysilane significantly weaken the Nicalon fibers. There is no degradation in strength after drying; thus the weakening occurs during the calcination process. Various weight percents of polysilane resin in xylenes, 0.01 to 10 wt % polysilane, were used for dip coating with no improvement. In an attempt to protect the fiber from a chemical interaction, a tow was precoated with a thin, ~50 Å, coating of yttria before coating with polysilane. The tow still exhibited substantial degradation.

Silicon nitride and silicon carbide coatings were applied from polymer solutions on Nicalon fibers with a CVD BN precoat. Provided the BN coating is thick enough, ~1 μm, considerably less degradation in strength was observed than without the BN coating.

BN coatings obtained by dip coating in a solution of a polymer precursor developed by Dietmar Seyferth (Ref. 28) or dip coating in a solution of a polymer precursor developed at

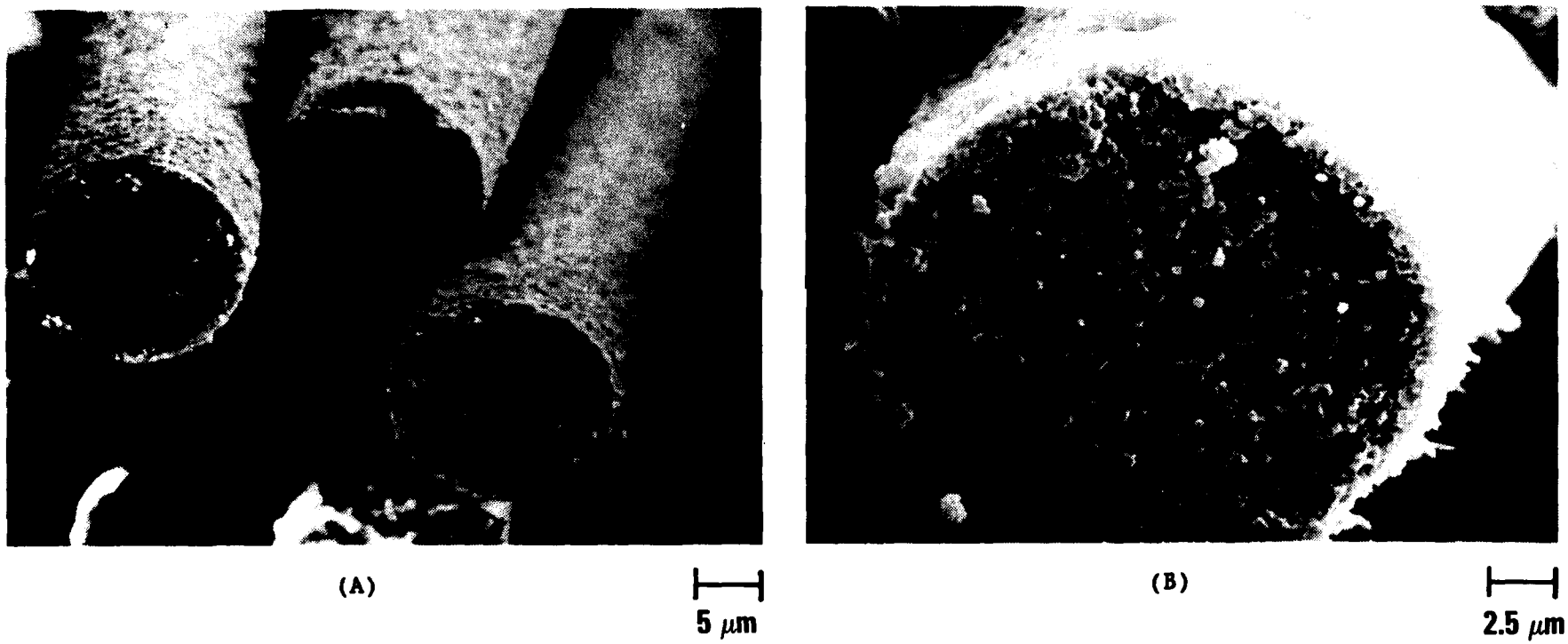


Fig. 9 $Si_3N_4$ and SiC coatings on FP-PRD-166 from a preceramic polymer solution. Panel A is a $Si_3N_4$ coating. Panel B is a SiC coating.

GA have been discontinuous and granular. However, coatings "grown" from a solution of trichloroborazine have been continuous and smooth with little bridging or tracking. The process involves first applying a thin coating of a borazine polymer with free amine groups. The tows were dip coated in a solution of trichloroborazine and the coating formed in-situ by curing with ammonia. The fiber tows were then redipped in the trichloroborazine solution resulting in a reaction between the amine groups and the trichloroborazine. The trichloroborazine monomer becomes bound to the existing coating and the excess coating solution was then rinsed off using pure solvent. The tows were then treated with ammonia to convert the newly bound trichloroborazine to triaminoborazine. Thus, new amine groups were produced and the reaction bonding process can be repeated. Typical coating thickness after three to five reaction bonding cycles are estimated to be 0.1 to 0.2 $\mu$m from SEM micrographs. The principle problem has been that some of the coating is often porous. This appears to be due to volatile removal during the calcination procedure. The problem has been substantially alleviated by removing the volatiles at a slower rate. Another problem encountered with this process is that coating quality has been dependent on the fiber substrate composition. Thus, different coating conditions may be required for different fibers.

Further work on the processes for producing BN coatings yielded improvements in continuity and density. However, the coatings are not as smooth as the oxide coatings. The best results were obtained with the reaction bonding process. This process involves:

1) A thin coating of aminoborazine is prepared by dipping the fibers in a ß-trichloroborazine solution and curing in-situ with ammonia.

2) The tow is then redipped in the ß-trichloroborazine solution, and the free amine groups react with the ß-trichloroborazine.

3) Excess solution is rinsed from the fibers to avoid precipitation of unbound ß-trichloroborazine.

4) The bound aminochloroborazine is converted to aminoborazine by curing with ammonia.

5) Steps 2 through 4 are repeated to increase the thickness.

This process nearly eliminates bridging and tracking. Tensile strengths of Nicalon fibers before and after coating by reaction bonding were measured by individual filament testing. There was a minimal decrease in tensile strength of the coated fibers. Oxidation testing at 1000°C for 24 hours resulted in little or no further degradation of the coated fibers. Coatings produced by in-situ curing instead of reaction bonding result in a large decrease in tensile strength. Samples of BN polymer precursors from Dr. Robert Paine of the University of New Mexico and Dr. Larry Sneddon of the University of Pennsylvania were obtained. Coatings from these polymer precursors were prepared by dip coating. The coatings obtained will be compared with the reaction bonding coatings.

Silicon nitride coatings from polysilane solutions on CVD BN coated Nicalon were produced. SEM micrographs of the silicon nitride on BN-coated Nicalon are shown in Figure 10. The BN coating is approximately 2 $\mu$m thick. The $Si_3N_4$ coating is smooth and uniform with a thickness between 1000 and 2000Å. Thus, the parameters to allow production of silicon nitride coatings by a relatively easy method of dip coating from a preceramic polymer were established.

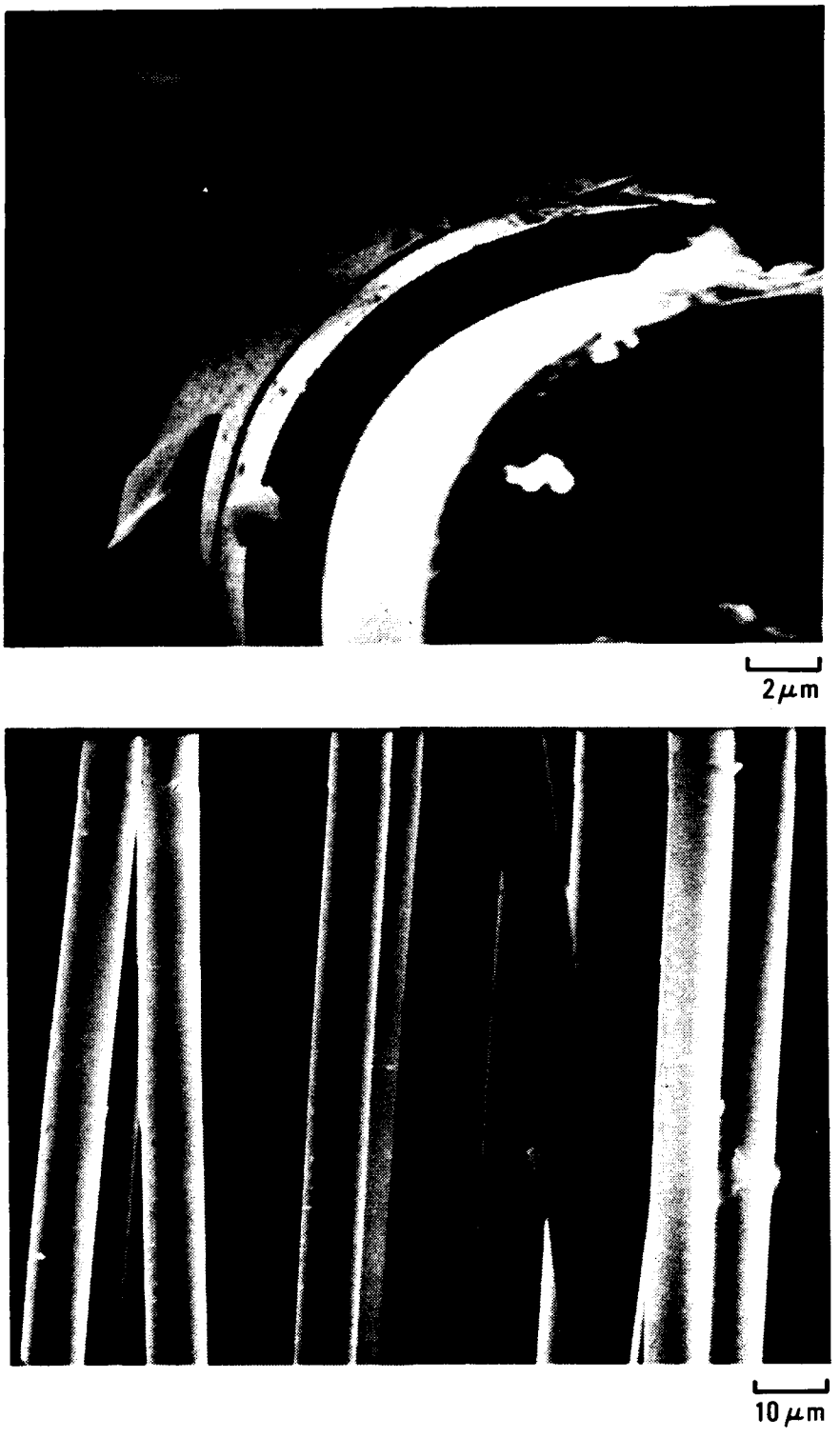


Fig. 10 Scanning electron micrographs of $Si_3N_4$ coating prepared from polysilane polymer precursor on CVD BN coated Nicalon. Top panel (5000X) shows dual nature of coating. Bottom panel 1000X.

## TASK 1-3 GAS-PHASE PROCESS DEVELOPMENT

### Desizing Experiments

Thermal and plasma processes for desizing ceramic tows were examined initially. Auger analysis of three of the thermally desized Nicalon samples showed the presence of carbon still on the surface after a 30 min treatment in hydrogen at 10 torr and 600°C. The level of carbon was however, approximately the same as that of a sample of unsized Nicalon tow. Examination of a control filament with sizing showed a carbon content of 80 atomic % which dropped to approximately 46% after sputter removing approximately 400 Å of material. The thermally desized fibers were tested for strength by measuring the tensile properties and comparing the values with the untreated fibers. Four individual filaments from each desizing test and the control were tested. The average failure load for the desized samples was slightly greater than the as received sample uncorrected for filament diameter.

The plasma desizing process comes from the sputter removal of the sizing material in a glow discharge. The parameters examined in this process were: (1) pressure, (2) power into the glow discharge, and (3) gas composition and flow rate. Three desizing experiments were completed. Evaluation of these plasma desized samples showed the sizing is removed in 30 s, with a 475 W, 0.5 torr, 13.56 MHz, 25 sccm hydrogen plasma.

The sizing of the Nicalon fibers, which is polyvinyl acetate, can be effectively removed from the fibers using a

relatively low energy, $H_2$ plasma. The same is not true, however, for fibers such as Nextel, which have a modified epoxy sizing. At present the only effective means for removing this sizing, which is compatible with PACVD, is to thermally remove it. Several tests in the plasma assisted coater with different plasma energies were unsuccessful at removing the epoxy sizing. A possible solution is to add a small tube furnace to the uppermost section of the continuous coater. Thermal gravimetric analysis of the fibers sized with the epoxy sizing shows that at 500°C the sizing is removed after 5 min. To evaluate this as a solution to the sizing problem a small tube furnace was installed in the continuous fiber coater with external controls to maintain the temperature at 500°C. Desizing can now be accomplished continuously as the fibers pass through the furnace.

PACVD Filament Coatings

Plasma-assisted chemical vapor deposition (PACVD) BN coatings were made from $B_2H_6$ in $H_2$ and $NH_3$ gas precursors. These gases were the principle precursors evaluated. Process parameters examined were: (1) gas composition, (2) gas flow rates, (3) power into the plasma and (4) gas pressure. Preliminary trials examined process parameters reported in the literature with subsequent iterative changes in these parameters. Evaluation of these coatings include: coating thickness, coating uniformity of outer and inner filaments of the tow, deposition rates, coating uniformity along the length of the tow, chemical composition of the coating, and effect of the filament coating on the tensile strength of the tow.

Initial deposition experiments on the PACVD of BN were accomplished. Fibers coated during this initial trial were Nicalon, FP-PRD-166, Nextel 480, and graphite. The

objectives of this initial study were to determine the effective coating zone of the system with respect to uniformity and growth rate of the film, and to determine the operating parameters for the different coatings.

CVD Fiber Coating

The chemical composition of BN depends on the $NH_3$ to $B_2H_6$ ratio in the reactants, and the deposited films are a mixture of B and BN. Adams and Capio (Ref. 29) report a boron to nitrogen ratio of six for films deposited at 340°C with $NH_3$ to $B_2H_6$ ratio greater than 0.5. They also report that the films appear to have a composition of approximately $B_6NH_x$, where x has a strong dependence on deposition temperature.

A series of experiments was performed where the deposition temperature was varied between 500°C and 900°C and the $NH_3$ to $B_2H_6$ ratio was varied from 5 to 50. Scanning Auger depth profiles of some of the BN coated Nicalon fibers were obtained by Dr. John Brennan at UTRC. Coatings deposited at 550°C resulted in a quite stoichiometric BN with very little C and 0 contamination as shown in Figure 11. The coatings deposited at 750°C exhibited good stoichiometry with low oxygen but contained a lot of carbon, Figure 12. BN coatings were successfully deposited on Nicalon, HPZ, Nextel 480, and FP-PRD-166 fibers. Figure 13 shows a ~0.2 $\mu$m thick BN coating on a HPZ fiber deposited at 900°C.

The deposition temperature affects the B:N ratio in the film. BN deposited at 500°C was richer in boron (B:N ratio 2.5:1) than films deposited at higher temperatures. At 900°C the B:N ratio was 1.2:1. Our observation agrees with that reported by Murarka, et al. (Ref. 30) where a similar trend was observed. The two curves are superimposed in Fig. 14.

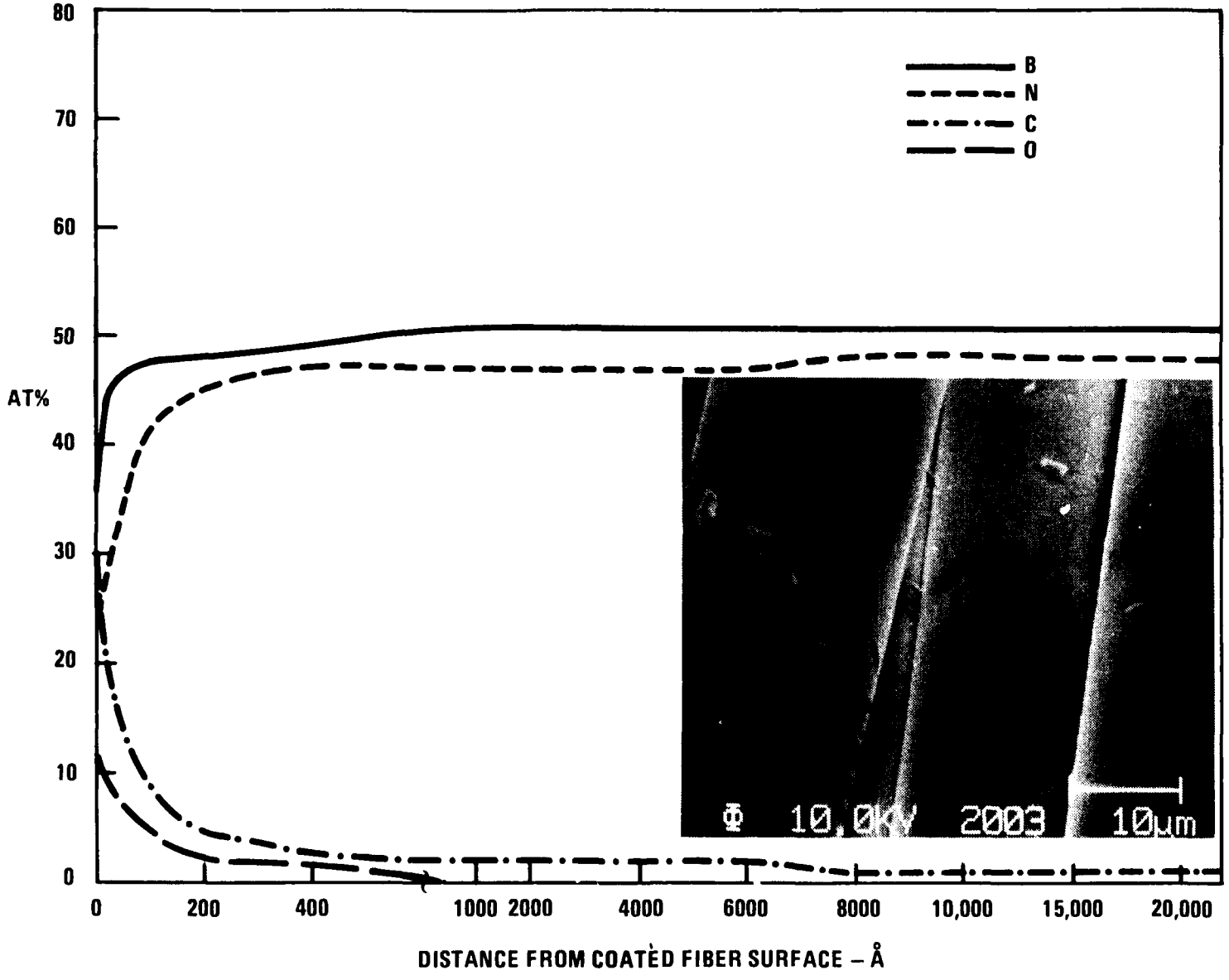


Fig. 11 Auger depth profile of BN coated Nicalon deposited from diborane and ammonia at 550°C (from J. Brennan, UTRC).

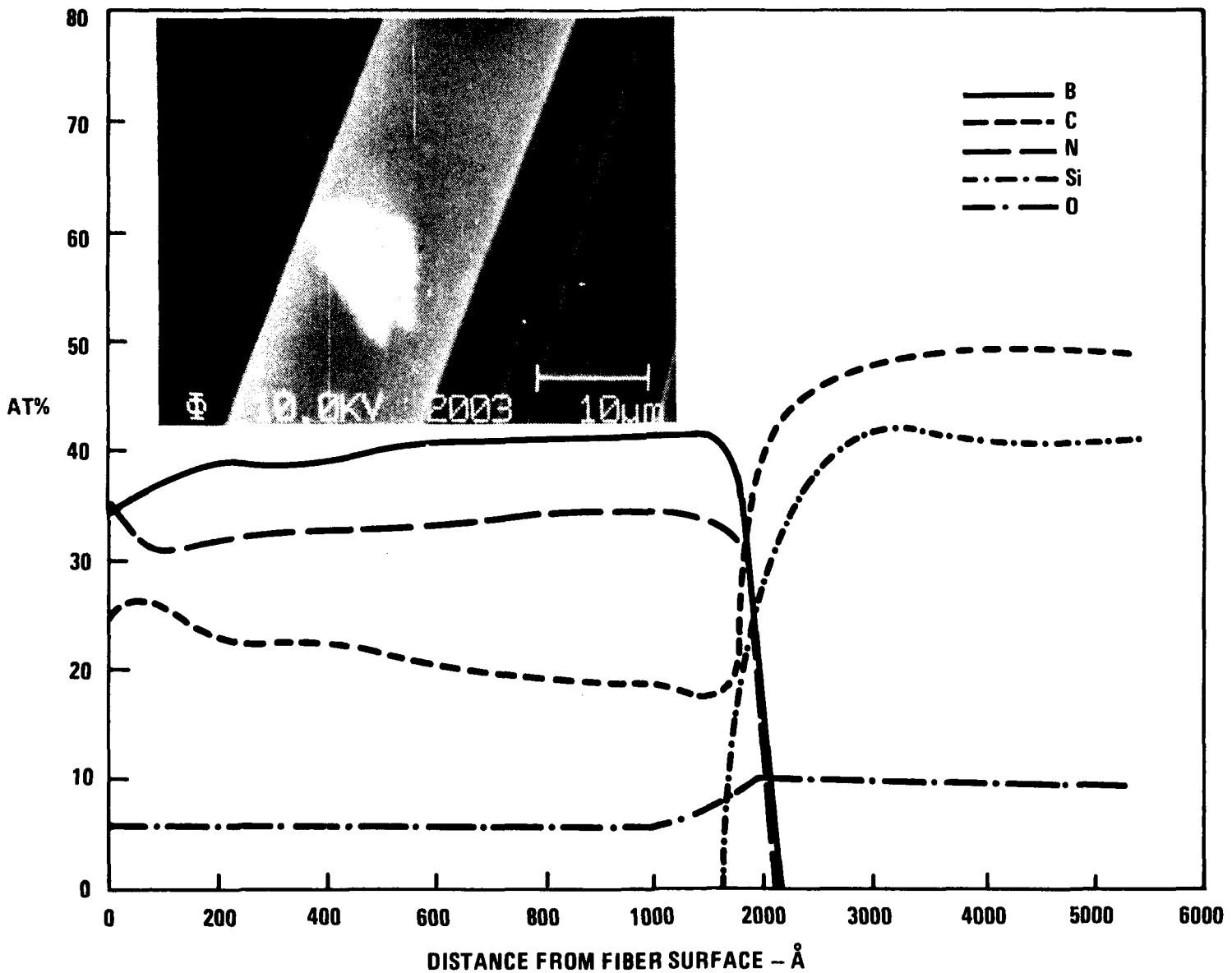


Fig. 12 Auger depth profile of BN coated Nicalon deposited from diborane and ammonia at 750°C (from J. Brennan, UTRC).


Fig. 13 Chemical vapor deposition coating of BN on HPZ fiber produced at 900°C

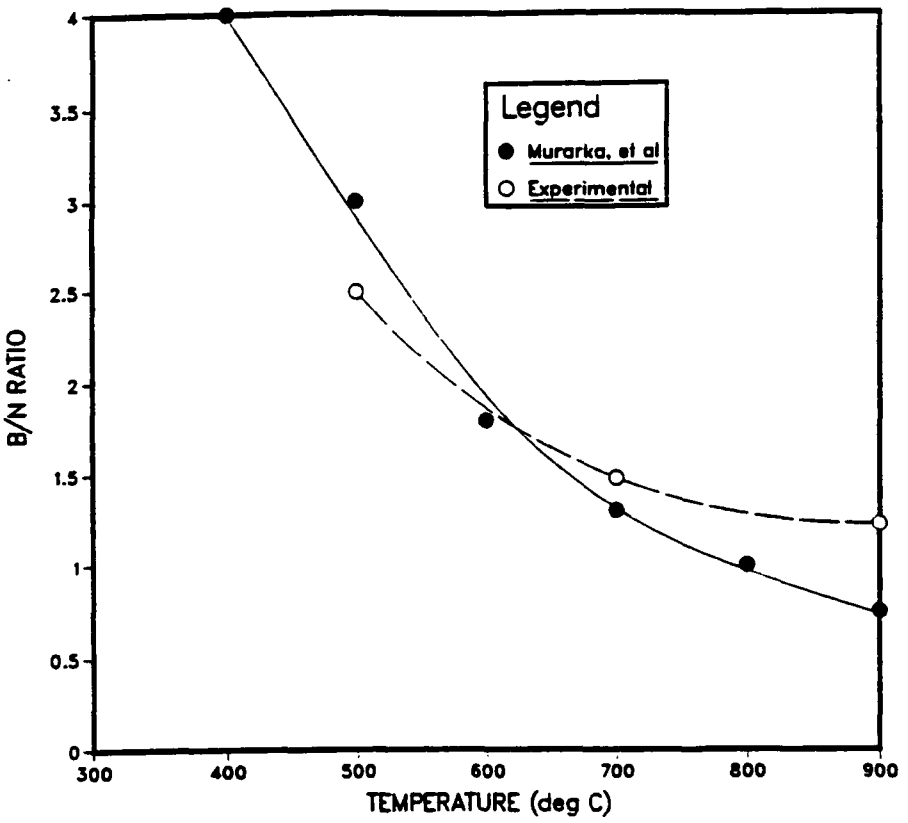


Fig. 14 Ratio of boron to nitrogen as a function of temperature

The deposition temperature also affects the growth rate of the film. The growth rate determined for BN films deposited on Nicalon and carbon fibers increased as the deposition temperature increased from 500°C to a maximum at 700°C then dropped off again at 900°C.

In the previously referenced work by Murarka (Ref. 30), they published results which showed a deposition rate dependence on the ratio of reactants in the feed stream. When growth rate for our deposited films is plotted against the ratio of reactants, the same shape of curve is obtained as presented by Murarka, but displaced due to different flow rates and temperatures. The two curves are plotted in Fig. 15.

Although the mechanism is not yet understood there appears to be a substrate dependence on the initial film growth, or nucleation. One hypothesis is that the nucleation phase involves the formation of $B_2O_3$ for those substrates which have oxygen absorbed on the surface.

The strengths of the Nicalon filaments coated with BN from the $B_2H_6$ + $NH_3$ reaction were compared to the as-received filaments and the heat-cleaned filaments. The results are summarized in Table 3 and show that there is no significant loss of strength resulting from the deposition process.

Silicon carbide coatings were made on Nicalon, HPZ, and FP-PRD-166 fibers. Auger analyses of these first coatings show a carbon-rich coating. These deposits were made at a $H_2$:$CH_3SiCl_3$ ratio of 5:1, chamber pressure of 1.0 torr and deposition temperature of 1000°C.

Pressure , reactant gas ratio and temperature were varied

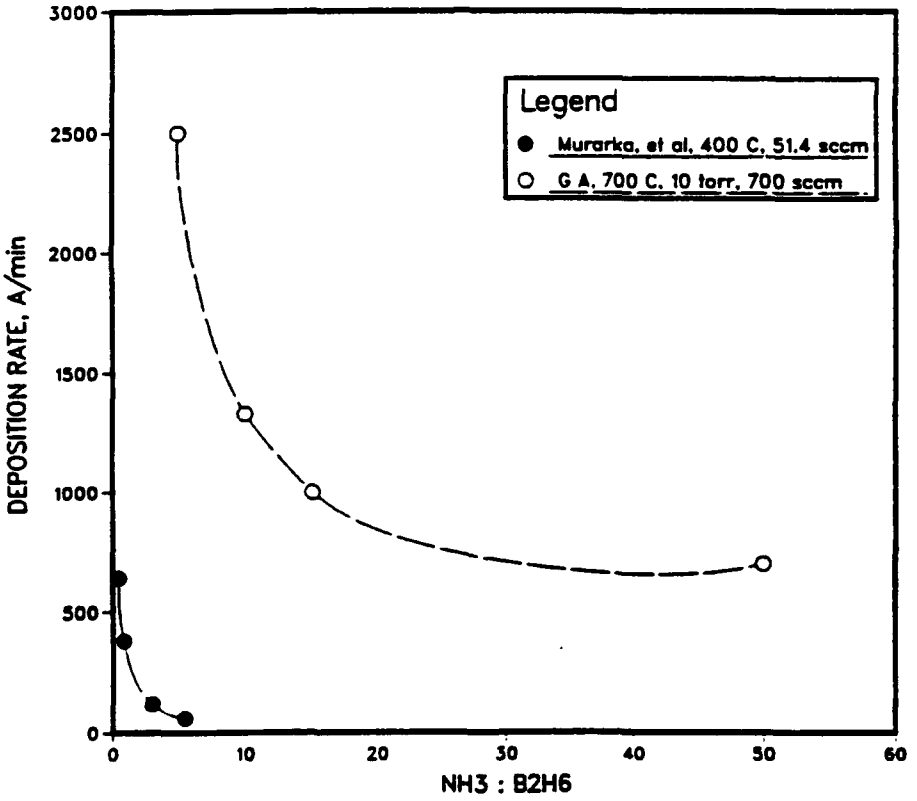


Fig. 15 Deposition rate dependence on ratio of reactants

Table 3
BN DEPOSITION CONDITIONS AND FAILURE LOAD FOR INDIVIDUAL FILAMENTS

| ID | Substrate | Reactants | Temperature (°C) | Pressure (torr) | Time (min) | Flow (sccm/min) | Ratio B:N | Failure Load (g) |
|---|---|---|---|---|---|---|---|---|
| 10193-17 | Nicalon | $B_2H_6/NH_3$ | 500 | 10 | 5.0 | 650 | 5:1 | 31.4 |
| 10193-18 | Nicalon | $B_2H_6/NH_3$ | 700 | 10 | 5.0 | 650 | 5:1 | 49.9 |
| 10193-19 | Nicalon | $B_2H_6/NH_3$ | 900 | 16 | 5.0 | 650 | 5:1 | 50.0 |
| 10193-20 | Nicalon | $B_2H_6/NH_3$ | 700 | 10 | 10.0 | 320 | 15:1 | 51.0 |
| 10193-22 | Nicalon | $B_2H_6/NH_3$ | 500 | 10 | 10.0 | 320 | 15:1 | 47.7 |
| 10193-23 | Nicalon | $B_2H_6/NH_3$ | 700 | 10 | 10.0 | 670 | 50:1 | -- |
| 10193-24 | Nicalon | $B_2H_6/NH_3$ | 900 | 30 | 10.0 | 1340 | 10:1 | 46.7 |
| 10193-26 | Nicalon | $B_2H_6/NH_3$ | 700 | 10 | 7.5 | 800 | 10:1 | 45.8 |
| 10193-28 | Nicalon | $B_2H_6/NH_3$ | 900 | 10 | 7.5 | 800 | 10:1 | 48.7 |

in a systematic manner to optimize coating rate and stoichiometry. A dual coating of BN and SiC was deposited on Nicalon cloth and displayed in Fig. 16. A smooth continuous coating was obtained with a high degree of uniformity. The SEM micrograph does not show the dual nature of the coating due to lack of contrast between the BN and SiC.

Boron nitride was successfully deposited continuously on Nicalon tow. The $B_2H_6$ + $NH_3$ chemistry, a deposition temperature of 1000°C, and a system pressure of ~1.0 torr were used. The fiber speed through the 40 cm coating zone was 7.5 cm per minute. The coater was run continuously for 12 h, producing about 55 m of coated tow.

The coated fiber is visibly different from the uncoated fibers; the fibers exhibit optical interference patterns on the surface under ordinary white light. The colors range from green to red. For these interference patterns to develop, the film thickness must be at least $\lambda/4\ \mu$ (where $\mu$ is the index of refraction of the film). Assuming $\mu$ ~2 indicates the coating is on the order of 1000 Å. We should be able to take advantage of the optical properties of very thin films to control the film thickness while coating continuously.

The coatings were successfully resolved on the new Cambridge 360 SEM recently acquired by General Atomics. The thickness of these coatings as viewed with the SEM appears to be on the order of 1500 Å. This thickness agrees with the presumed thickness based on light interference.

Further studies of BN coating parameters on Nicalon were studied in the 5 cm coater. Deposition conditions for the $B_2H_6$

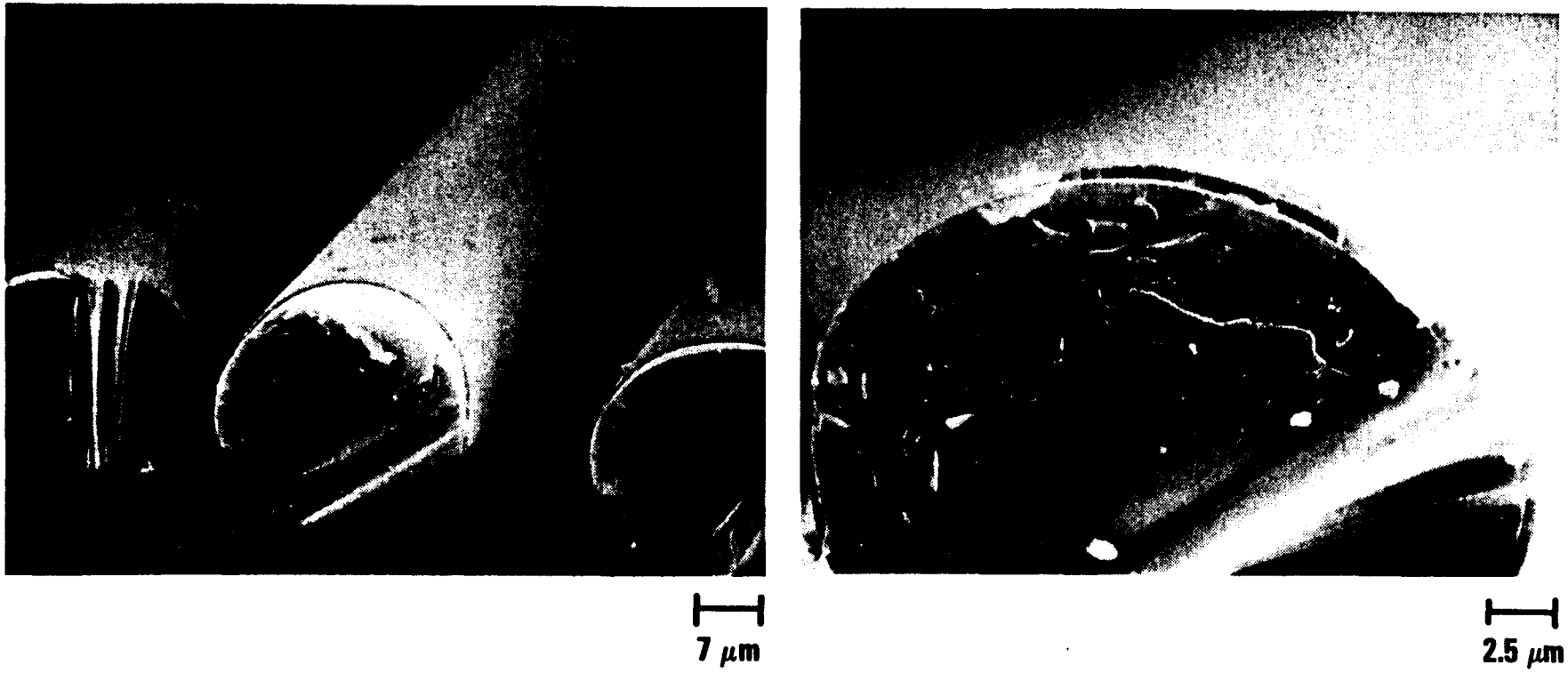


Fig. 16 Dual coating of CVD BN and SiC on Nicalon cloth

+ $NH_3$ reaction were: substrate temperature between 500°C and 550°C, coater pressure 3 to 5 torr, and a $NH_3$ to $B_2H_6$ ratio of 10.

A second set of conditions were: substrate temperature 1000°C, coater pressure 10 torr and a $NH_3$ to $B_2H_6$ ratio of 10.

Under the same coating conditions, boron nitride was also successfully deposited on HPZ (Dow Corning) ceramic fiber with mixed results. The boron nitride coating deposits onto the HPZ with good penetration into the tow and good adherence to the fiber. However, the chemical conditions inside the coater appear to embrittle the fibers.

Samples of the statically coated Nicalon and HPZ fibers were supplied to Dr. John Brennan at United Technologies Research Center for evaluation. He performed TEM, EDS, and scanning Auger analysis in addition to preparing an LAS matrix composite with BN coated Nicalon fabric.

TEM data for BN coatings on Nicalon deposited at 500° and 1000°C are shown in Figures 17 and 18, respectively. It is apparent that the 500°C coating is totally amorphous, while the 1000°C coating does contain some structure and could be considered to be microcrystalline. The electron diffraction pattern of the 1000°C coating shows a distinct ring structure of hexagonal BN. The EDS data for the two coatings distinctly show a higher B and O content for the 1000° coating than the 500°C coating, which is exactly what was found previously from scanning Auger analysis.

The optical micrographs and TEM replica of a LAS composite (#237-90) are shown in Figures 19 and 20, respectively. The BN coating thickness on the Nicalon fabric

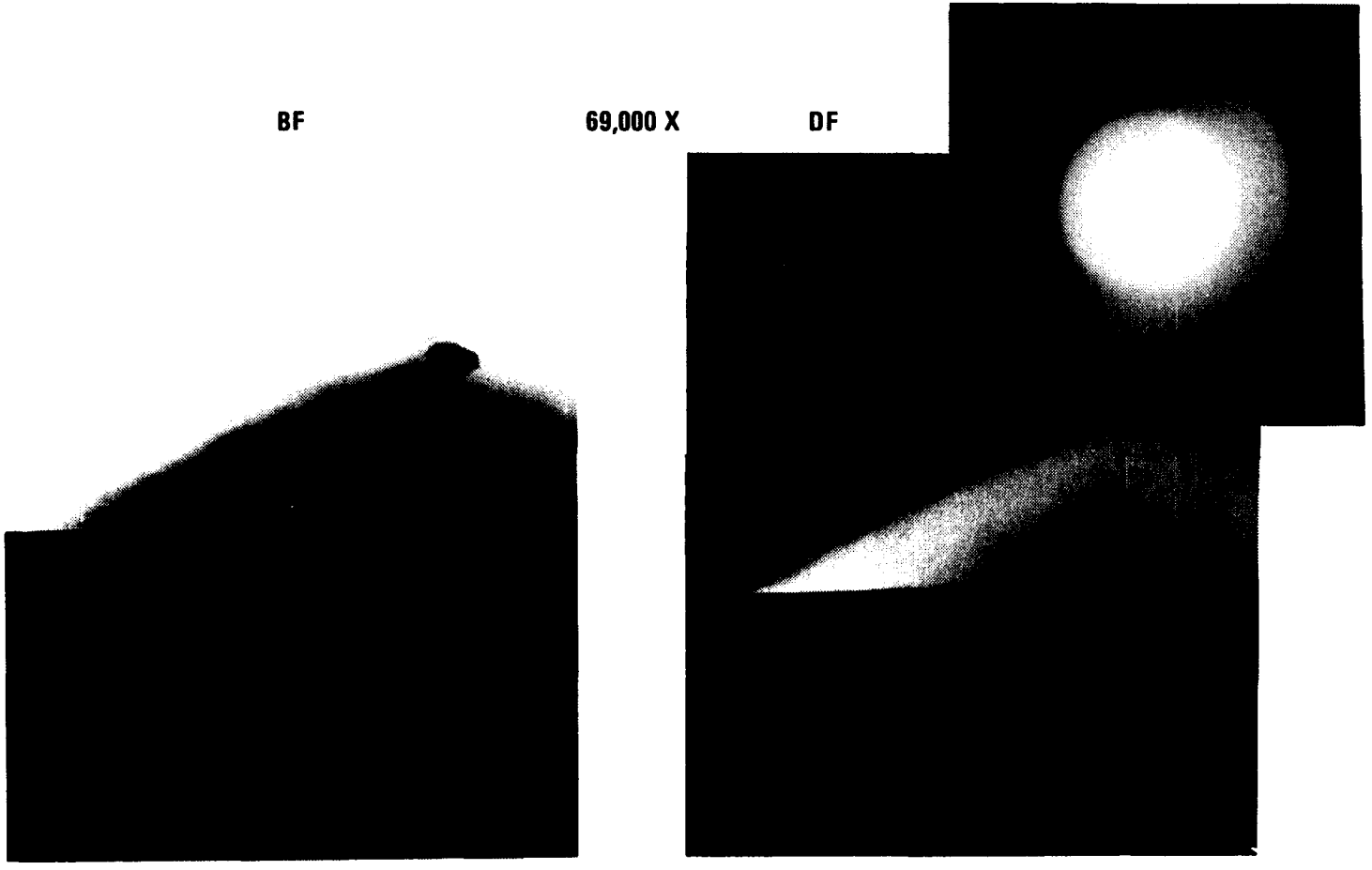


Fig. 17 Bright field and dark field transmission electron micrographs of BN coating on Nicalon deposited at 500°C. Insert shows electron diffraction pattern. (from J. Brennan, UTRC)

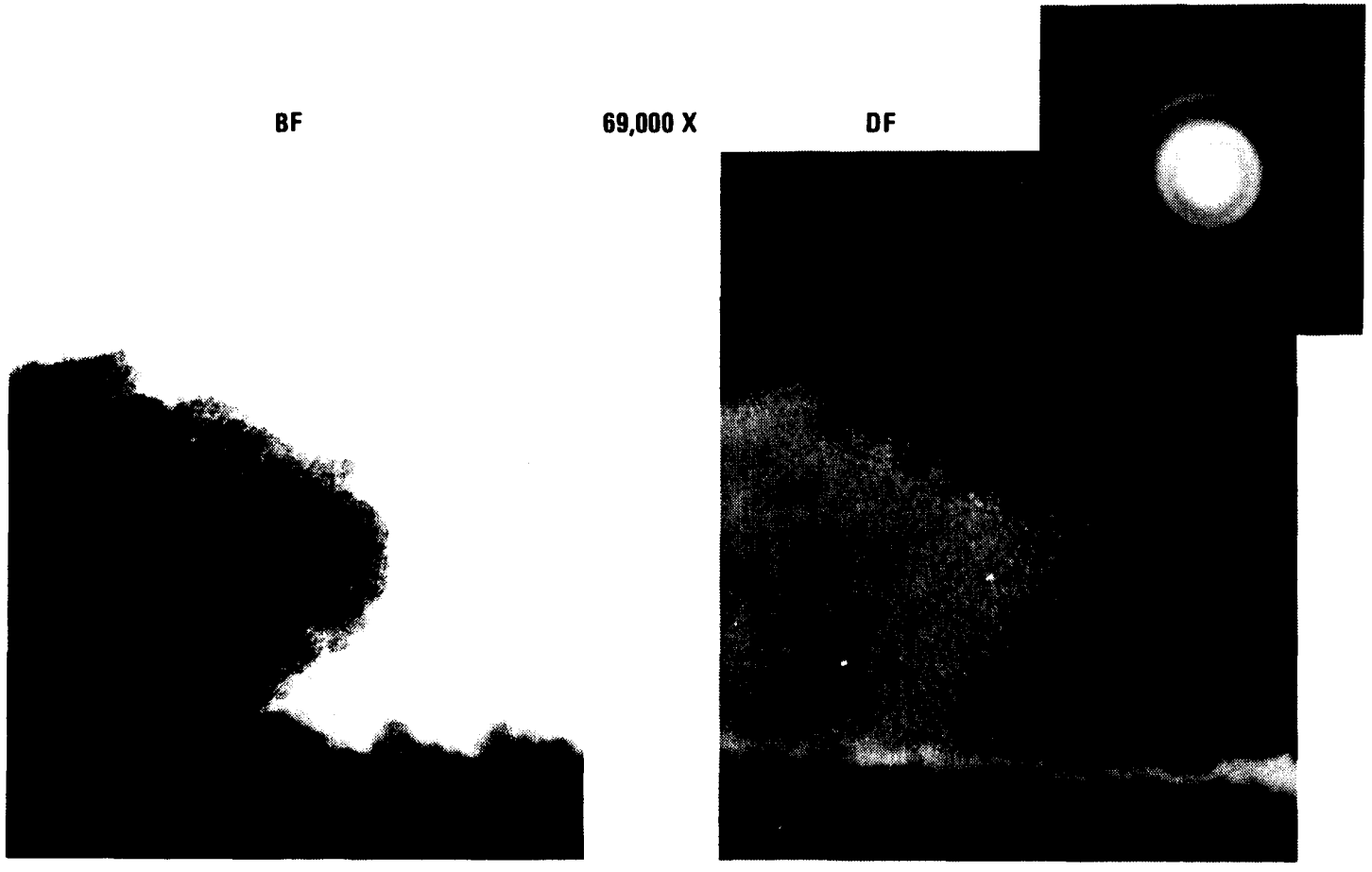


Fig. 18 Bright field and dark field transmission electron micrographs of BN coating on Nicalon deposited at 1000°C. Insert shows electron diffraction pattern. (from J. Brennan, UTRC)

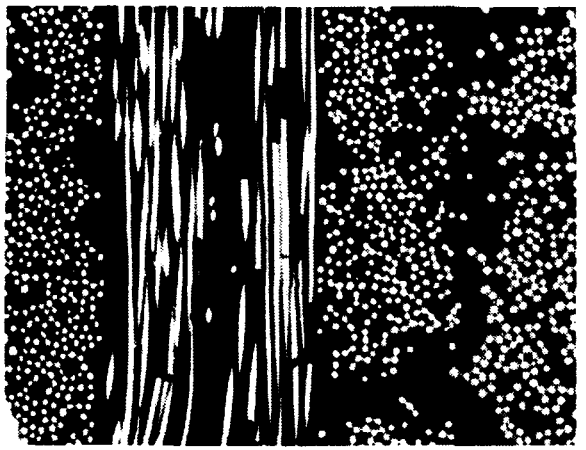


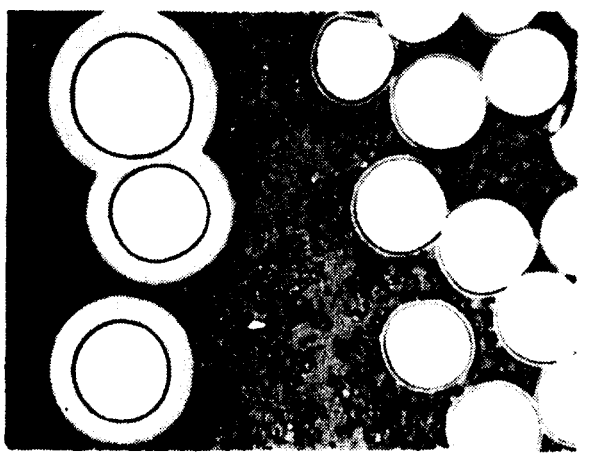


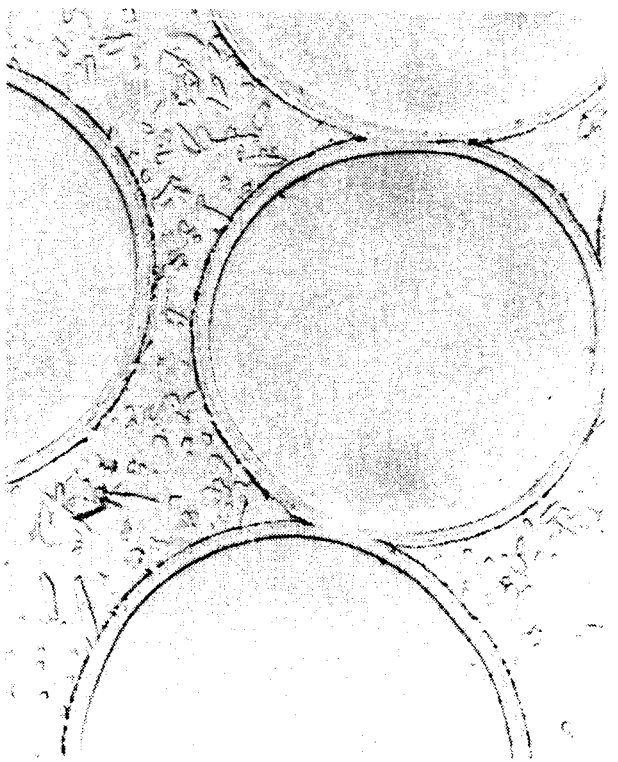


Fig. 19 Optical micrograph of LAS/BN coated Nicalon fiber composite. Coating temperature 550°C. Hot pressed at 1350°C, 13.8 Mpa. (from J. Brennan, UTRC)

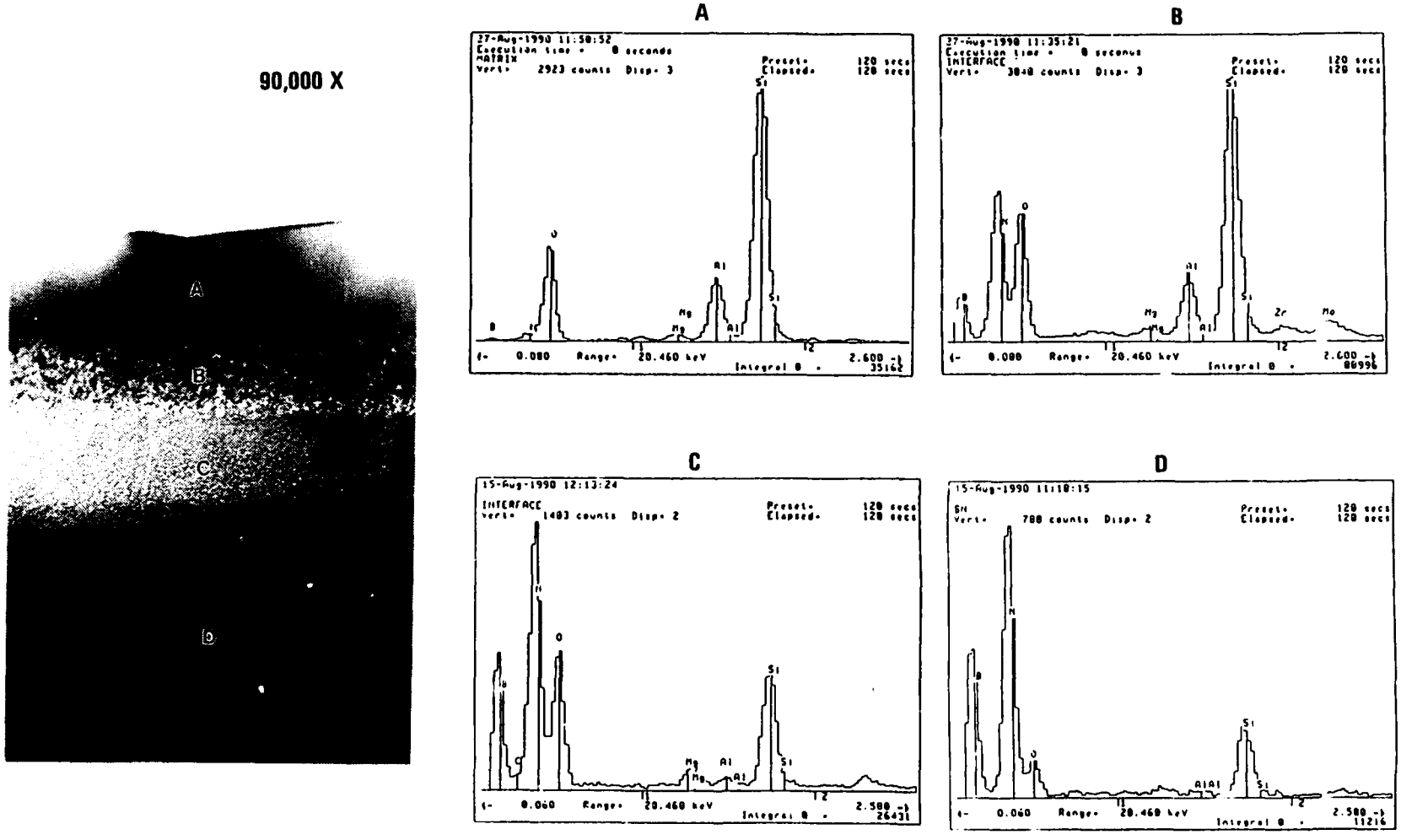


Fig. 20 TEM/EDX thin foil analysis of LAS/BN interface of composite shown in Figure 8.
(from J. Brennan, UTRC)

varies from ~4 μm to <0.1 μm.

The TEM replica of a relatively thick (~1 μm) BN coated region indicates at least two different structures are present in the BN layers. The TEM thin foil taken from a rather thick BN coating at the BN/LAS matrix interface shows that the BN layer (B) next to the matrix (A) has become quite crystalline (hexagonal BN) as a result of composite processing (1350°C), with the next layer (C) becoming coarser in structure compared to the bulk of the BN coating (D). The EDX data taken from the three BN regions show that region B contains a considerable amount of Si, O, and diffusion from the matrix (also slight Mg), while region C contains lesser amounts of these elements and region D contains only Si and O in small amounts. Carbon, which is also present in the BN layer, cannot be picked up by EDX in the presence of Si.

This particular composite exhibited a 3-point flexural strength of 200 Mpa. At 900°C the strength of a ceramed (matrix crystallized) composite was about 190 Mpa, while at 1100°C it was 270 Mpa.

The scanning Auger depth profile of a fiber surface and a matrix trough on a longitudinal fracture surface of this composite is shown in Figure 21. It is apparent that the BN coating of ~14,000Å in thickness stays on the matrix trough when the sample fractures. The points to note from this data are that, as was seen from the TEM results, Si, Al and O are diffusing into the BN from the matrix perhaps contributing to the crystallization of the BN. The C is diffusing into the BN from the fiber, and both B and N are diffusing into the Nicalon fiber from the BN coating to a depth of ~1000Å. Some B is diffusing into the LAS matrix, and no distinct carbon

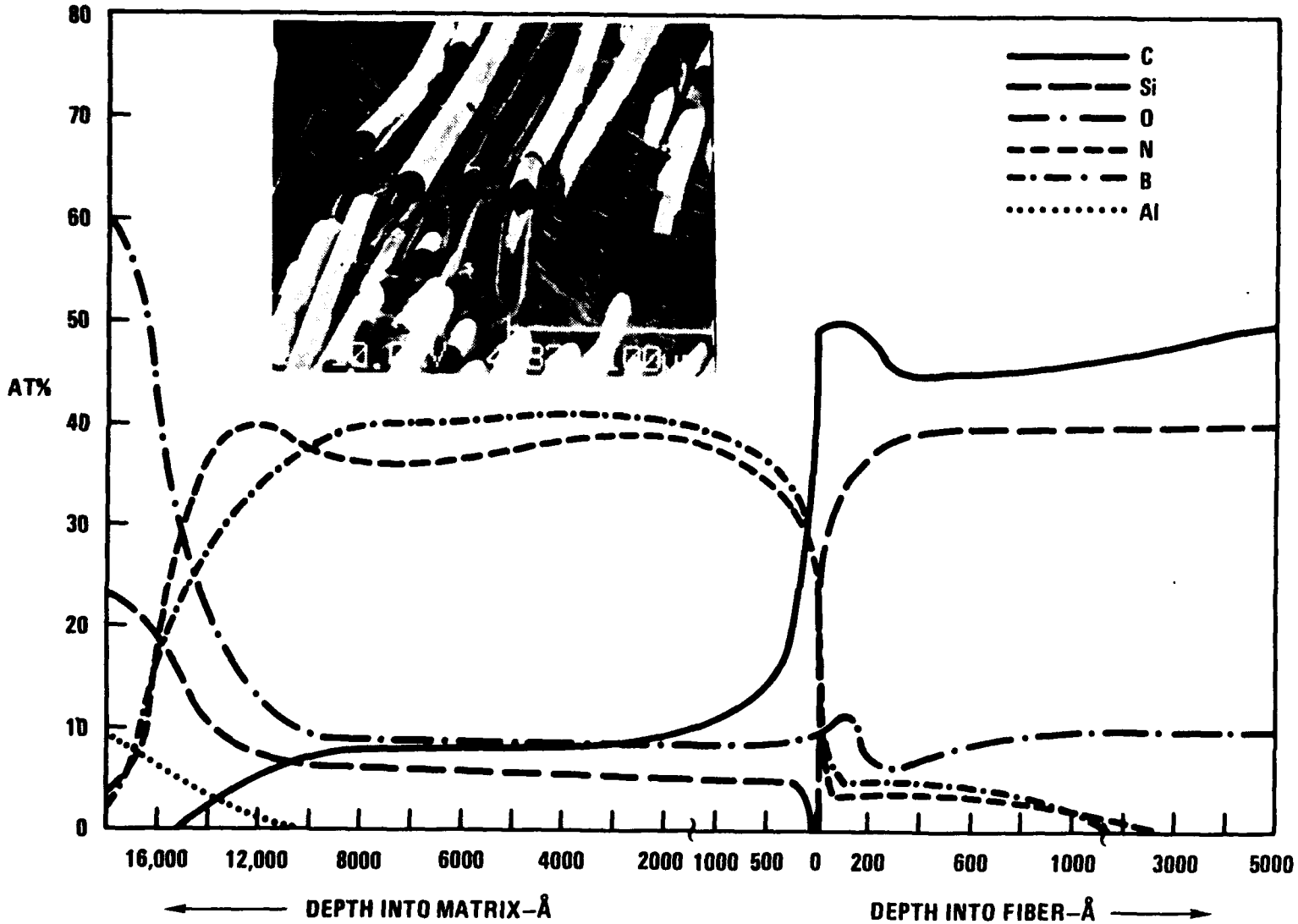


Fig. 21 Scanning Auger depth profile of LAS/BN interface of composite shown in Figures 19 and 20. (from J. Brennan, UTRC)

layer has formed at the BN/NICALON fiber surface. The latter observation is important for the oxidative stability of the composite.

The scanning Auger depth profile of the BN coated HPZ fiber sample is displayed in Figure 22. The coating is relatively smooth with a uniform composition throughout the entire thickness of ~5000Å. A relatively stoichiometric B/N ratio and fairly small amounts of C and O impurities are apparent. The measured tensile strength of the BN coated HPZ fibers was only 760 ± 400 Mpa.

CVD Fabric Coating

Another effort in this area involved coating trials on Nicalon fabric by conventional chemical vapor deposition methods. Experiments were designed to coat uniformly both in area and in thickness a single layer of fabric.

A number of configurations to deliver the reactant gases were designed and tested. The two major problems encountered involved nonuniform coatings and cracking of the reactant gases prior to deposition which led to "sooty" coatings. The problem of nonuniform coatings was minimized by reconfiguring the gas inlet path and adjusting the flow rates of reactants. The problem of "sooty" coatings was minimized by preventing the reactant gases from encountering hot surfaces prior to the surface intended for coating. Also, adjustments of flow rates and gas concentrations were necessary. Coatings produced were BN and dual coatings of BN and SiC.

Equilibrium Calculations

A theoretical examination of the gas flow profiles and equilibrium conditions in the continuous fiber coater was

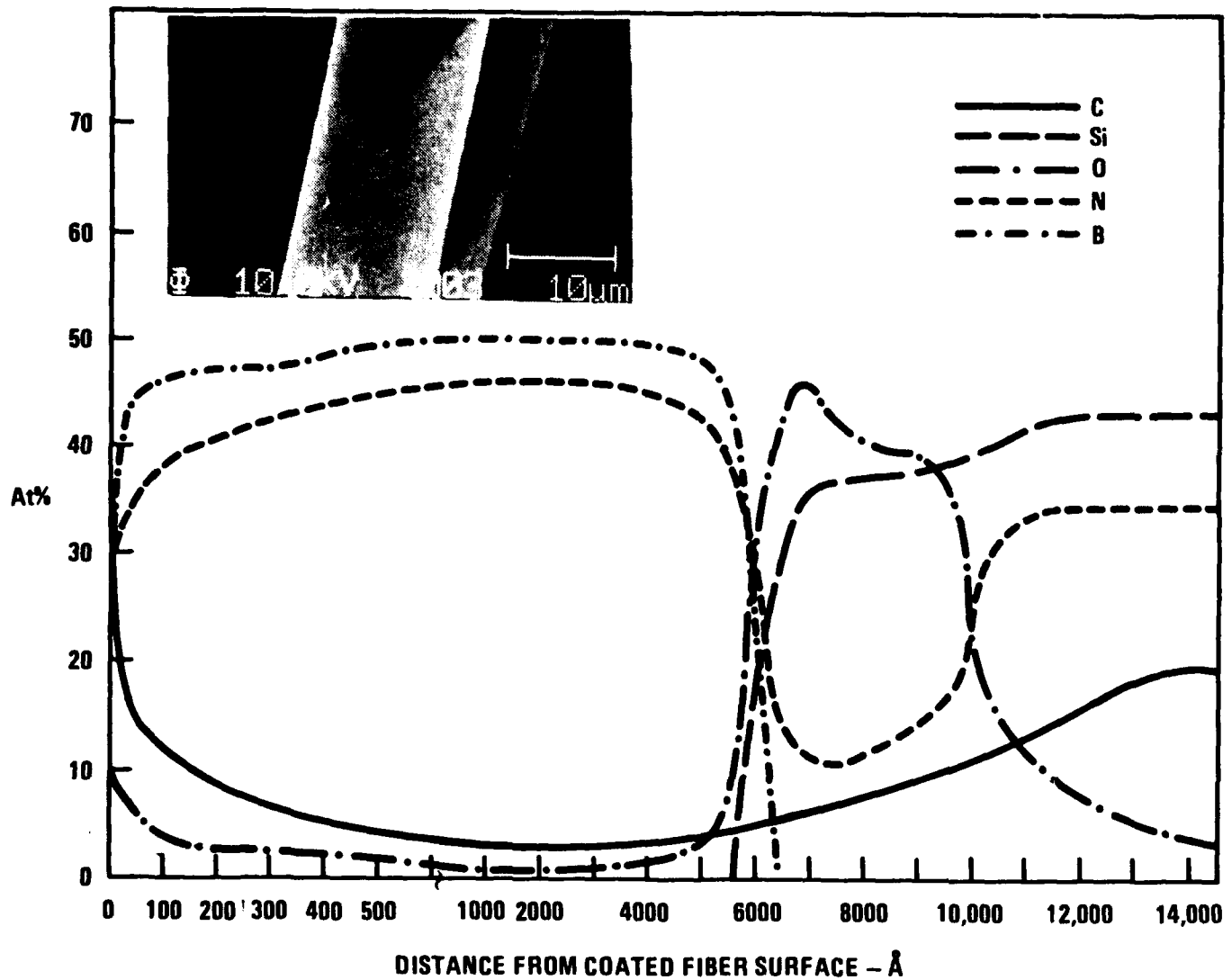


Fig. 22 Scanning Auger depth profile of BN coated HPZ fiber. (from J. Brennan, UTRC)

performed with the help of Professor Middleman at the University of California, San Diego.

Equilibrium calculations were carried out for three CVD systems:

1. $(BCl_3, NH_3, H_2) = (BN, NH_4, Cl)$

   The boron trichloride/ammonia system yields boron nitride films and an undesired deposition of ammonium chloride. The presence of hydrogen has a minor effect on the appearance of trace compounds in the gas phase.

   The stoichiometry is expected to be

   $$BCl_3 + 2NH_3 = BN + NH_4Cl + 2HCl \qquad (18)$$

   This predicts that the ratio of the moles of ammonium chloride deposited to the input moles of nitrogen (as ammonia) is 0.5. Below ~200°C the equilibrium follows the simple stoichiometry given above. Above 200°C, this critical temperature depends upon pressure, ammonium chloride is not deposited, and nitrogen and additional HCl appear in the gas phase.

2. $(SiCl_4, NH_3, H_2) = (Si_3N_4, NH_4Cl)$

   The silicon tetrachloride/ammonia system yields silicon nitride and ammonium chloride films. The feed gas flows

specified correspond to the following stoichiometry:

$$SiCl_4 + 4.42\ NH_3 + 8.85\ H_2 = 0.33\ Si_3N_4 + 3.1\ NH_4Cl + 9.28\ H_2 \quad (19)$$

If this stoichiometry were followed we would find 3.1/4.42 = 0.70 moles of ammonium chloride per input mole of nitrogen (as atomic N), and 0.33 moles of silicon nitride per input mole of silicon tetrachloride.

Figure 23 shows that the ammonium chloride remains slightly above stoichiometric with respect to Eq. 19 until some critical temperature above which there is no longer any ammonium chloride deposition. At higher temperature HCl appears in significant amounts in the gas phase.

The silicon nitride deposition is always below the expected 0.33 moles per mole of $SiCl_4$ because the reaction of $SiCl_4$ is incomplete. The efficiency of conversion of the chloride to the nitride film ranges from 0.92 to 0.67.

3. $(B_2H_6, NH_3, H_2) = (BN)$

The diborane/ammonia system yields boron nitride film over the entire range of temperature (500 <T< 700°C) and pressures (10 < P < 50 torr) studied. The feed gas

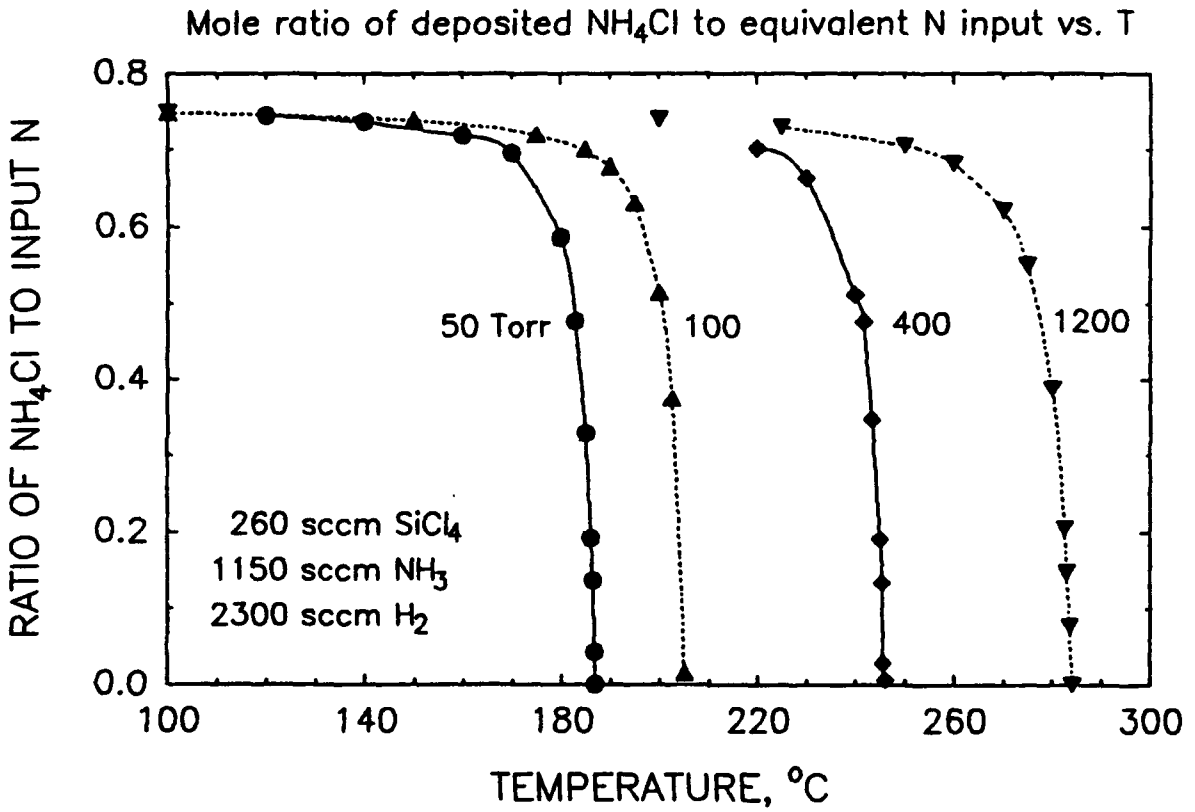


Fig. 23 *Effect of feed gas ratio and system pressure on deposition of silicon nitride and ammonium chloride*

specified, and the expected stoichiometry, was

$$B_2H_6 + 10NH_3 + 15.8\ H_2 = 2BN + 4N_2 + 33.8\ H_2 \qquad (20)$$

Except for trace amounts of unreacted ammonia the equilibrium results are consistent with this stoichiometry. The efficiency of conversion of diborane to boron nitride is 100%.

Boron-rich films have been reported in the laboratory. Such results cannot be predicted by an equilibrium analysis. There is no other boron compound of significance formed from this feed, at equilibrium. It is possible that the kinetics of this reaction could lead to an intermediate boron species that deposits under nonequilibrium conditions at a rate comparable to the boron nitride deposition. Alternatively it is possible that boron deposits directly by a surface reaction of diborane:

$$B_2H_6 = 2B + 3H_2 \qquad (21)$$

Such a speculation has been offered by Murarka, et al. (Ref. 30) but without any supporting evidence.

There is a possibility of oxygen intrusion into reactors used for growth of solid films by chemical vapor deposition.

Because oxygen has the potential to react with precursor gases, its presence could exert a significant influence on film growth. A study of the effect of oxygen on equilibrium in several CVD systems has been carried out.

Boron Nitride from Boron Trichloride and Ammonia

We study the following gas mixture:

$$BCl_3 + 2NH_3 + 4H_2 + xO_2$$

which yields the following solid films:

$$BN,\ B_2O_3,\ NH_4Cl$$

The results are similar to the previous results in the absence of oxygen. The temperature above which no ammonium chloride is formed is a function of reactor pressure, and has not changed significantly because of the presence of oxygen.

The major change is in the increased efficiency of conversion of ammonia to ammonium chloride - about 75% at 5% oxygen, compared to 50% in the absence of oxygen.

Figure 24 shows the fraction of solid films formed from the feed gas as a function of oxygen in the range of 0% to 5% oxygen. The presence of oxygen leads to the removal of some boron as boron oxide. This frees ammonia, making more of it available for production of ammonium chloride. This removes nitrogen from the system and leads to reduced deposition of boron nitride.

These results are essentially independent of temperature and pressure in the range studied.

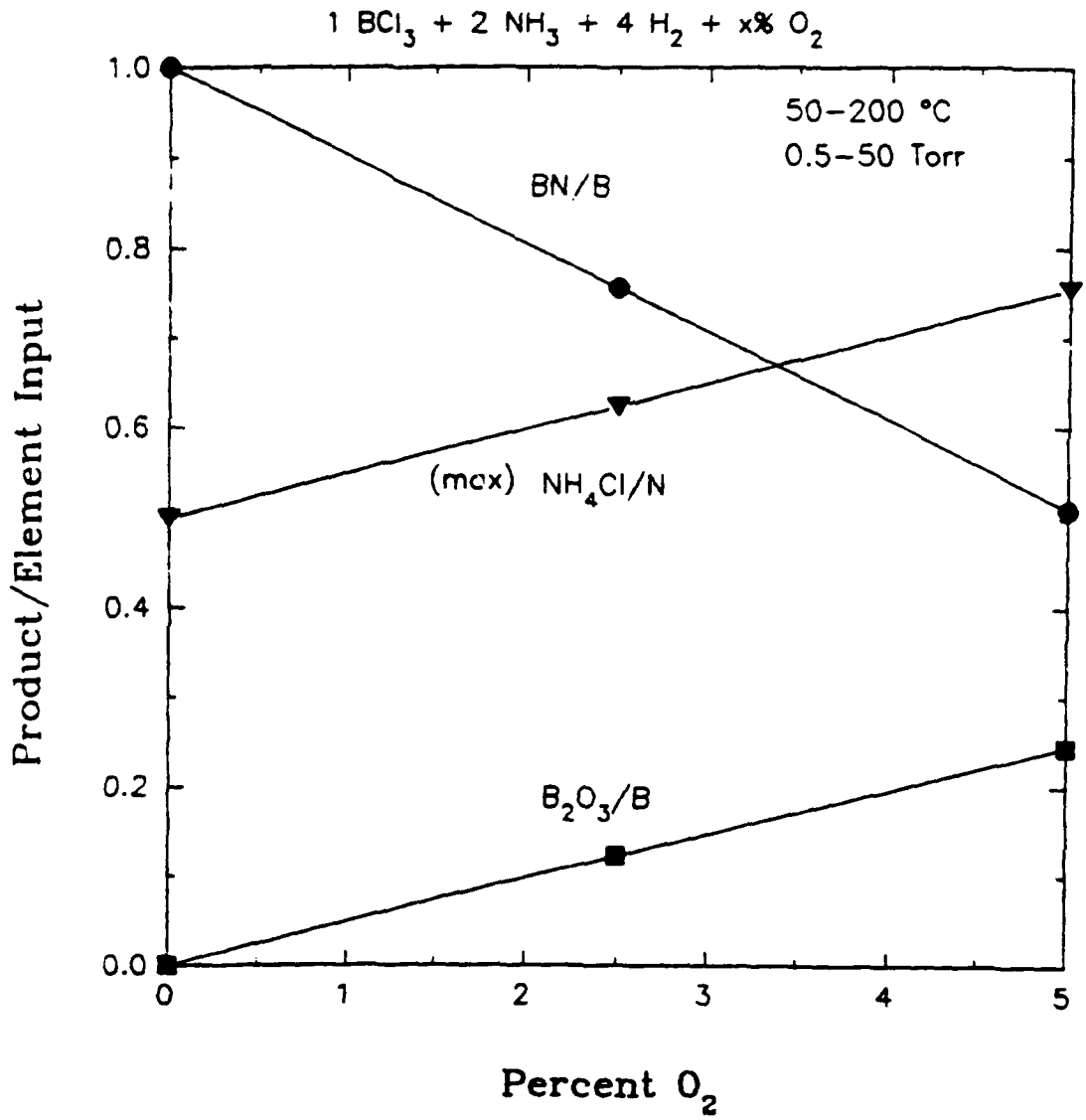


Fig. 24 Effect of oxygen on the deposition of boron nitride from $BCl_3$ and $NH_3$

Boron Nitride from Diborane

We study the following gas mixture:

$$B_2H_6 + 10NH_3 + 15.8\ H_2 + xO_2$$

which yields boron nitride solid and $B_2O_3$ as a liquid film, since the crystal to liquid transition occurs at 450°C.

Figure 25 shows the ratio of solid film to the input elemental boron concentration. As oxygen increases, boron oxide is produced. This removes boron from the system making it unavailable for boron nitride production. Above 5% oxygen practically no boron nitride is produced.

These results are nearly independent of temperature and pressure in the range studied.

Silicon Nitride from Silicon Tetrachloride and Ammonia

We study the following gas mixture;

$$SiCl_4 + 4.42\ NH_3 + 8.85\ H_2 + xO_2$$

which yields the following solid films:

$$Si_3N_4,\ SiO_2,\ NH_4Cl$$

Figure 26 shows the effect of oxygen concentration on nitride and oxide formation at 900°C and 100 torr. Clearly, oxide is preferred and deposited at the expense of nitride as the amount of oxygen increases. Above 5% oxygen very little nitride can grow.

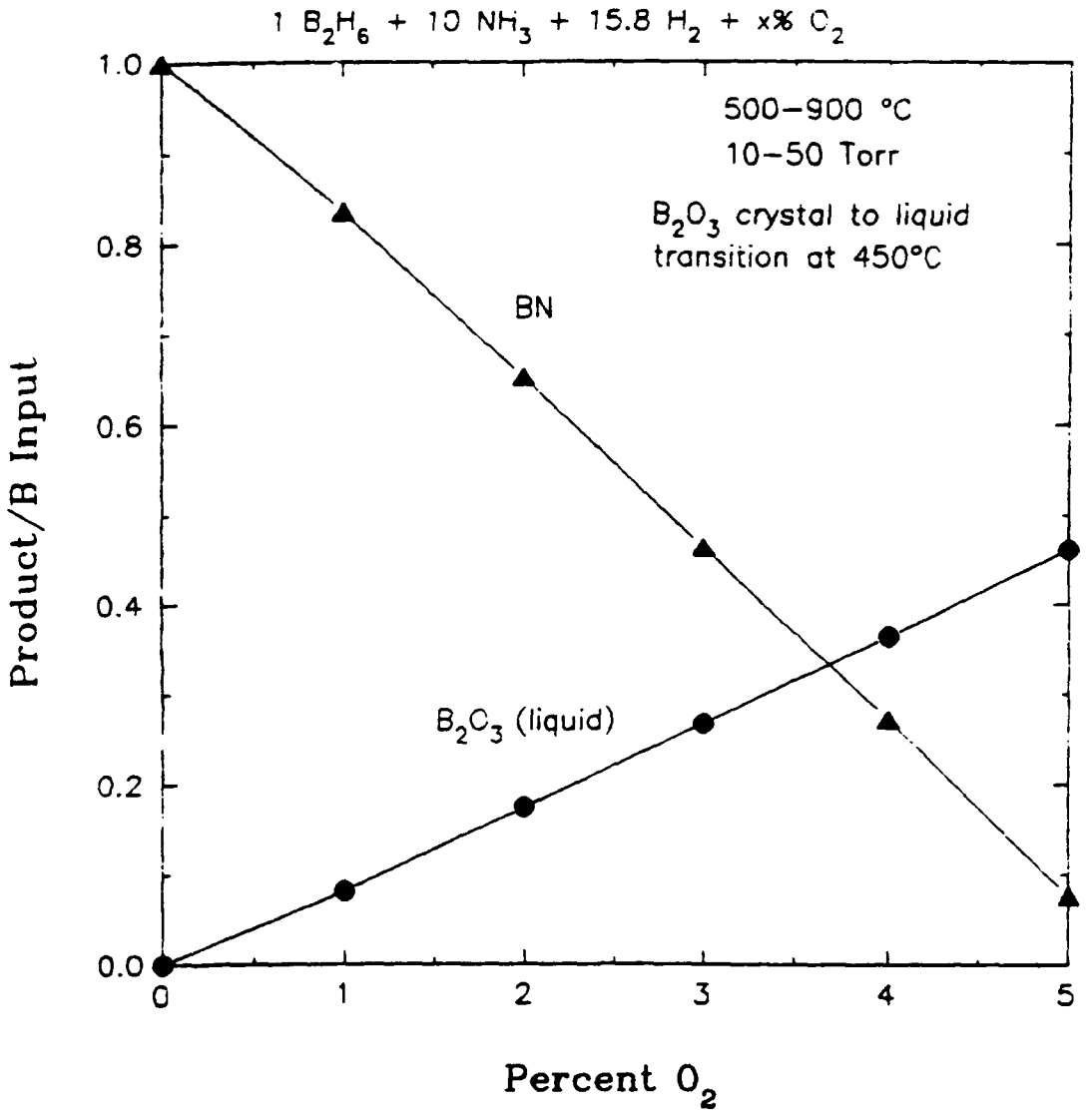


Fig. 25 Effect of oxygen on the deposition of boron nitride from diborane and ammonia

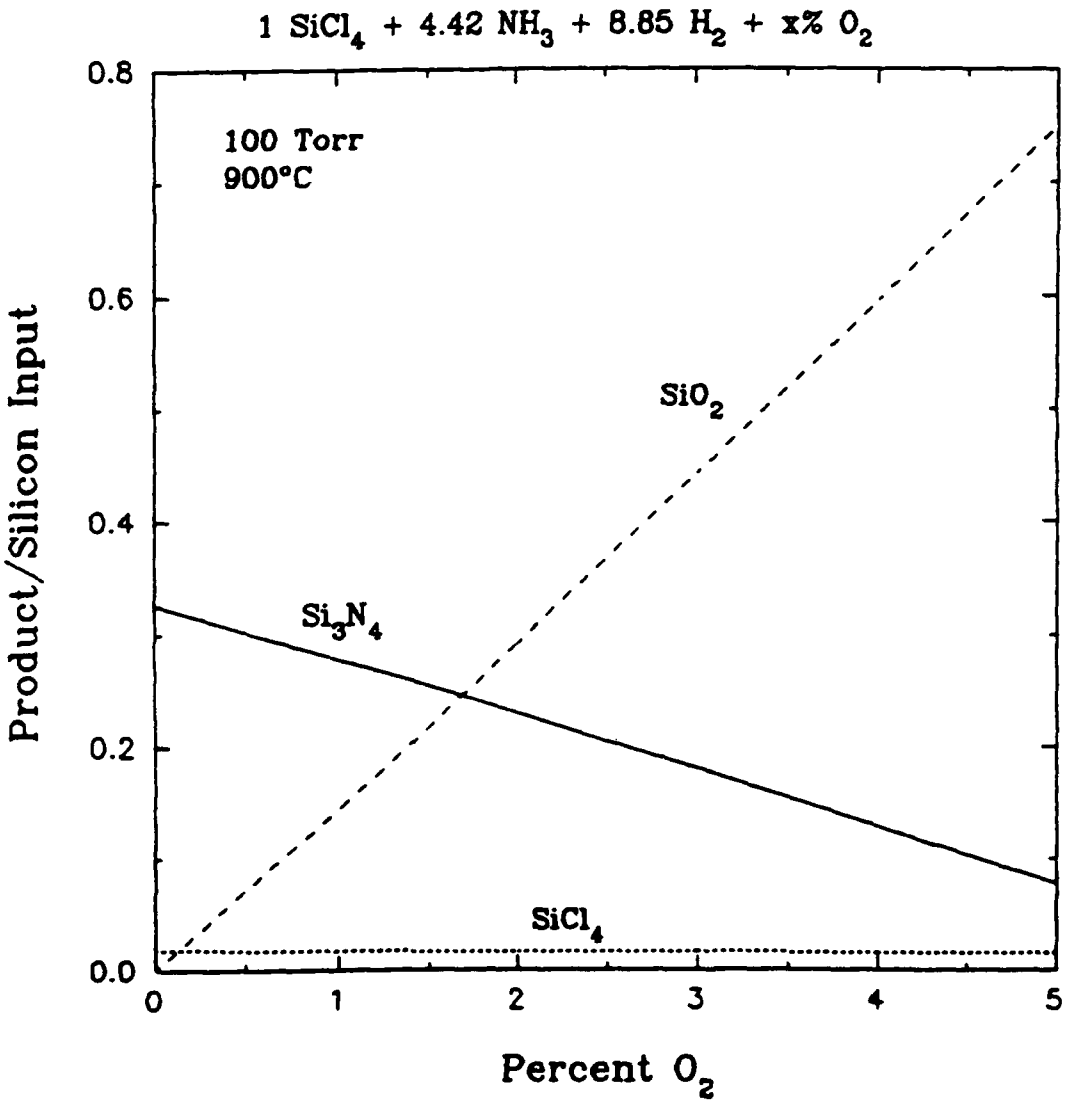


Fig. 26 Effect of oxygen on the deposition of silicon nitride from $SiCl_4$ and $NH_3$

## TASK 1-4 COATED FIBER EVALUATION AND SCREENING

Characterization and evaluation efforts of the coated ceramic fibers were performed by several microanalytical techniques. The characterization and evaluation techniques include tensile testing, scanning electron microscopy (SEM), energy dispersive spectroscopy (EDS), transmission electron microscopy (TEM), and scanning Auger microscopy (SAM).

Tensile tests of coated and uncoated Nicalon fiber tows from lot No. 127 were performed according to a modified ASTM D4018-81 method and summarized in Table 4.

Average failure loads and tensile strengths of the $Y_2O_3$ dip coated fiber tows are comparable to the as-received Nicalon fiber tows. Tensile strengths for the $Al_2O_3$ coated Nicalon are approximately 80% of the as-received. The degradation is probably due to the diffusion of $SiO_2$ from the fiber into the coating. Substantially higher tensile strength values for the desized lots of fiber specimens compared to the as-received material was indicated. The cause of this increase in tensile strength is probably due to a surface "healing" effect and is under investigation.

The desizing operations were performed at 500°C and 700°C in air. Fiber tows run through the continuous sol-gel coater without coating, identified as control runs in Table 4, were also tested and showed no degradation in tensile properties due to the operation of the coater.

Tensile testing of uncoated and coated Nicalon fibers, by individual filament testing was performed and the test results are reported in Table 5.

TABLE 4
SUMMARY OF TENSILE TEST RESULTS OF FIBER TOWS

| Nicalon Fiber Treatment | Number of Tests | Failure Load (Kg) | Tensile Strength (MPa) |
|---|---|---|---|
| As-received | 10 | 13.75 | 1700 |
| Desized - 500°C | 9 | 23.27 | 2880 |
| Desized - 700°C | 6 | 19.88 | 2460 |
| Control Run | 10 | 20.11 | 2490 |
| $Y_2O_3$ coated (0.05M) | 5 | 13.66 | 1680 |
| $Al_2O_3$ coated (0.1M) | 5 | 11.31 | 1400 |

TABLE 5
SUMMARY OF TENSILE TEST RESULTS OF INDIVIDUAL FILAMENTS

| Nicalon Fiber and Condition | Number of Tests | Failure Load (Kg) | Tensile Strength (MPa) |
|---|---|---|---|
| Lot 095 unsized as-received | 15 | 21.92 | 2720 |
| Lot 127 - M sizing as-received | 14 | 28.06 | 3480 |
| GA desized at 700°C | 12 | 31.60 | 3910 |
| $Al_2O_3$ coated continuously | 15 | 24.64 | 3050 |
| $Y_2O_3$ coated continuously | 14 | 21.40 | 2650 |

The individual filament tensile tests were run on a GA designed test rig using a 250 g load cell and SENSOTEC Model GM signal conditioner The Table 5 test results for the Nicalon filaments (lot No. 095), unsized from the manufacturer, showed an approximately 20% reduction in tensile strength compared to as-received Nicalon filaments with M sizing (lot No. 127). The individual filament data supported the reduction in tow failure load of the unsized fibers, as seen in Table 8. Surface flaws could account for the difference in the reduced strength of the lot No. 095, unsized Nicalon fibers from the manufacturer.

An increase in tensile strength for the GA desized (at 700°C) Nicalon filaments compared to the as-received, M sized, Nicalon filaments confirmed the fiber tow data reported previously.

Continuous coating of the Nicalon fiber with $Al_2O_3$ resulted in a mean tensile strength of 3050 MPa, approximately 10% less than the as-received Nicalon tensile strength. Continuous coating of the Nicalon fiber with $Y_2O_3$ produced fiber tow tensile strengths of 2650 MPa, a greater than 20% reduction in strength compared to the as-received material. Additional continuous coating runs of $Y_2O_3$ on Nicalon were performed. The coating runs were performed with different ratios of nitrogen ($N_2$) to ammonia ($NH_3$) in the curing step. The failure load and the tensile strength data are reported in Table 6.

Table 6 data indicate the lowest tensile strength values were recorded from the lowest $N_2$:$NH_3$ ratios. Conversely, the higher $N_2$:$NH_3$ ratios resulted in the highest tensile strengths.

The same continuously $Y_2O_3$ coated Nicalon fiber (samples 38 A, B, F) that provided the test data presented in Table 6

TABLE 6

SUMMARY OF TENSILE TEST RESULTS ON INDIVIDUAL FILAMENTS FOR $Y_2O_3$ COATED NICALON

| Sample No. | Gas Ratio $N_2$ : $NH_3$ | | Average Failure Load (Kg) | Tensile Strength (MPa) |
|---|---|---|---|---|
| 38A | 50 | 50 | 21.95 | 2720 |
| 38B | 100 | 50 | 26.55 | 3280 |
| 38C | 25 | 50 | 20.95 | 2600 |
| 38D | 50 | 70 | 21.55 | 2670 |
| 38E | 50 | 25 | 21.20 | 2630 |
| 38F | 100 | 25 | 26.6 | 3300 |

were reheated to 1100°, 1200°, and 1300°C to determine the effect of temperature on the coated fibers. A standard, uncoated Nicalon fiber was heated in each furnace run. The results are provided in Table 7.

A comparison of tensile strength values of $Y_2O_3$ coated Nicalon before (see Table 6) and after reheating, shown in Table 7, revealed degradation from 10% to 40%. The greatest degradation occurred with a higher $N_2$:$NH_3$ ratio (2:1), which had the highest strength originally. However, the lowest percentage of tensile strength degradation with increasing elevated temperature exposure (1100°, 1200°, and 1300°C) was also reported with this same 2:1 ratio coated material.

The tensile strength values for the elevated temperature furnace cycle after $Y_2O_3$ coating, compared to the standard uncoated Nicalon fiber, indicated lower than standard values for the 1100°C run. Tensile strength values above standard values are reported for the 1200°C run, and equivalent to standard values for the 1300°C furnace run.

SEM and EDS were used as qualitative fiber coating evaluation tools. SEM photomicrographs document bridging, cracking, spalling, and tracking problems. Coating appearance and the EDS relative peak intensities of the characteristic energy levels for the elements making up the coating were evaluated, providing important inputs toward optimization of the coating parameters and conditions.

SAM at Charles Evans and Associates and at the University of Pennsylvania was also performed. The resulting coating chemistry profiles are used to determine if there are any surface and bulk chemical, as well as coating-to-fiber interface problems. An example of an Auger depth profile of

TABLE 7
EFFECT OF TEMPERATURE ON TENSILE STRENGTHS
OF $Y_2O_3$ COATED NICALON

| Sample Number | Reheat Temperature (°C) | Failure Load (Kg) | Tensile Strength (MPa) |
|---|---|---|---|
| 38A-1 | 1100 | 16.45 | 2040 |
| 38A-2 | 1200 | 12.30 | 1520 |
| 38A-3 | 1300 | 10.20 | 1260 |
| 38B-1 | 1100 | 16.00 | 1980 |
| 38B-2 | 1200 | 14.50 | 1800 |
| 38B-3 | 1300 | 12.85 | 1590 |
| 38G-1 | 1100 | 18.25 | 2260 |
| 38F-2 | 1200 | 13.65 | 1690 |
| 38F-3 | 1300 | 12.75 | 1580 |
| Standard | 1100 | 26.95 | 3340 |
| Standard | 1200 | 9.90 | 1230 |
| Standard | 1300 | 12.80 | 1590 |

an alumina coating on Nicalon fiber is presented in Fig. 27. The alumina coating is approximately 1000 Å thick with a rather abrupt transition to the substrate fiber. A considerable amount of $SiO_2$ has diffused from the fiber into the coating. The separate Si and $O_2$ peaks are probably from $SiO_2$ that was cleaved during the Ar ion sputtering process. The SAM quantitative data for a particular coated fiber is also correlated back to the SEM/EDS data for that same coated fiber run to aid in making more useful comparative analyses.

TEM specimens were prepared from TEM grids that were $Al_2O_3$ coated from aluminum ethoxide in 2-ethoxy ethanol. A bright-field TEM micrograph of a sample annealed at 700°C is shown in Fig. 28(a), and an electron diffraction pattern of this material is shown in Fig. 28(b). Both figures suggest that the material is amorphous. There is no diffraction contrast typical of a crystalline material in the bright field image, and only diffuse scattering is present in the diffraction pattern.

The bright-field TEM micrograph and the electron diffraction pattern of a coating annealed at 800°C (Fig. 29), however, do reveal evidence of crystallinity. Diffraction contrast from regions about 30 Å in size are present and the electron diffraction pattern is composed of spotty rings. The four largest atomic-plane spacings determined from this pattern are compared with those of the various reported transition phases of hydrated alumina and with alpha alumina in Table 8A. The atomic-plane spacings determined from the electron diffraction pattern are closest to those of eta and gamma alumina. Note that there are only small differences in the planar spacings of eta and gamma alumina, the largest difference being for the planes with the largest spacing. This difference cannot be used to identify the phase in the

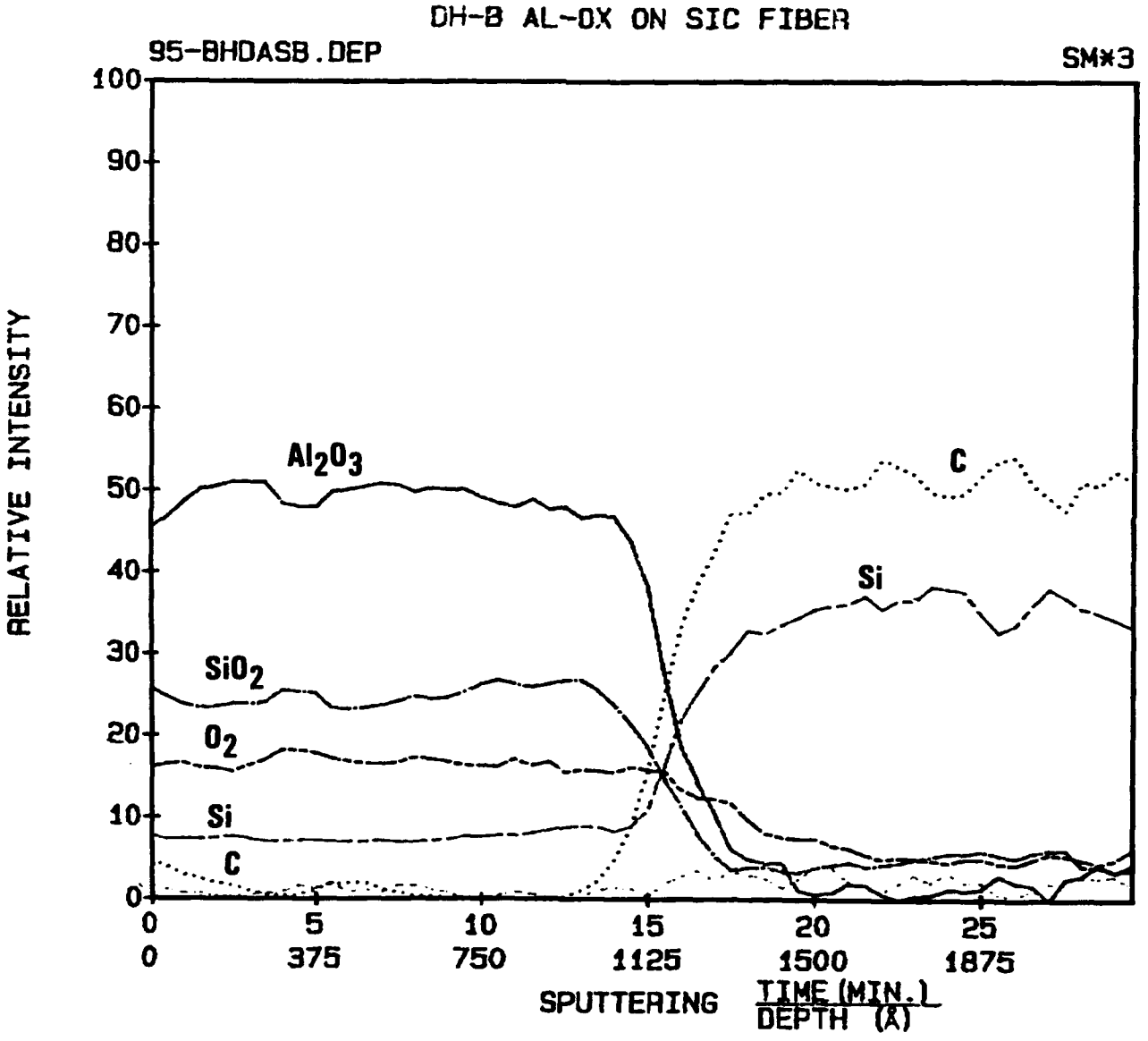


Fig. 27 Auger depth profile of alumina coating on Nicalon made from a 0.1M aluminum sec-butoxide sol.

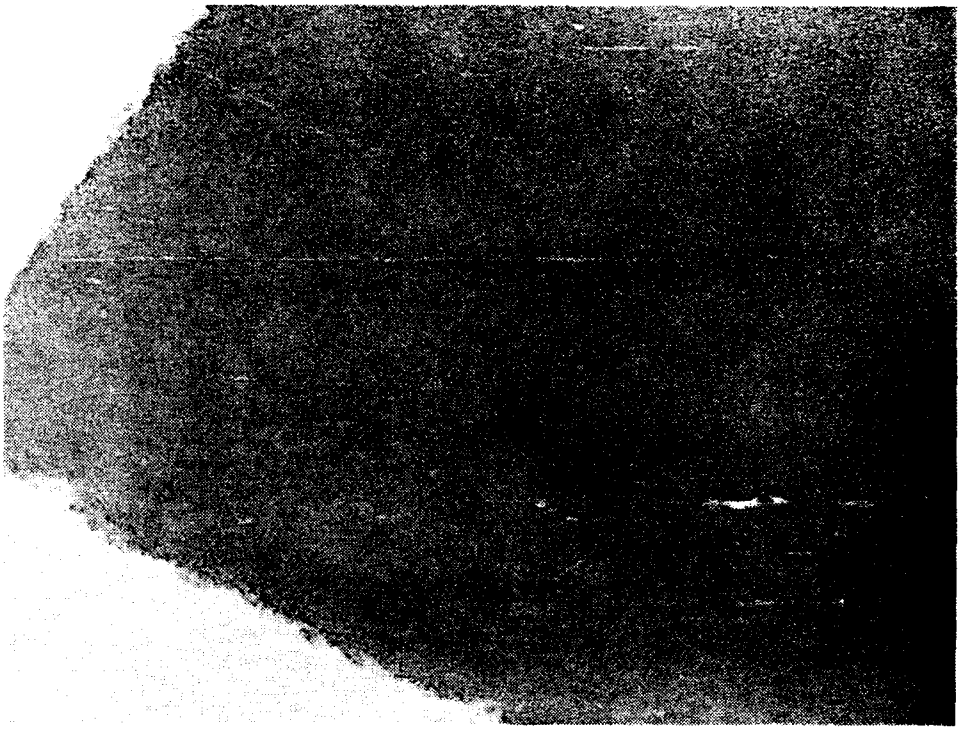


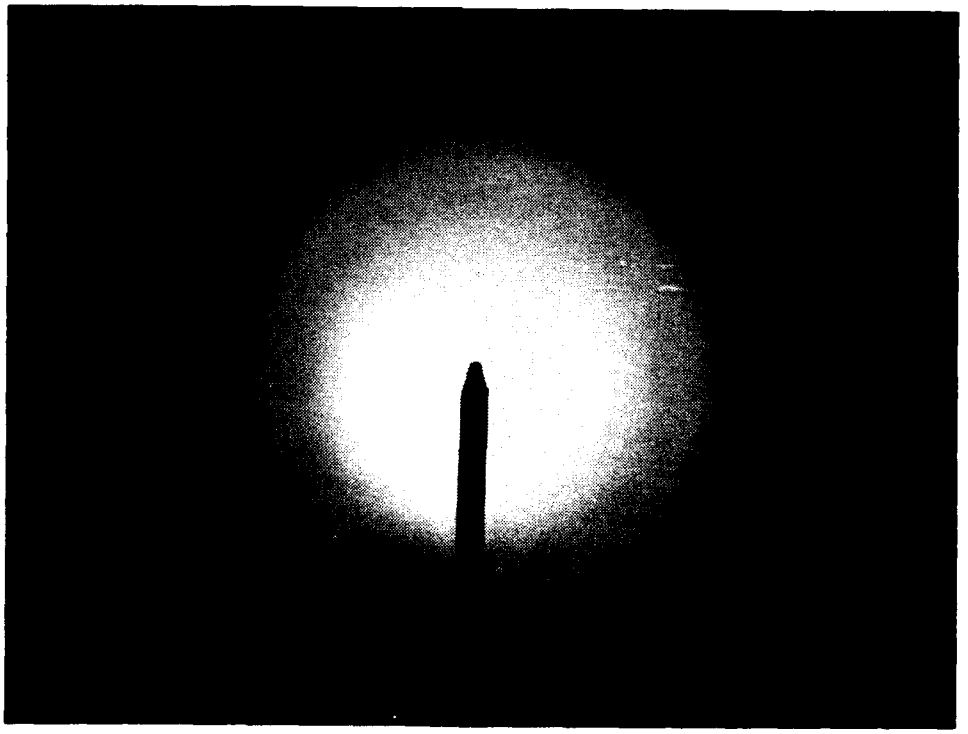


Fig. 28 Panel A - bright field transmission electron micrograph of $Al_2O_3$ coating annealed at 700°C. Panel B - electron diffraction pattern of coating in Panel A.

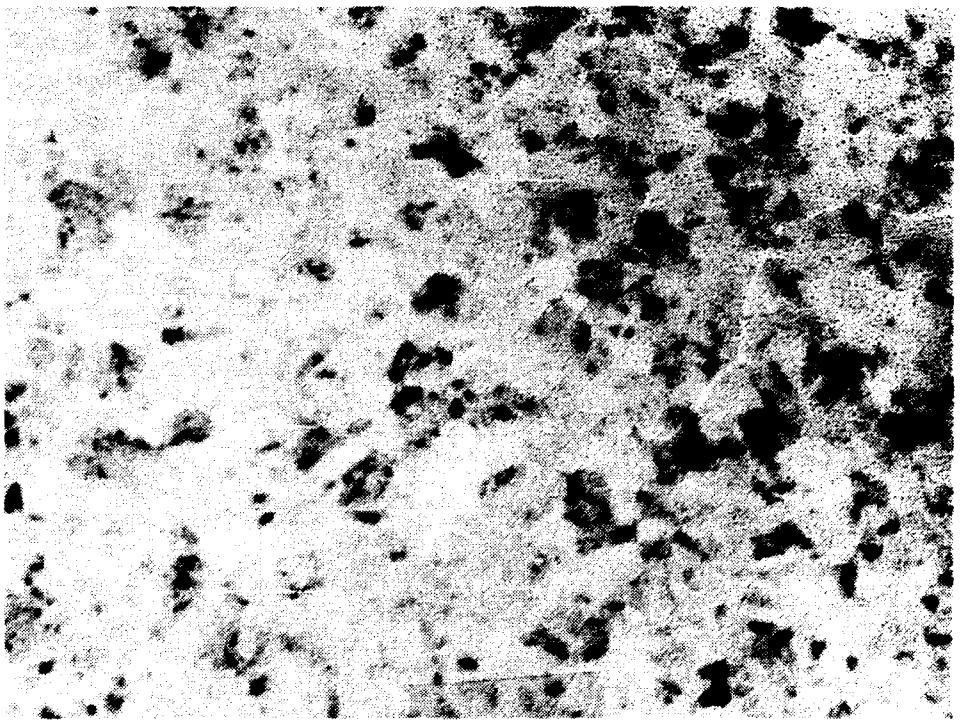


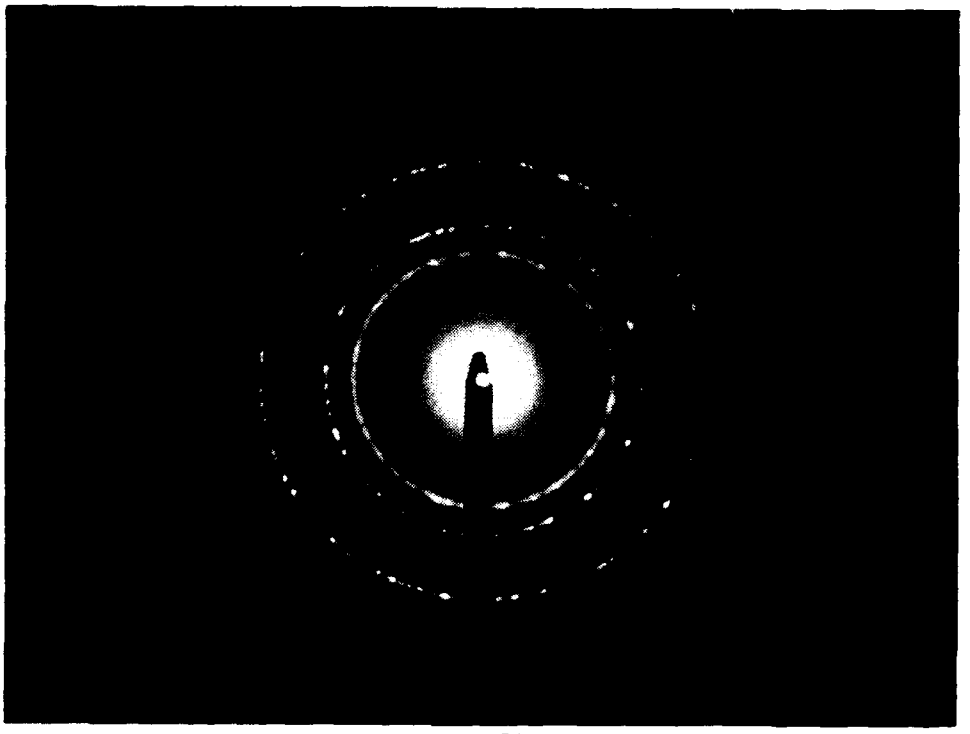


Fig. 29 Panel A - bright field transmission electron micrograph of $Al_2O_3$ coating annealed at 800°C. Panel B - electron diffraction pattern of coating in Panel A.

(A)

100 Å

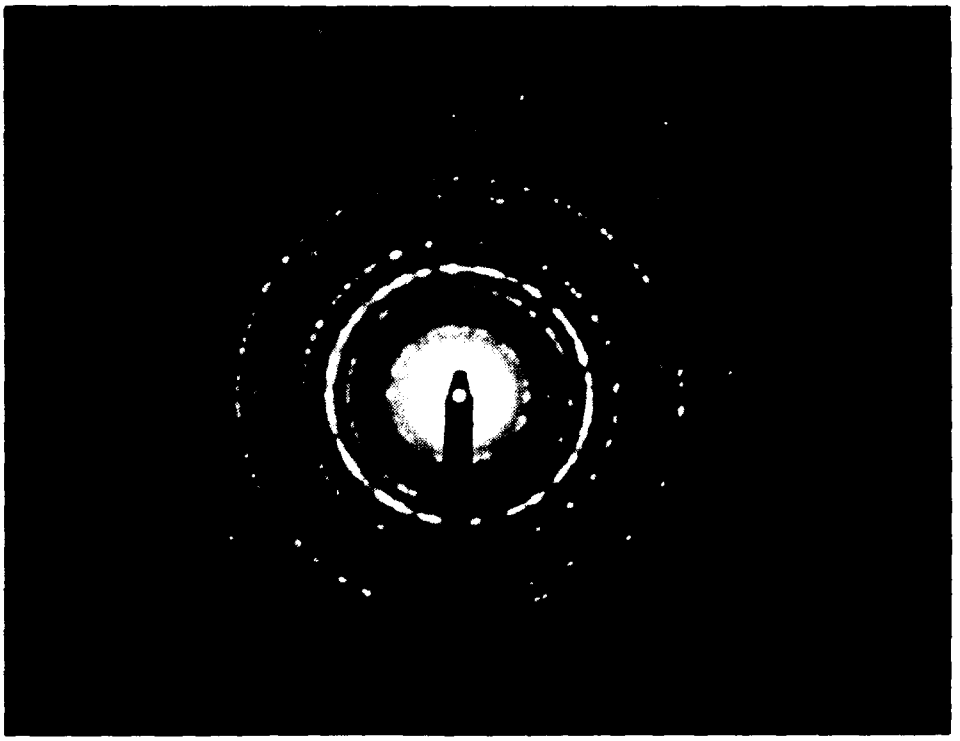

(B)

Fig. 30 Panel A - bright field transmission electron micrograph of $Al_2O_3$ coating annealed at 900°C. Panel B - electron diffraction pattern of coating in Panel A.

Table 8

PLANAR SPACINGS OF VARIOUS ALUMINA PHASES AND PLANAR SPACINGS OF THE COATINGS PREPARED IN THIS STUDY

A. Planar Spacings of Various Hydrated Alumina Phases

| Phase | Eta | Chi | Gamma | Kappa | Delta | Theta | Alpha |
|---|---|---|---|---|---|---|---|
| Planar spacings (Å) | 4.6 | 4.50 | 4.53 | 6.2 | 7.6 | 5.45 | 3.48 |
| | 2.8 | 4.11 | 2.80 | 4.5 | 6.4 | 4.54 | 2.55 |
| | 2.40 | 3.23 | 2.39 | 4.2 | 5.5 | 2.84 | 2.38 |
| | 2.27 | 2.81 | 2.28 | 3.04 | 5.1 | 2.73 | 2.16 |
| | 1.97 | | 1.98 | | | | |

B. Planar Spacings Determined from Electron Diffraction Patterns

| Treatment | 800°C | 900°C |
|---|---|---|
| Planar spacings (Å) | 4.45 | 4.56 |
| | 2.73 | 2.77 |
| | 2.35 | 2.39 |
| | 1.96 | 1.97 |

coating, however, because the 4.45 Å planar spacing of the coating differs significantly from the values for both eta and gamma alumina. Also, one diffraction ring, the ring for a 2.28 Å spacing, is missing from the coating pattern.

A bright-field TEM micrograph of a coating annealed at 900°C and the corresponding electron diffraction pattern are shown in Fig. 30. The crystalline regions are larger than those in the 800°C annealed coating, measuring about 100 Å in size. The four largest atomic-plane spacings determined from the spotty ring electron diffraction pattern are listed in Table 8B. They agree well with those of the 800°C coating. As with the 800°C annealed coating the ring for a 2.28 Å spacing is missing.

## TASK 2-1 COATING PROCESS SCALE-UP

In Phase I of this program a wide variety of methods for coating multifilament ceramic tows was developed. Both gas phase and liquid phase techniques were employed to develop coating procedures for depositing mainly oxides, nitrides, and carbides. The more promising coating methods were developed to a level where short (~60 m) continuous runs were performed to demonstrate production feasibility. The objectives of Phase II were to identify the most promising coating candidates and to develop methods for coating these at production levels. An additional objective was to demonstrate economic feasibility of ceramic fiber coating. This development occurred on both gas phase (Task 2-1-1) and liquid phase (Task 2-1-2) processing.

## TASK 2-1-1 GAS PHASE PROCESS SCALE-UP

Several different coatings for fiber/matrix interface control were explored including BN derived from diborane. Additionally, BN coatings derived from boron trichloride, and a dual coating of BN were investigated. The dual coating is a layer of BN from diborane (subsequently referred to as low temperature BN) followed by a layer of BN derived from boron trichloride (subsequently referred to as high temperature BN). In addition to these coatings, samples with CVD coatings of pyrolytic carbon and with titanium diboride were prepared. All of the coatings discussed here were made on Nicalon cloth. The cloth was cut into strips, 5 cm by 20 cm and placed inside a cylindrical graphite susceptor. The susceptor was 5 cm ID by 25 cm long, and supported inside a quartz tube. The graphite was inductively heated. Coating gases were fed in through the top of the quartz tube and evacuated through the bottom. High temperature CVD BN was prepared by reacting boron trichloride with ammonia in the presence of hydrogen. The following first order reaction is assumed:

$$BCl_3 + NH_3 = BN + 3HCl$$

This reaction for depositing BN on Nicalon cloth was carried out at 1000°C and a pressure of 3.5 to 4 torr. The reaction proceeds rapidly at these conditions. The micrograph in Figure 31 shows a 3.5 $\mu$m coating of high temperature BN on Nicalon that was deposited in 20 minutes.

The dual BN coating was prepared in two steps. The first step consists of reacting diborane and ammonia in the presence of hydrogen according to the following reaction:

$$B_2H_6 + 2NH_3 = 2BN + 6H_2$$

Figure31. Scanning electron micrograph (4000X) of a thick coating of BN on Nicalon made from $BCl_3$ and $NH_3$ at 1000°C.

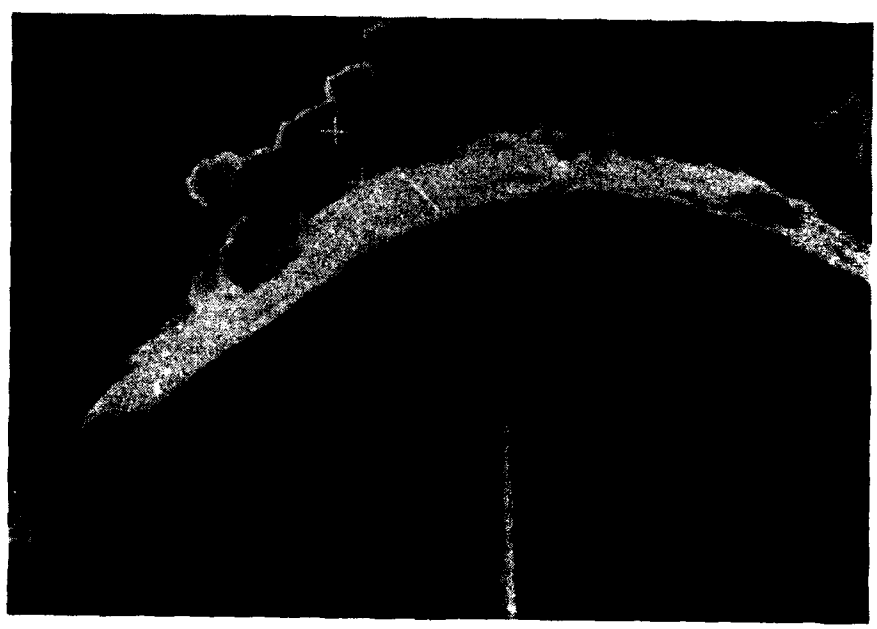

Figure 32. Scanning electron micrograph (7000X) of $B_2H_6$ and $NH_3$ at 500°C followed by $BCl_3$ and $NH_3$ at 1000°C.

This low temperature BN could protect the fibers if they are susceptible to chemical attack by the Cl from the $BCl_3$ reaction. The second step in the dual coating is the deposition of high temperature BN as described previously. The micrograph in Figure 32 shows a dual coating of about 750 nm thickness.

Pyrolytic carbon is a CVD coating that has been studied extensively; because of its chemical stability in the absence of oxygen, it is a good baseline material by which to measure fiber matrix interaction. The preferred method for preparing the pyrolytic carbon coating was the thermal decomposition of propylene. Propylene was fed into the reactor at a rate of 100 sccm. The Nicalon cloth was coated for 1 hour, inverted, and coated for 1 more hour. The coating was performed at 1120 and 1150°C and a pressure of 3.5 torr. The resulting coating is shown in Figure 33.

Titanium diboride was prepared from titanium tetrachloride and diborane. The titanium diboride reaction is complex but may be expressed simply as:

$$TiCl_4 + B_2H_6 + H_2 = TiB_2 + 4HCl + 2H_2$$

Hydrogen is bubbled through $TiCl_4$ transporting a known amount of vapor to the CVD reactor. The vapor flow rate of $TiCl_4$ is easily calculated making use of Raoult's law, which for this pure liquid system defines the partial pressure as equal to the vapor pressure. The vapor pressure of $TiCl_4$ at room temperature is quite low, ~10 torr. In order to introduce more vapor into the reaction, the liquid reservoir was heated. By heating the $TiCl_4$ to 40°C the vapor pressure was raised to 25 torr. This is the partial pressure of $TiCl_4$ maintained in

Figure 33a. Pyrolytic carbon coating on Nicalon showing good fiber bundle penetration.

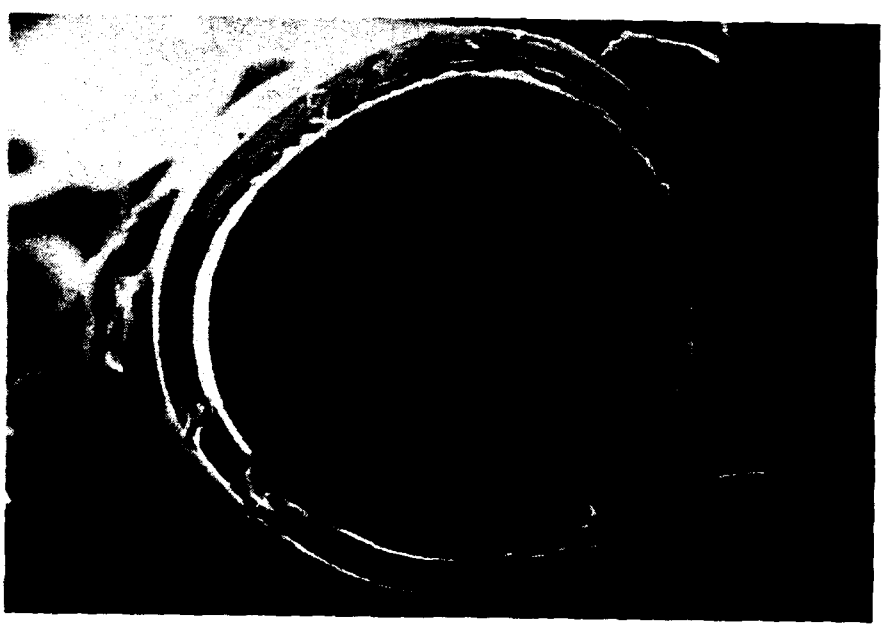

Figure 33b. 1.0 micron thick pyrolytic carbon coating on an individual filament of Nicalon.

the reservoir for the $TiB_2$ coating. Diborane was fed into the reactor through a separate line. The coating, shown in Figure 34, was made at 700°C and a reactor pressure of 15 to 25 torr. The deposition rate of $TiB_2$ is quite slow (2 nm/min) using these conditions but provides a very uniform coating through the fiber bundle. The $TiB_2$ coating was examined using Auger analysis. Figure 35 shows the energy distribution for the sample with a boron peak (179 eV) and two dominant titanium peaks (387 eV, 418 eV). A depth profile is shown in Figure 36 which indicates a fairly uniform composition through the coating.

## CONTINUOUS CVD FIBER COATING

A demonstration of the capacity of the continuous fiber coater to process multiple tows simultaneously was completed successfully. Four spools of Nicalon CG fiber were loaded into the top of the coater in their as-received condition as supply spools. The fibers then passed through the coating zone where BN was deposited and wound onto the take-up spools in the bottom of the coater. The coater was run continuously for about 3½ hours. The fiber speed through the coater was 20.7 cm/min. This rate equates to a throughput of about 50 meters per hour.

The coating chosen for this demonstration was BN derived from $B_2H_6$. This reaction, though the section on composite fabrication would indicate that it is not the coating of choice for these fibers, was chosen because it is clean and demonstrates the efficacy of coating four tows simultaneously.

A filament winder was completed and installed in the take-up section of the continuous coater. The winding pattern and the spacing on the spools are the same as that received from most

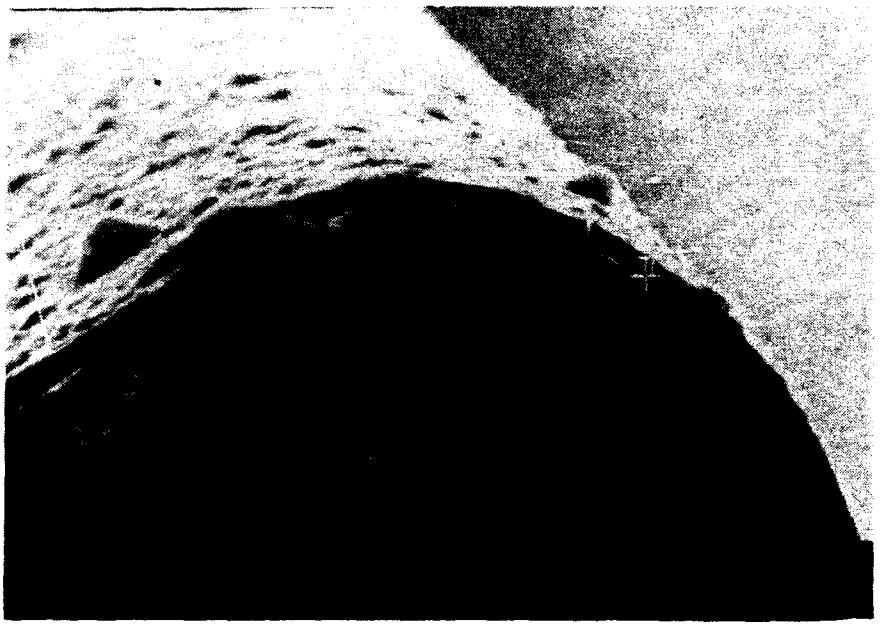

Figure 34. Scanning electron micrograph (4000X) of $TiB_2$ coating on a Nicalon filament. Coating is 250 nm thick.

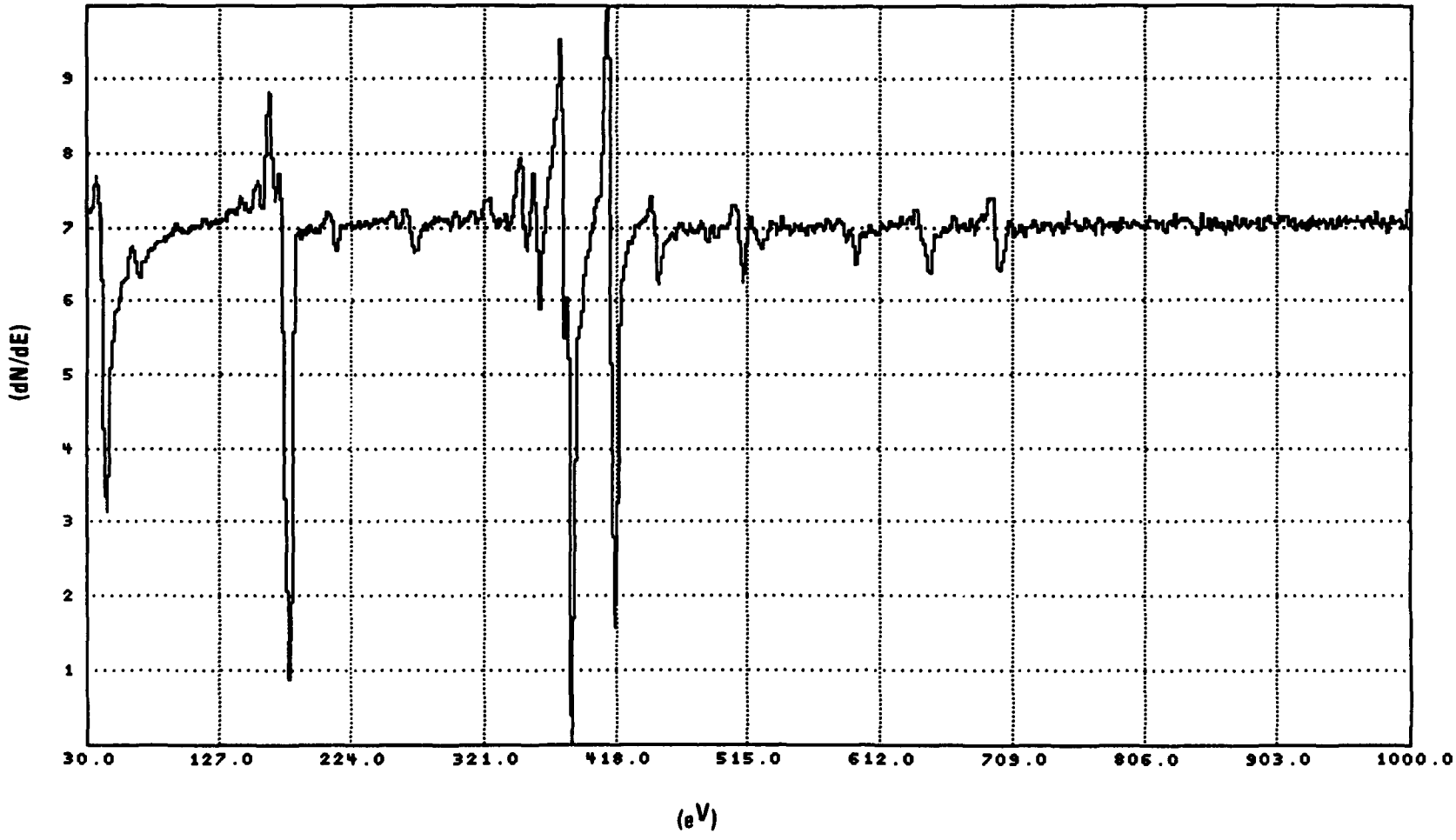


Figure 35. Auger electron spectroscopy survey of $TiB_2$ coating ...ces include boron peak at ... 387 eV and 418 eV.

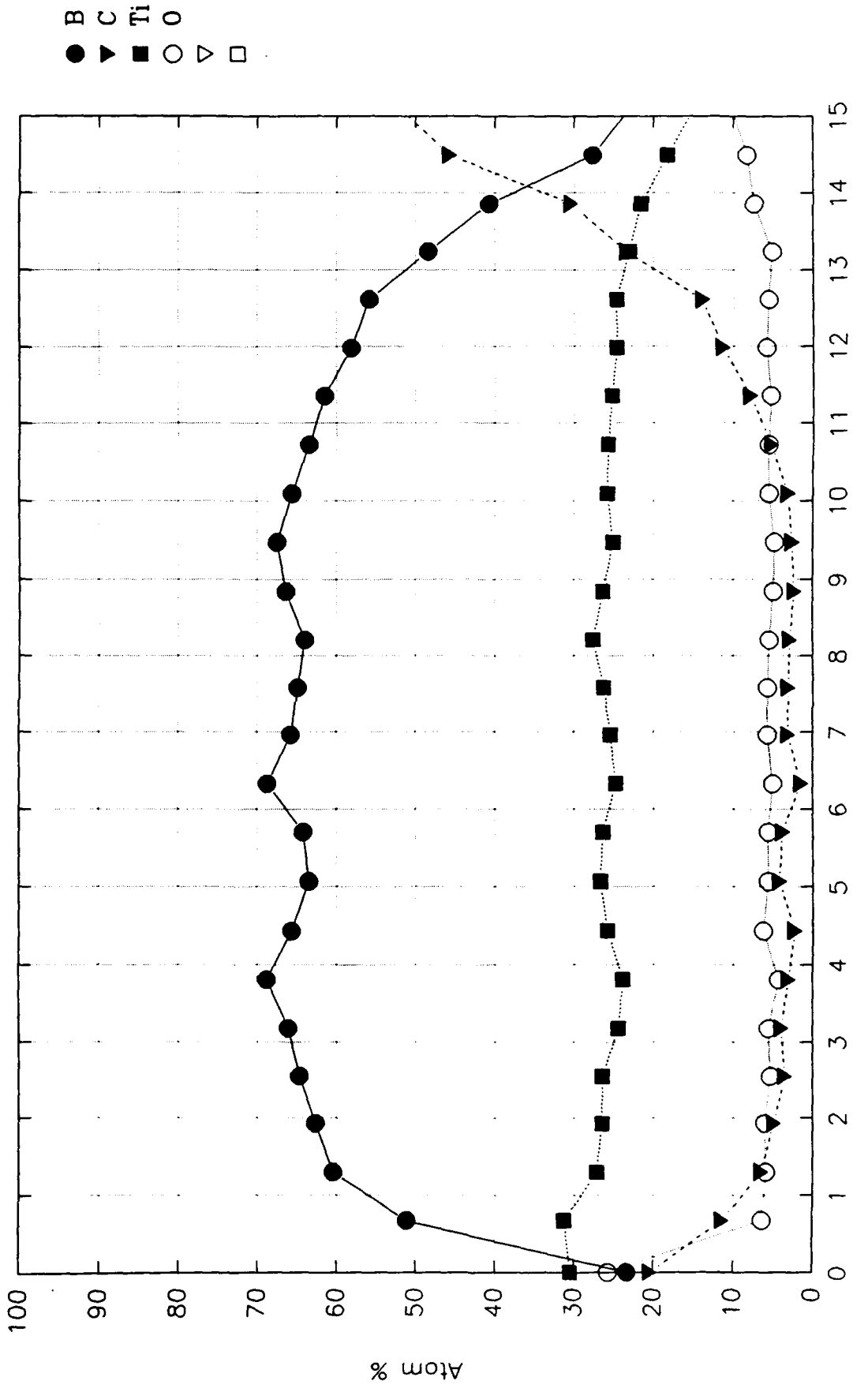


**Figure 36. Auger depth profile of $TiB_2$ coating on ceramic grade Nicalon. Sputter rate is approximately 200Å/min.**

commercial fiber suppliers. This will make the coated fiber spools easily adaptable to commercial weaving machines and rewinders. One effort with the continuous fiber coater focused on the deposition of boron nitride on Nicalon. BN derived from $BCl_3 + NH_3$ at a deposition temperature between 950 and 1000°C has thus far provided the most successful fiber/matrix interface coating. Once the optimum coating conditions have been established for depositing approximately 500 nm thick coatings, handling criteria will be assessed including the minimum radius of curvature before damage occurs. This will determine whether further modification is required to the coater before producing larger quantities of coated fiber.

Two approaches to applying an interface coating were investigated. The first was to coat the fiber tows prior to weaving. The second approach was to weave the fiber into fabric and subsequently coat the fabric. There are certain advantages and disadvantages to each method. By first coating the fiber tows, greater uniformity of the coating is achieved, but more handling of the coated fibers during weaving and processing is required which can result in greater damage to the coated fibers. Coating the woven fabric may result in more non-uniformity of the coating as well as difficulty infiltrating the fiber tows. It is, however, attractive since little additional handling is required to fabricate a composite. Also, the throughput of coated material is increased substantially.

Another effort on the continuous fiber coater was directed towards optimizing the system for desizing tow on-line. The desizing is a critical step in the continuous coating of ceramic fibers. The sizing must be stripped from the fibers and the residue carried away without mixing with the coating

gases. The system under development consists of a tubular furnace placed in the coater a short distance above the coating zone. After passing through the desizing furnace, the fibers travel through an orifice into the coating zone. The orifice, though not extremely small, allows the top chamber to be purged and exhausted separately, creating little interference with the coating zone. The coating gases are introduced below the orifice and exhausted in the direction away from the orifice.

While continuing to optimize the continuous fiber coater, work was continued on coating large pieces of woven material. From an economic viewpoint, it would be desirable to coat fabric instead of tow, because the throughput is potentially much greater. The quality of the coating on fabric needs to be examined to determine if it is acceptable.

The technique presently under investigation is one where the cloth is fixed in a cylindrical shape supported only at the top edge and at the bottom edge of a graphite mandrels. The free edges of the cloth are stitched together so that the permeability of the cloth is fairly uniform. Support for the cloth is provided by graphite rings which press the top and bottom edge of the cloth against a graphite mandrel of the same diameter. The free height of the cloth is 30 cm. Through the center of the fixture is a perforated graphite gas distributor with a diameter of 7.5 cm. The cloth and mandrel sit inside of a 28 cm ID graphite susceptor. The cloth is then heated from the outside and the reactant gases are forced through the cloth from the cold side. We successfully coated Nicalon cloth using this process applying both BN and BN with a $Si_3N_4$ overcoat. The coating uniformity is somewhat compromised; the coating thickness varies by about a factor of two over the entire piece of fabric. The fabric becomes

slightly more rigid due to bridging of filaments where the tows from the fill and warp directions cross. However, we think that this approach to batch coating large pieces of cloth will yield itself to design of a continuous fabric coater. Such a coater might be visualized as passing the cloth through a zone where heat is supplied on one side and coating gases are forced through the cloth from the opposite side.

Beside better mechanical performance (i.e., higher toughness) control of the fiber-matrix interface has other significant benefits. This is clearly a critical region for controlling many of the electrical characteristics and possibly some of the thermal characteristics of composites. It is also one of the key factors in contributing to the high temperature stability of ceramic fiber composites to prevent their embrittlement as a result of exposure to high temperatures. It is apparent that fiber coating technology is rather complex, involving different chemical compositions and thicknesses, depending upon the application, and possible need for multi-layer coatings. An example is a three-layer fiber coating scheme where the first layer protects the fiber; the second layer controls mechanical, electrical, or thermal properties; and the third layer acts as a chemical barrier between the matrix and the other layers.

Fibers with multiple coatings were prepared by chemical vapor deposition in a batch mode to study coating conditions and in a continuous mode to establish production parameters. Dual and triple coatings were deposited sequentially in the static coater described previously. After the first coating was deposited the coating gases were shut off, the coater was purged of any reactant gases and subsequently the coating conditions for the next layer were established.

Figure 37 is SEM of a dual coating of SiC on top of BN deposited on Nicalon tow in the static coater. The BN was deposited from $BCl_3$ and $NH_3$ at 900°C and 100 Pa for 3 minutes. The SiC was deposited from the decomposition of $CH_3SiCl_3$ at 1050°C and 260 Pa for 3 minutes. Figure 38 shows a SEM of a triple coating fabricated in the static coater of BN followed by Si followed by $Si_3N_4$. The BN was deposited from $BCl_3$ and $NH_3$ at 925°C for 2 minutes; the Si was deposited from the decomposition of $SiH_4$ at 700°C for 5 minutes and the $Si_3N_4$ was deposited from $SiF_4$ and $NH_3$ at 1340°C for 5 min.

Figure 39 is an end on view of triple coating on a Nicalon fiber produced in the static coater. The coating consists of a layer of BN deposited from $BCl_3$ and $NH_3$ at 950°C for 2 minutes. Subsequently, a layer of Si was deposited from $SiH_4$ at 700°C for 5 minutes. Finally, another layer of BN was deposited under the same conditions as the first layer. Figure 40 displays a fiber coated under the same conditions as the fiber in Figure 39. The fiber has partially debonded from the coating, leaving the coating exposed.

A coating produced on Nicalon in the continuous coater is shown in Figure 41. It consists of a dual coating of BN followed by SiC. The BN was made from $BCl_3$ and $NH_3$ at 1050°C. The SiC was prepared from $CH_3SiCl_3$ at 1070°C. The fiber speed for both coatings was 15 m/hr. Figure 42 shows a coating fabricated under similar conditions except that the fiber speed for the SiC coating was 7.5 m/hr.

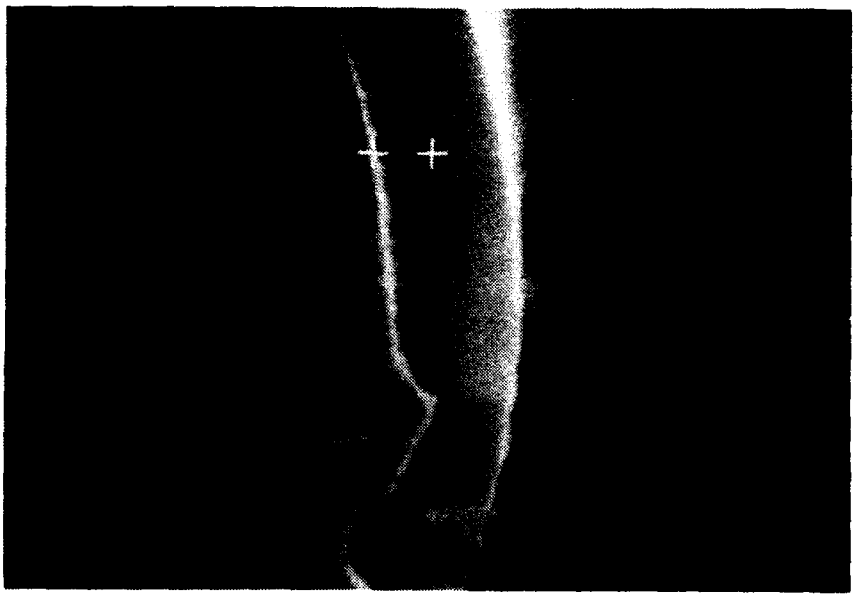

Figure 37. Scanning electron micrograph (15000X) of dual coating consisting of BN followed by SiC on a Nicalon fiber substrate prepared in static coater.

Figure 38. Scanning electron micrograph (5000X) of triple coating consisting of BN followed by Si followed by $Si_3N_4$ on Nicalon tow prepared in static coater.

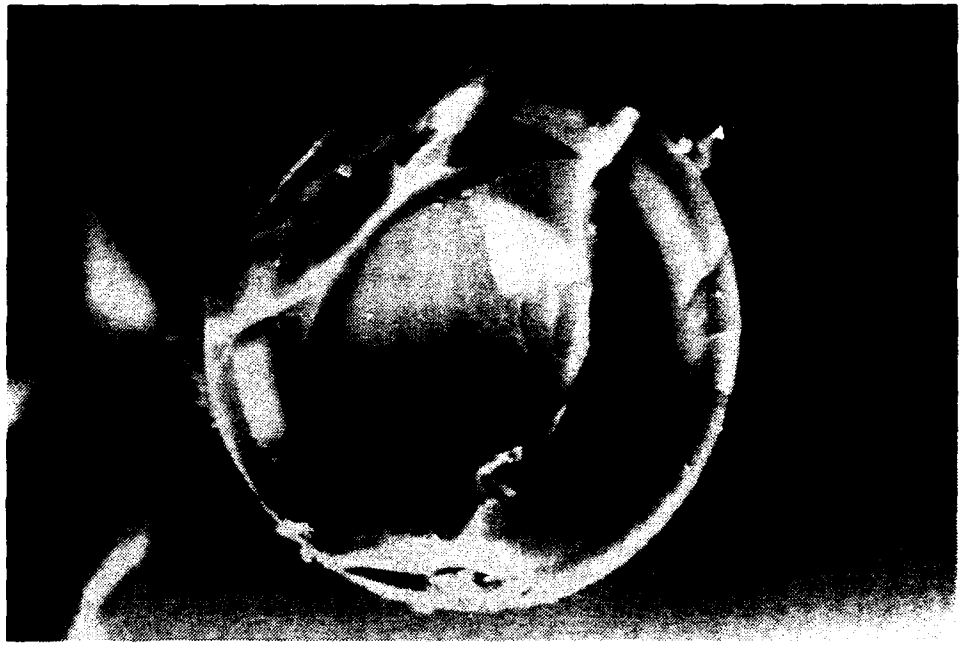

Figure 39. Scanning electron micrograph (2500X) of triple coating consisting of BN followed by Si followed by BN on Nicalon.

Figure 40. Scanning electron micrograph (1500X) of triple coating consisting of BN followed by Si followed by BN on Nicalon.

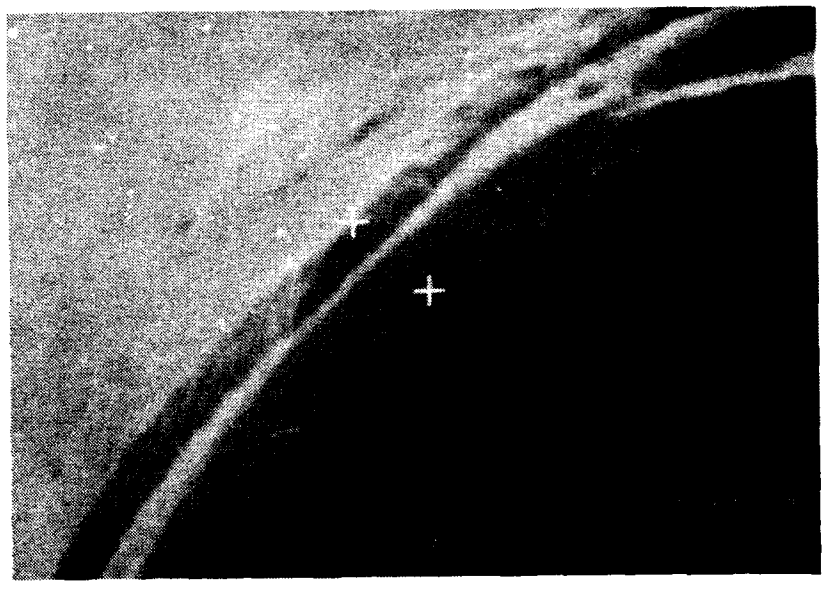

Figure 41. Scanning electron micrograph (20,000X) of dual coating consisting of BN followed by SiC deposited on Nicalon. Continuous coating produced at 15 m/hr.

Figure 42. Scanning electron micrograph (15,000X) of dual coating consisting of BN followed by SiC deposited on Nicalon, BN coating produced at 15 m/hr, SiC produced at 7.5 m/hr.

A conceptual design of a continuous fiber coater with multiple coating zones was prepared. Multiple coating zones require a number of modifications to the current coater including independent gas inlet and exit lines, independent hot zones, and a means to adjust system pressure, at least over a limited range. A number of concepts to incorporate these features are under consideration.

## TASK 2-1-2 LIQUID PHASE PROCESS SCALE-UP

### REVIEW OF COATING METHODS

Tows coated were Nicalon, Nextel 480, FP-PRD-166, and HPZ. All processes required the tows to be desized and coated tows to be calcined. Desizing was accomplished by heating in air to between 550°C and 700°C for up to thirty minutes. Oxide coated fibers were calcined at 800°C to 1000°C for six to sixty minutes. Silicon carbide coated fibers were calcined at 800°C in nitrogen for 24 minutes. Boron nitride and silicon nitride coated fibers were calcined at 1000°C in ammonia.

A schematic and chemistry summary of the traditional dip coating process are shown in Fig. 43. The process consists of:

1. Desize tow
2. Dip tow into sol or solution
3. Dry solvent from coated tow

(3a) Optionally cure coating

4. Repeat steps 2 and 3 to obtain desired thickness
5. Calcine coated tow

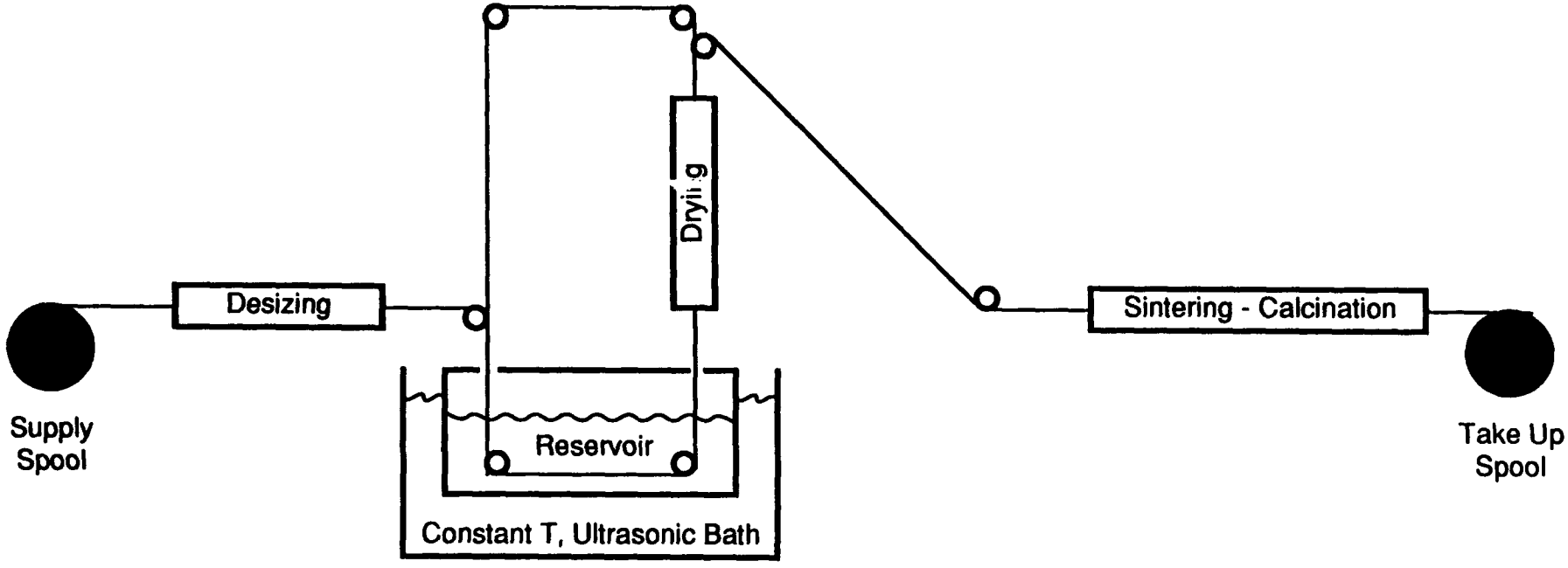


Reservoir: Metal Alkoxide Sol

Drying: $nMO_i(OR)_{j(alcohol)} + Fiber \rightarrow nMO_i(OR)_j \bullet Fiber$

Calcination: $MO_i(OR)_j \bullet Fiber \rightarrow MO_k \bullet Fiber + H_2O(g) + CO_2(g)$

Figure 43. DIP COATING PROCESS SCHEMATIC AND CHEMISTRY.

Calcining and desizing were described above. Solutes used in nonaqueous solvents were polysilane resin, decaborane based polymer, yttrium isopropoxide, ß-trichloroborazine, aluminum sec-butoxide, yttrium 2-ethoxyethoxide, and zirconium n-butoxide. Solutes used in water were yttrium nitrate, aluminum hydroxide, yttrium hydroxide, and zirconium hydroxide. Drying temperatures ranged from 100°C to 500°C. Curing was performed with water vapor, dry ammonia, or wet ammonia.

A schematic and chemistry summary of the in-situ curing coating process are shown in Figure 44. The process consists of:

1. Desize tow
2. Dip tow into sol solution
3. Cure coating
4. Dry solvent from coated tow
5. Repeat steps 2 to 4 to obtain desired thickness
6. Calcine coated tow

Calcining and desizing were described above. Solutes used in non-aqueous solvents were hafnium, n-butoxide, zirconium n-butoixde, aluminum sec-butoxide, yttrium isopropoxide, and ß-trichlorobo-razine. Solutes used in water were yttrium nitrate, hafnium chloride, aluminum nitrate, aluminum hydroxide, yttrium hydroxide, and zirconium hydroxide. Alkoxides were cured with water vapor, aqueous solutions were cured with wet ammonia, and ß-trichloroborazine was cured with dry ammonia. Drying temperatures ranged from 100°C to 500°C.

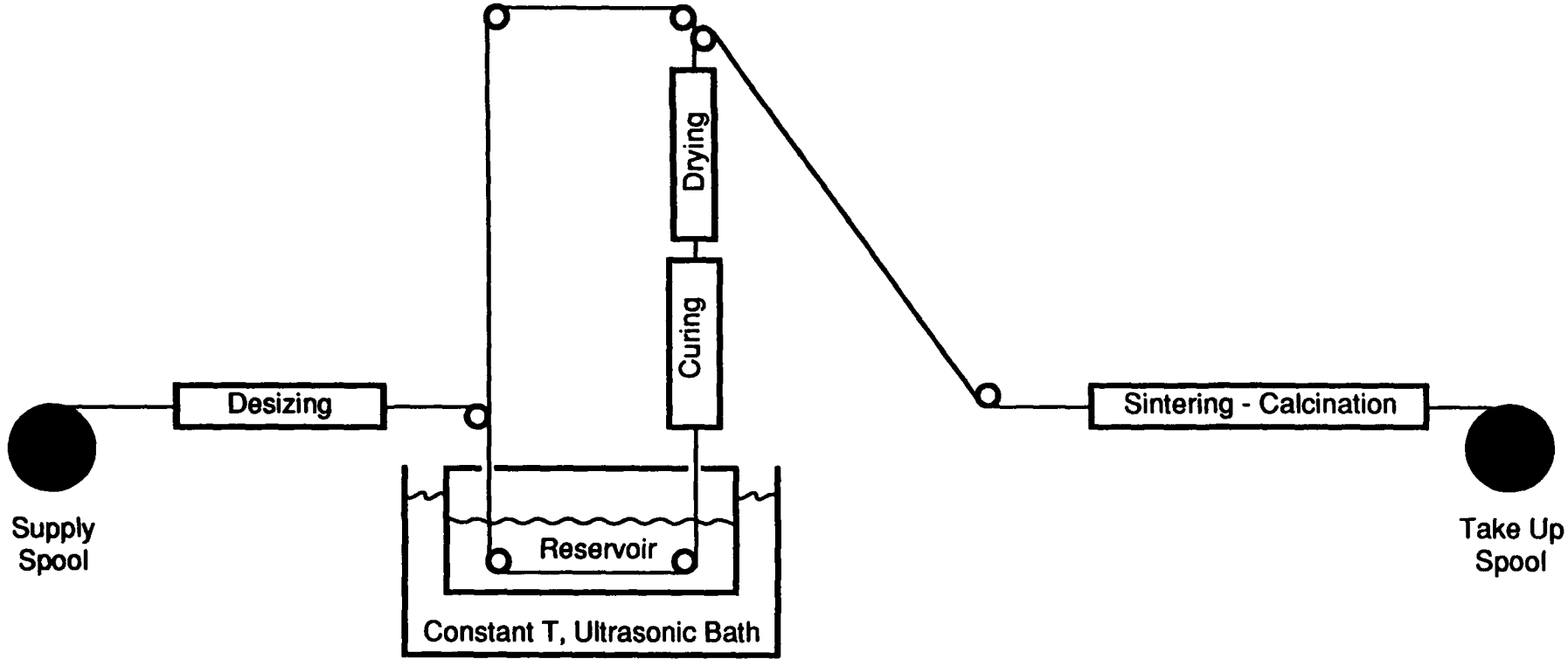


Reservoir: Metal Salt Solution

Curing: $M^{(i)+}(aq) + H_2O + OH^- \rightarrow MO_j(OH)_k(aq)$

$MO_i(OH)_j(aq) + Fiber \rightarrow MO_i(OH)_j \bullet Fiber$

Drying: Remove $H_2O$ Solvent

Calcination: $MO_i(OH)_j \bullet Fiber \rightarrow MO_k \bullet Fiber + H_2O(g)$

**Figure 44. IN-SITU CURING PROCESS SCHEMATIC AND CHEMISTRY.**

A schematic and chemistry summary of the reaction bonding coating process are shown in Figure 45. The process consists of:

1. Desize tow
2. Produce a thin hydroxide or amine coating using either traditional dip coating with a curing step or in-situ curing
3. Dip tow into the solution allowing the coated and cured tow to react with solute
4. Rinse excess solution from tow with pure solvent
5. Dry solvent from coated tow
6. Cure new coating layer
7. Repeat steps 3 to 6 to obtain desired thickness
8. Calcine coated tow

Calcining and desizing were described above. Hafnium n-butoxide, zirconium n-butoixde, aluminum sec-butoxide, and yttrium isopropoxide were used for reaction with hydroxide films. ß-trichloroborazine was cured with dry ammonia. Drying temperatures ranged from 100°C to 200°C.

## SUMMARY OF RESULTS FOR LIQUID PHASE METHODS

### DIP COATING

The traditional method of dip coating in a sol or solution is the simplest process of the methods investigated because no curing is necessary. The process variables that exhibit the greatest affect on the coating properties are the type of sol or solution, the degree of polymerization of the solute, the concentration of the solute, and the drying rate. There are a number of other variables in the coater design, such as the type of rollers, which also affect the coating properties.

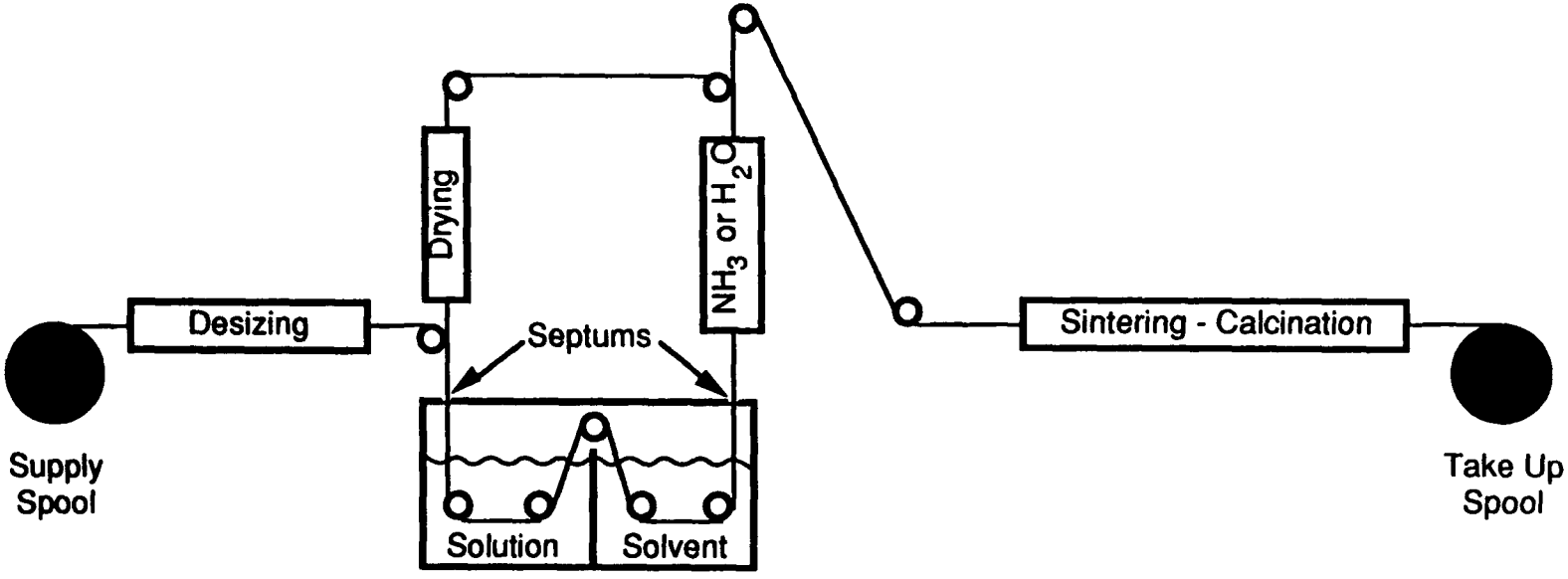




Reservoir:

$$M(OR)_{i(alcohol)} + M_jO_k(OH)_l\bullet Fiber \rightarrow M_{j+l}O_{k+l}(OR)_{(i-1)l}\bullet Fiber + ROH$$

Curing: $M_iO_j(OR)_k\bullet Fiber + H_2O \rightarrow M_iO_j(OH)_k\bullet Fiber + ROH$

Drying: Remove Alcohol Solvent

Calcination: $MO_i(OH)_j\bullet Fiber \rightarrow MO_k\bullet Fiber + H_2O(g)$

Figure 45. REACTION BONDING PROCESS SCHEMATIC AND CHEMISTRY.

The calcination rate, the solvent, the rate of withdrawal, and the residence time in the solution have little affect on the coating properties.

Coatings produced using aqueous or non-aqueous sols typically are smoother and more adherent than coatings produced using aqueous or non-aqueous solutions. However, more bridging and tracking is observed in the higher the degree of polymerization. The bridging and tracking can be reduced by lowering the concentration of the solute and applying more coats. Thus, there is a tradeoff between the smoothness, adherence, and thickness of the coating versus the degree of bridging or tracking. The uniformity of the coating throughout the tow is controlled by the drying rate. A drying rate that is too fast will result in thicker coatings near the surface of the tow, and a drying rate that is too slow will result in thicker coatings in the center of the tow. An intermediate drying rate that achieves uniformity of deposition throughout the tow can generally be found.

The most difficult problem with many of the aqueous sols and solutions as well as the preceramic polymer solutions was maintaining the strength of the fibers. Often the fibers would be embrittled to such an extent that the tow would break during or following the calcination step. The mechanism of this embrittlement has not yet been elucidated. The embrittlement occurs during the calcination step. Embrittlement of the tow was not as significant a problem for highly polymerized sols, but adding a curing step to polymerize the coatings from solutions and slightly polymerized sols before calcining did not eliminate the problem. This embrittlement was prevented by precoating the fibers with several microns of boron nitride by CVD before dip coating with another compound. However, there is no longer any advantage of dip coating if the fibers must be precoated by a CVD process.

The dip coating method requires about ten passes to fabricate a 100 nm coating. This is not difficult for aqueous sols and solutions and non-aqueous polymer solutions that are very easy to maintain. Non-aqueous sols and alkoxide solutions are much more difficult to maintain, and multiple passes are more difficult unless the coating is performed in a dry box. The throughput is limited by either the drying rate and the height of the drying tower or the minimum calcination time and the length of the calcination furnace(s).

## IN-SITU CURING

The in-situ curing coating method is designed to overcome some of the limitations of the simple dip coating process. The process is more difficult to implement than simple dip coating because the curing gases must be excluded from the coating chamber without the tow contacting a roller or septum. This is accomplished by using a diffusion resistance tube and maintaining a flow of gas from the coating chamber into the curing zone. The important processing variables are similar to the traditional dip coating method except that the curing rate is a new critical variable. The curing rate is controlled by the concentration of the curing gas and the reactivity of the solute.

The primary difference between in-situ curing and simple dip coating is that monomers are used in the solution rather than polymers, and that the deposition of coating material occurs while the tow is still wet. Both of these differences reduce the amount of bridging and tracking. As a result, a thicker coating is produced without increasing the degree of bridging or tracking. Many hydroxides, such as yttrium hydroxide, do not form stable, highly polymerized aqueous sols. Because in-situ curing uses metal salts rather than metal hydroxide polymers, deposition from aqueous solution is possible for

these hydroxides. A very important benefit of in-situ curing is that the problem of fiber strength degradation encountered with traditional dip coating is eliminated. The uniformity of the coating throughout the tow is controlled by the reactivity of the solute and the curing rate. A curing rate that achieves uniformity of deposition throughout the tow is not always attainable. Another problem with in-situ curing is that a smoother coating is not always obtained. In some cases the precipitation is so fast that a smooth polymerized coating does not form.

The in-situ curing coating method requires about five passes to fabricate a 100 nm coating. Although fewer passes are required than for traditional dip coating, excluding the curing gas from the coating chamber adds to the complexity. Non-aqueous alkoxide solutions are much more difficult to maintain than the aqueous salt solutions. The throughput is limited by either the curing and drying rate or the minimum calcination time. Thus, the individual tow speed through the coater is lower for the in-situ curing method than the traditional dip coating method with the same total height of the curing and drying tower. However, fewer passes through the coater are required for the in-situ curing method, so the total throughput is similar for both methods.

## REACTION BONDING

The reaction bonding method is designed to achieve a very uniform and very smooth coating without bridging or tracking. The thickness of coating per pass through the coater is reduced compared to the other methods. However, the thickness is larger than might be anticipated. This is because the curing gas is adsorbed by the previous coating layer providing more reactant than expected, and the deposited species have multiple hydroxide or amine groups available for the reaction.

Reaction bonding produces the highest quality coatings provided the tow is completely precoated with a thin layer by one of the previous methods. The smoothness, adherence and uniformity of the coatings produced by this method are significantly improved over the other methods because the coating growth is determined by the availability of reactants on the individual fibers rather than the amount of coating precipitated out of solution. In addition to uniform coating growth, little bridging or tracking occurs because the coating is bonded to the individual fibers. As with in-situ curing, the problem of fiber degradation by the coating process is eliminated.

The reaction bonding coating method requires about fifteen passes to fabricate a 100 nm coating. Additional steps are added to the process by the requirement to produce a thin ~5 nm coating on the fibers first. Furthermore, the process is more difficult to maintain than in-situ curing or simple dip coating because the rinse bath must be replaced periodically to avoid build up of coating precursors, and the precursors are very reactive with water vapor in the air. The throughput is limited by either the reaction time and length of the reaction chamber or the minimum calcination time and the length of the calcination furnace(s). The drying rate and curing rate are no longer limited steps because they can be performed in a horizontal chamber. This flexibility is achieved because the rinsed tow may contact a roller or septum after leaving the coating chamber. The overall throughput is reduced compared to the other methods due to the greater number of dips required.

## CONCLUSIONS

Simple dip coating is the easiest process to implement provided the desired coating qualities can be achieved.

However, problems with bridging, tracking and degrading of the fibers are likely. Also, the sols are often difficult to maintain, and sols of complex oxides with the appropriate stoichiometry in the polymers may be difficult to fabricate. The easiest way to overcome these problems is to use in-situ curing. Mixed oxides are easy to fabricate using in-situ curing, and metal salts may be used as precursors, simplifying the bath maintenance. If problems with the smoothness or uniformity of the coating are encountered using in-situ curing, then reaction bonding may be the solution. Reaction bonding is not particularly useful for multi-component oxides, but reaction bonding is an effective method for improving the smoothness and uniformity of single component coatings.

In-situ curing is the method of choice, because higher coating rates can be obtained without degradation in coating properties. Thus, the continuous coater has been configured for in-situ curing. Although primary emphasis is on in-situ curing, the coater has been built in a very modular fashion that allows coating by any of the three methods. This will allow use of dip coating or reaction bonding if a satisfactory coating cannot be obtained by in-situ coating.

## LIQUID PHASE PROCESS SCALE-UP

The continuous coater was modified to enable coating of full-size spools and multiple passes through the coating chamber before calcining. The modifications allow coating eight layers on tows at a rate of 4 to 6 meters per hour. The flexibility of the coater was improved so that larger curing and drying zones can easily be added to increase the rate to 20 to 30 meters per hour with eight layers and so that in-situ curing and reaction bonding can also be performed in the continuous mode.

Sols from the ethyl hexanoate method were produced for zirconia, hafnia, yttrium aluminum garnet, and titania. Standard dip coating, solvent exclusion, and in-situ curing were tested with these sols. Good coatings were obtained from zirconia and hafnia sols, relatively poor coatings were obtained for yttrium aluminum garnet, and no continuous coatings were obtained for titania. A silica sol was mixed with zirconia sol (from 1 to 5 weight percent silica in zirconia) to determine if zirconium silicate would improve coating density and uniformity. The hafnia sol was also used to obtain a thick (~1 $\mu$m) coating on SCS-6.

Further progress was made on coating of BN from ß-trichloroborazine. However, comparison with coatings made from borazine polymer from the University of Pennsylvania was not possible because the polymer could not be redissolved. A new batch of polymer was received, and a different solvent was ordered.

In-situ curing of stable alkoxide solutions for zirconia, silica, and titania was attempted. Low temperature water vapor was used rather than steam so that the solvent would not be dried before hydrolysis of the alkoxide. High quality coatings were obtained for zirconia, and no continuous coatings were obtained for titania. Hafnia and niobium oxide coatings should also be amenable to this method. Production of niobium sols was initiated.

Composites were fabricated using a CVI silicon nitride matrix and Nicalon with 100 nm coatings of yttria, yttrium aluminum garnet and zirconia. The composites made from coated Nicalon demonstrated no improvement over uncoated Nicalon. (See section of composite fabrication and evaluation.) As a result of a study of the thickness of CVD BN required to obtain maximum improvement in the composite strength, the target coating thickness was increased from 10 nm to 200-500 nm.

The coating conditions for yttria were optimized for the in-situ curing process using a yttrium nitrate coating solution and ammonium hydroxide curing gas. Coating thicknesses of 200-400 nm were achieved using 5 to 8 passes through the coating chamber. Longer coating runs of approximately 10 hours were conducted to prepare for coating entire spools. No significant problems were encountered during the longer runs. End on and transverse scanning electron micrographs (SEM) of a yttria coating on Nicalon are shown in Figure 46. The coating was made using a 0.1 molar yttrium nitrate solution, water saturated ammonia curing, 160°C drying temperature and seven passes through the coating chamber. All of the fibers appear to be coated with at least 300 to 500 nm of yttria, but there is some tracking and some particulate on the surface of the coating. Typically, coating solutions were made using double distilled water. Two solutions were made using the as-received distilled water. In these cases, the coatings were not adherent after several passes through the coater, and the solutions were not as stable. The mechanism of the instability in the solution and the poorer coatings has not been determined.

Zirconia coatings on Nicalon using the in-situ curing process with a zirconia alkoxide solution and a water vapor curing environment were used to coat fabric for composites and to coat monofilaments. The process was transferred to coating tows on the continuous coater. The general operating conditions were elucidated, although optimization is still required. The primary problems were cracking of the coating which was most likely caused by a high concentration of zirconium alkoxide and unstable solutions caused by partial hydrolysis. In addition to coater modifications to exclude water vapor, a lower concentration solution could be utilized to help alleviate these problems.

Figure 46. Scanning electron micrographs (top panel 500X, bottom panel 30,000X) of the yttria coated Nicalon coated continuously from yttrium nitrate coating solution.

Further, development of the liquid phase BN coatings continued with emphasis on obtaining smoother coatings using the ß-trichloroborazine system and testing the University of Pennsylvania's borazine polymer developed by Larry Sneddon. The difficulties with precipitation in the borazine polymer solutions continued and were discussed with Larry Sneddon. His group will study the concerns raised by our owrk in an effort to improve the polymer.

In addition to the problems with hydrolysis of the zirconia sols, other problems encountered with the continuous coater included excessive friction after exposure of the rollers to the solutions and curing gases, too little oxygen in the desizing furnace, and laborious threading of the coater for new runs. Modifications were made to remedy all of these problems: a) The stainless steel rollers were replaced with glass ball modifications and the long eight groove teflon rollers were bored out to allow the glass ball bearing rollers to be press fit into the ends, b) the quartz tube in the de-sizing furnace was replaced with a tube that has larger openings, c) a more efficient method of removing the curing gases from the curing chamber was implemented to avoid hy-drolysis of solutions by diffusion of the gases into the coating chamber, d) containers that can be filled with desiccant were installed around the openings in the coating chamber to prevent water vapor from reaching the non-aqueous solutions, e) the threading of the coater was greatly sim-plified by converting the coating, curing and drying chambers to hinged systems which allow complete access to the rollers during loading. In addition, variable length curing and drying zones were included to allow independent optimization of the curing and drying steps. The new curing and drying zones will enable coating rates to be increased to 8-12 meters per hour with eight passes through the coating chamber.

Samples of Saphikon were coated with 0.5 μm to 1 μm yttria and hafnia coatings for testing in metal matrix composites by Haydn Wadley at the University of Virginia. These complement the zirconia coated Saphikon delivered previously. The yttria coatings were made using an organic acid sol. Yttrium isopropoxide in isopropanol was reacted with ethyl hexanoic acid. The resultant polymers precipitated, and a mixture of toluene and water was added to bring the yttrium compound back into solution. A SEM of yttria coating on Saphikon is shown in Figure 47. This coating was made using five passes through the coating solution for a total thickness of 460 nm. The yttria coated Saphikon fibers sent to UVA were made using six passes through the coating solution. The hafnia was also made from an organic acid sol. Hafnium tert-butoxide in t-butanol was reacted with ethyl hexanoic acid. No precipitation was seen in the resultant sol, so the toluene and water mixture was not required. A SEM of a hafnia coating on Saphikon is shown in Figure 48. Coatings of approximately one micron were obtained on the Saphikon using five passes through the coating solution. For both the hafnia and the yttria coatings, the filaments were heated to 500°C in air between coating passes to oxidatively remove the organics. After the final coat, the filaments were heated to 800°C to insure the oxide was obtained.

A significant development was a modification to the coater which greatly improved the oxide coatings from nitrate solutions. Smooth yttria and zirconia coatings can now be routinely obtained throughout long coating runs. Work on BN coatings from the University of Pennsylvania's polyborazine precursor was completed with the determination that the system is not satisfactory for coating tows and fabric. The University of Virginia, therefore, received yttria, zirconia, and hafnia-coated Sophikon samples for examination in MMCs.

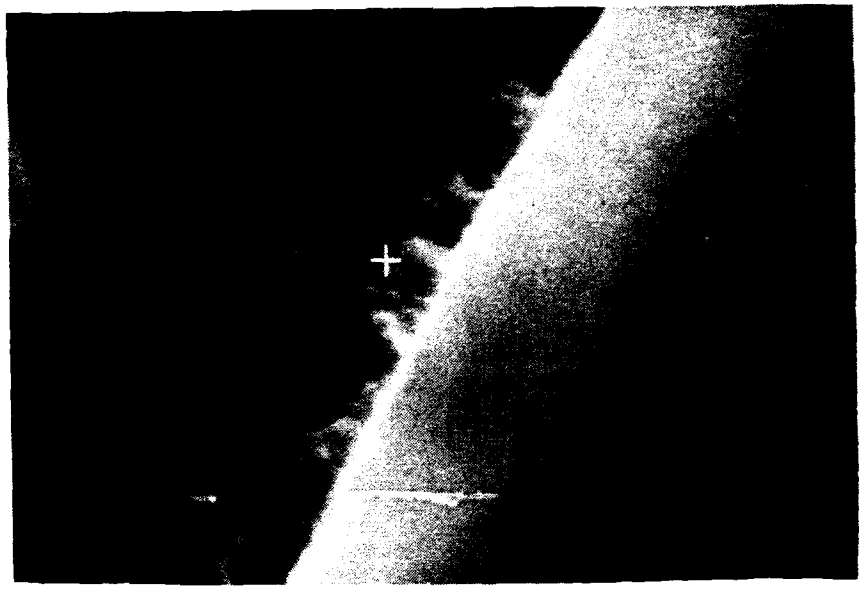

Figure 47. Scanning electron micrograph (20,000X) of yttria coating on Saphikon fiber. Coating is approximately 0.5 μm thick.

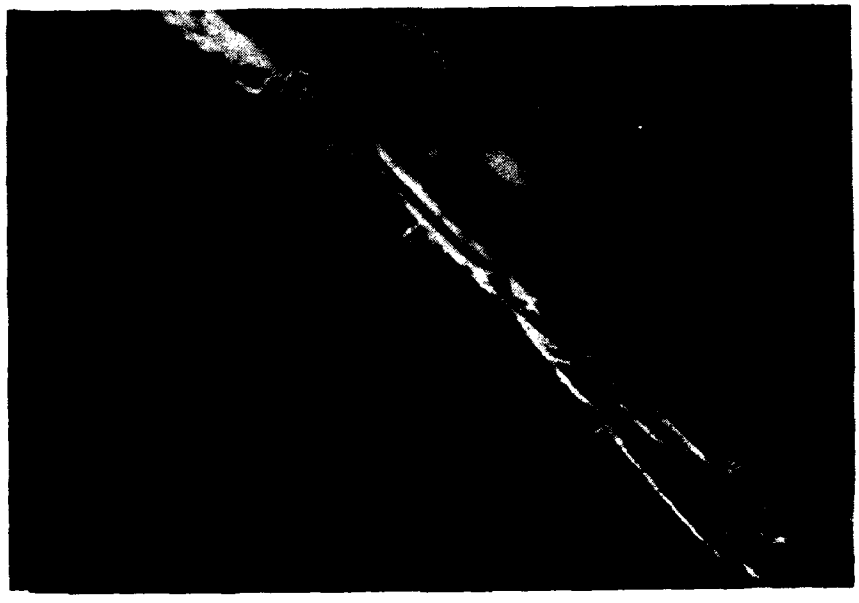

Figure 48. Scanning electron micrograph (10,000X) of hafnia coating on Saphikon fiber. Coating is approximatley 1 μm thick.

All of the modifications to the coater outlined previously proved successful, except the inclusion of desiccant containers on the openings to the coating chamber. The desiccant containers were not incorporated into the coater because the aqueous phase coatings for both yttria and zirconia were improved enough that non-aqueous coating methods are not warranted. One significant change was made to the coater which greatly improved the quality of the coatings. The solution is now continuously pumped into and out of the coating chamber, and the solution leaving the coating chamber is returned to a specified pH. As described below in the paragraphs on yttria and zirconia coatings, this change has resolved the problems with tracking, bridging, and particulate on the coatings.

The coating conditions for yttria and zirconia were optimized for an in-situ curing process using a yttrium nitrate coating solution and ammonium hydroxide curing gas. The optimum curing and drying conditions are saturated ammonia curing with a 160°C drying temperature. Eight passes through the coating chamber were used to obtain all coatings. A problem with the coating system was discovered when the run time was increased to 24 hours. The pH gradually rises during coating runs, and for 24 hours or longer the increase in pH causes the coating quality to significantly deteriorate and the solute to precipitate. The increase in pH of the coating solution is caused by ammonia which reaches the solution in two ways: diffusion from curing zone into the coating chamber, and transport of absorbed ammonia by the fibers into the coating solution. The diffusion from the curing zone into the coating chamber is minimized by maintaining a nitrogen flow out of the coating chamber, and by forced convention of air and ammonia to the top of the coating zone. The adsorption of ammonia on the fibers is likely to improve the coating uniformity and increase the coating thickness because the solute will react with the ammonia and cause precipitation near the fibers. Attempts to alleviate this problem by mixing the solution and

monitoring the pH improved the coatings, but the mixing was insufficient to disrupt pockets of high and low pH. Therefore, the solution was continuously pumped into and out of the coating chamber, and the pH was monitored and adjusted before flowing used solution back into the chamber. This process solved the problems created by the increasing pH and provided another variable for control of the coating quality.

Coatings of yttria on Nicalon were prepared after making the adjustments to the coating procedure described above. The resultant coatings were smooth and continuous, but the thickness was less than ~50 nm. A transverse scanning electron micrograph of yttria coated Nicalon from a 0.05M yttrium nitrate solution with a pH of 3.7 is shown in Figure 49. Increasing the concentration of yttrium nitrate to 0.10M resulted in 150 to 300 nm thick coatings, but there was a large amount of tracking. Transverse and end-on SEMs of yttria-coated Nicalon prepared from a 0.10M yttrium nitrate solution with a pH of 3.7 are shown in Figure 50. Using a 0.05M yttrium nitrate solution and increasing the pH to 6.0 resulted in smooth continuous coatings which were 150 to 300 nm thick. Transverse and end-on SEMs of a yttria coating on Nicalon using 0.05M yttrium nitrate solution at a pH of 6.0 are shown in Figure 51. All the fibers appear to be coated and there is very little bridging, tracking, or particulate on the coating.

The zirconium nitrate solutions are much lower in pH and are more sensitive to slight increase in pH than yttrium nitrate solutions. These differences appear to be the cause of poor coatings previously obtained from zirconium nitrate solutions. After incorporating adjustments to the coating system, quality of coatings obtained from zirconium nitrate solutions dramatically improved. A transverse SEM of a zirconia coating on Nicalon prepared from a 0.07M zirconium nitrate solution and a pH of 1.9 is shown in Figure 52. The coatings are smooth and continuous with very little tracking or particulate.

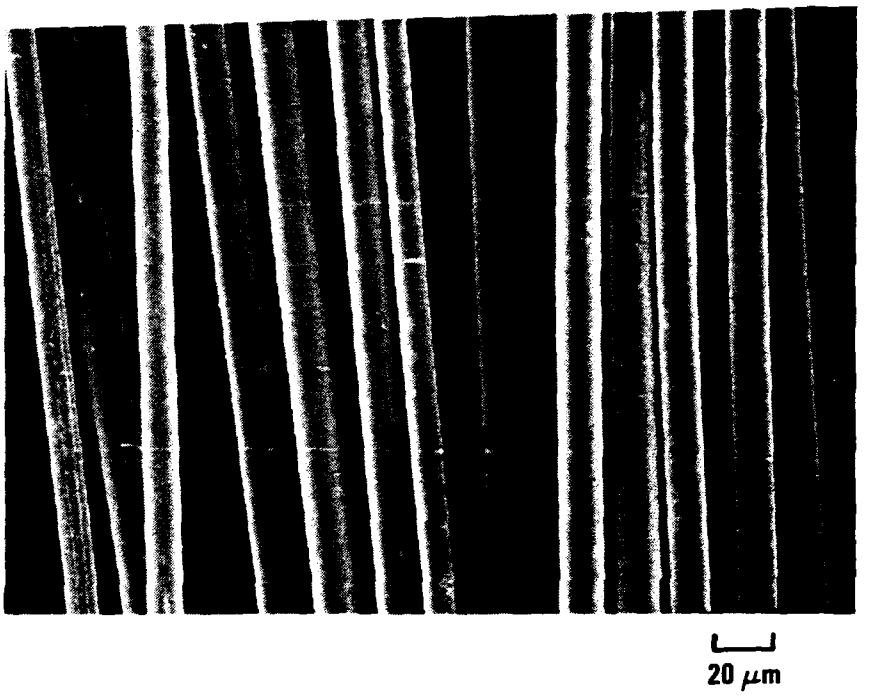


Figure 49.- Scanning electron micrograph of a yttria coating on Nicalon from a .05M, 3.7pH yttrium nitrate solution

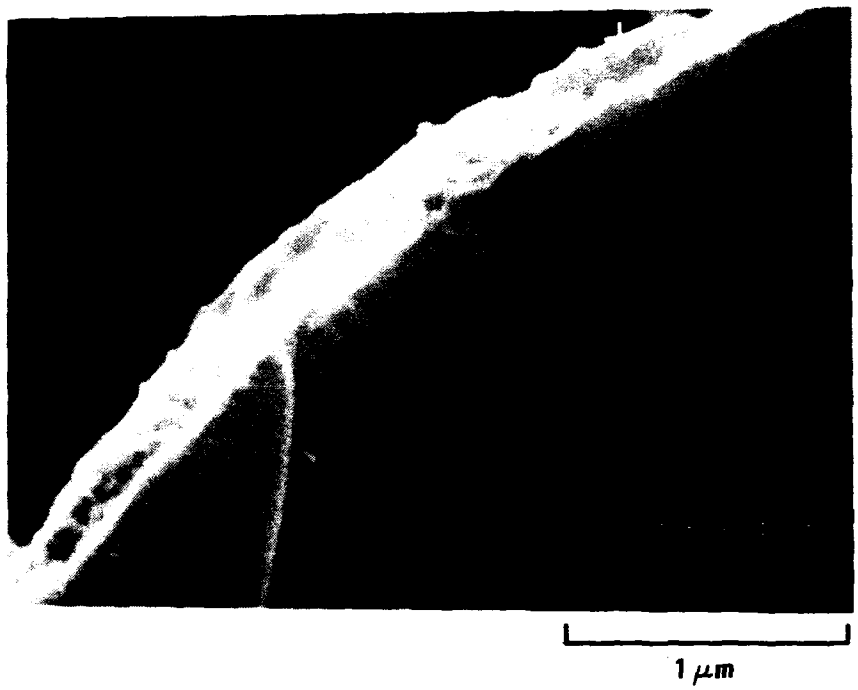


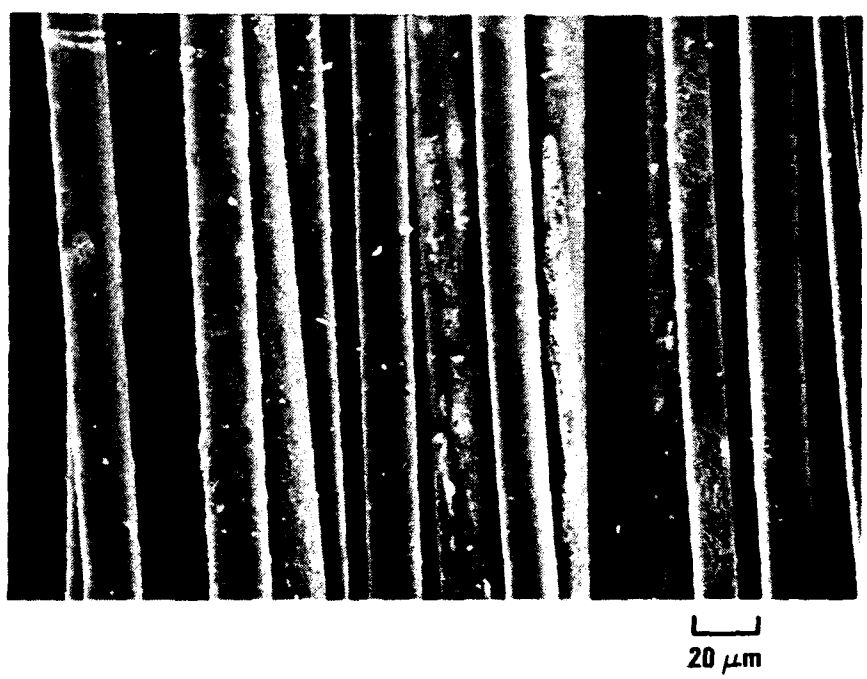


Figure 50.- Scanning electron micrograph of a yttria coating on Nicalon from a .10M, 3.7pH yttrium nitrate solution

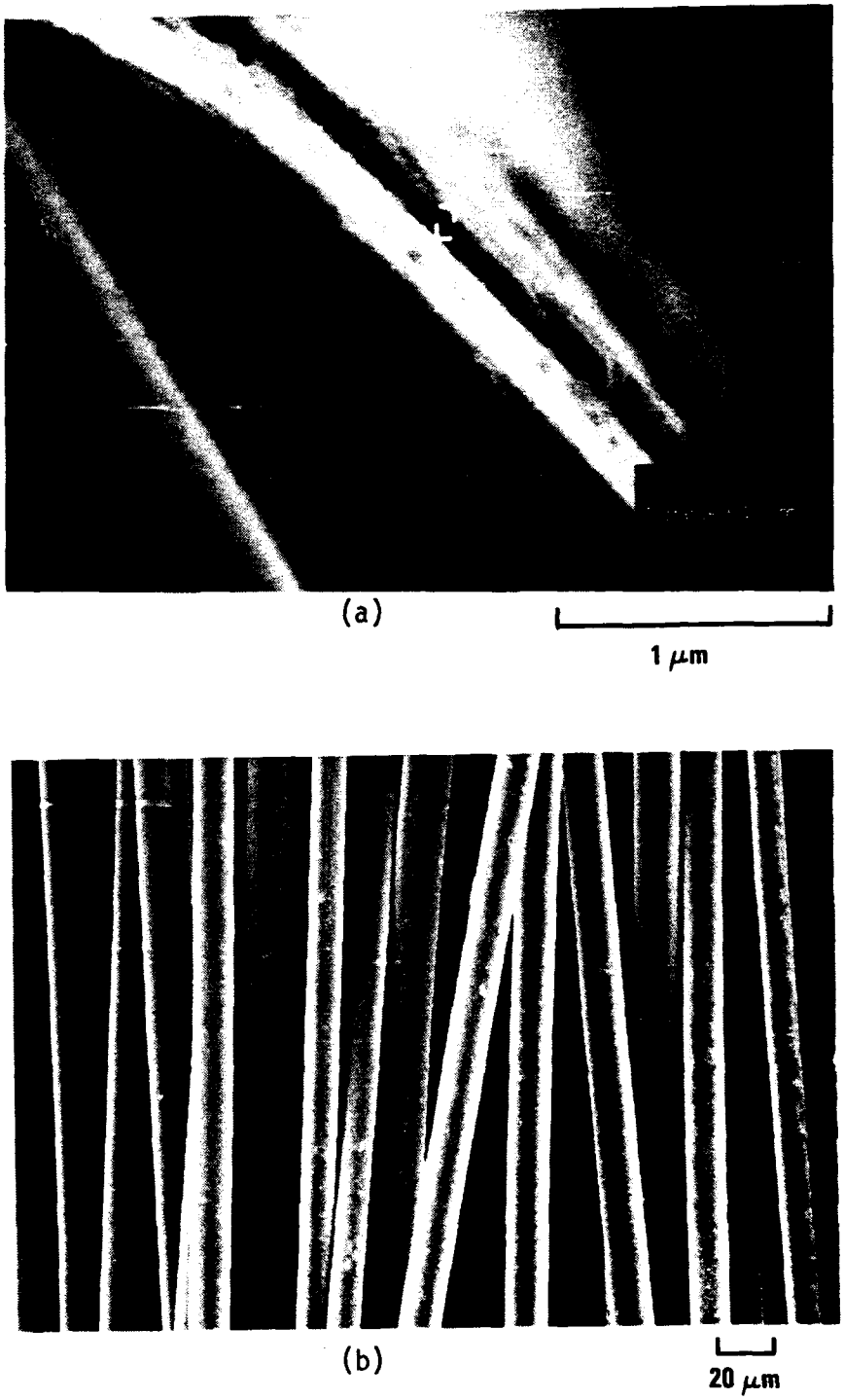


Figure 51. - Scanning electron micrograph of a yttria coating on Nicalon from a .05M, 6.0pH yttrium nitrate solution: a) end on view b) transverse view

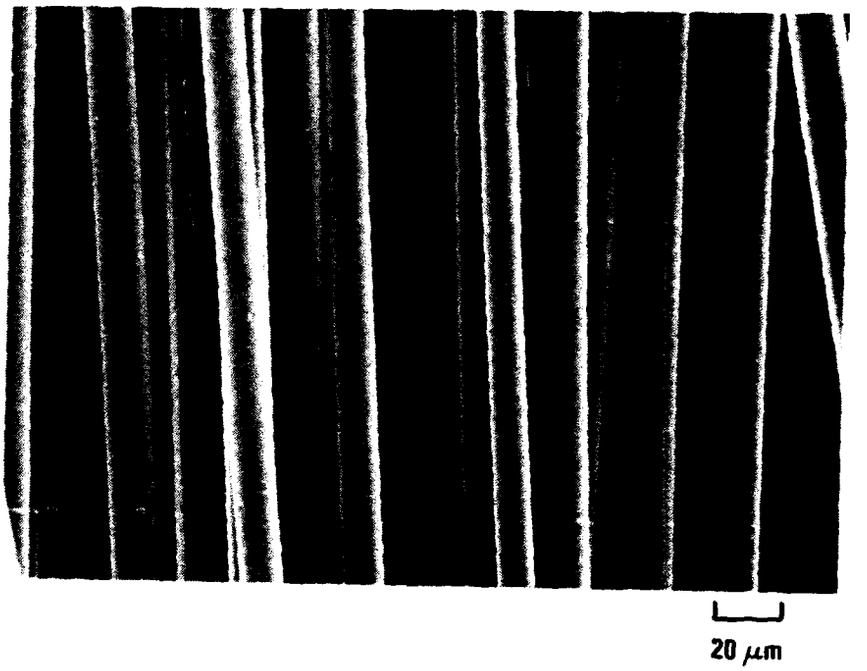


Figure 52.- Scanning electron micrograph of a zirconia coating on Nicalon from a 0.07M, zirconium nitrate solution

The strengths of as-received, desized, uncoated control (sent through coater with water as coating solucion), yttria coated (0.05M, 3.7 pH; 0.05M, 6.0 pH, and 0.10M, 3.7pH), and zirconia coated Nicalon fibers are presented in Table 9. The desized fibers are weaker than the as-received, but the uncoated control is stronger. A possible explanation for this discrepancy is that the silica layer which forms on the surface of the fiber during the calcining stage (800°C in air) heals surface flaws. The high strength of the uncoated control sample demonstrates that passing through the coater does not significantly degrade the fiber strength. The coated fibers have strengths approximately equal to the desized fiber. This may be because the coating blocks the silica on the fiber surface from flowing, thus surface flaws on the fibers are not healed. The high strengths demonstrate that the coatings and coating process do not significantly degrade the fibers.

Coatings were prepared and tested using the University of Pennsylvania's borazine polymer developed by Larry Sneddon. The difficulties with precipitation in the borazine polymer solutions were resolved, and ethylene glycol dimethyl ether distilled over sodium was used as the solvent. A transverse SEM of the coatings is shown in Figure 53. The coatings are heavily bridged with some tracking. Concentrations from 1.5% to 10%polyborazine were used, resulting in coating thicknesses of 100 to 600 nm. In all cases, the coatings were highly bridged. Another problem with this system is that the coating appears to react with the Nicalon fibers, dramatically weakening them. As a result of these problems, this coating system will not suffice for the coating of fabric and tows.

Good zirconia and yttria coatings were obtained using the continuous fiber coater as a result of improvements in coater design. A small scale continuous fabric coater was designed using these improvements and constructed to demonstrate that high quality coatings can be obtained on fabric . The fabric

| NICALON FIBER AND CONDITION | NUMBER OF TESTS | AVERAGE FAILURE LOAD (g) | STANDARD DEVIATION | AVERAGE TENSILE STRENGTH ($Kg/mm^2$) |
|---|---|---|---|---|
| AS RECEIVED | 15 | 50 | 10 | 454 |
| DESIZED (500°C/AIR: $O_2$) | 14 | 45 | 13 | 412 |
| CONTROL FOR CONTINUOUS COATER | 14 | 60 | 11 | 549 |
| $Y_2O_3$ (0.05 M/pH 3.7) COATED CONTINUOUSLY (800°C/AIR) | 15 | 43 | 15 | 394 |
| $Y_2O_3$ (0.05 M/pH 6.0) COATED CONTINUOUSLY (800°C/AIR) | 15 | 40 | 10 | 364 |
| $Y_2O_3$ (0.10 M/pH 3.7) COATED CONTINUOUSLY (800°C/AIR) | 14 | 48 | 16 | 439 |
| $ZrO_2$ (0.07 M/pH 1.9) COATED CONTINUOUSLY (700°C/AIR) | 14 | 41 | 11 | 375 |

K-020(16)
10-18-91

Table 9 - Strength comparison of as received, desized, control and coated Nicalon fibers.

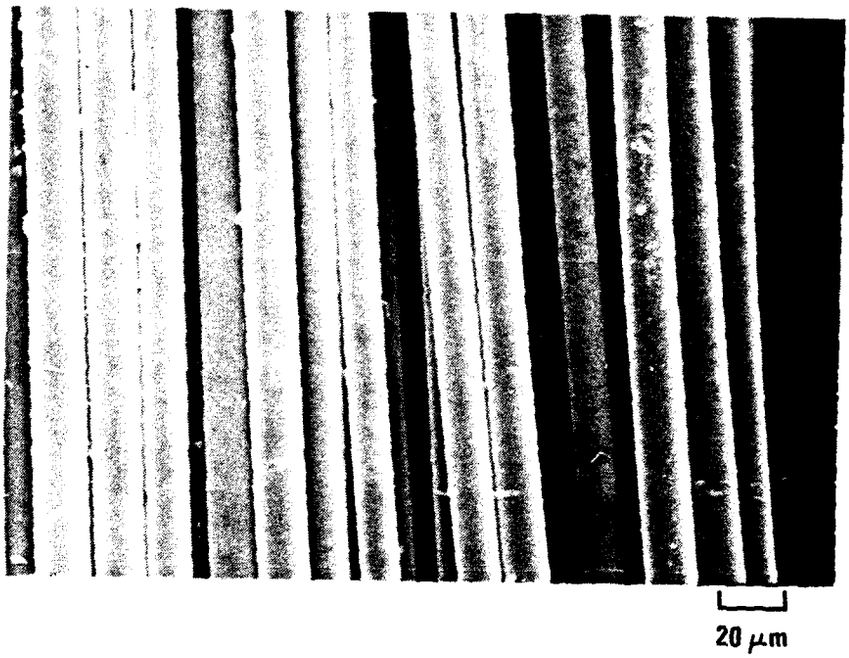


Figure 53. Scanning electron micrograph of a boron nitride coating on Nicalon from a 30 wt% polyborazine solution

coater will potentially increase the throughput by several orders of magnitude over the single tow fiber coater.

Two BN precursors and processes were selected for use with the continuous fiber and fabric coaters. One precursors is a preceramic polymer, polyborazylene, and the other is a monomemic compound, ß-trichloroborazine. Both of these are amendable to simple dip coating processes with no curing between dips. The lack of a curing step is critical because it greatly simplifies the shielding of these very reactive compounds from water vapor and ammonia.

FABRIC COATER

A conceptual design of the continuous fabric coater is illustrated in Figure 54. The small scale coater built can accomodate fabric widths of up to 15 cm; however, the basic design can readily be scaled to full width fabric with no significant modifications. The as-received fabric travels from supply spool 1 through the desizing furnace to the take up spool. Then the spool is moved to supply spool 2. The fabric travels from supply spool 1 through the coating, curing and drying chambers four times, and subsequently through the calcining furnace to the take up spool. Curing gases are pumped between each layer of fabric into and out of the curing chamber at the bottom and top, respectively. There are panel heaters on the interior of the curing chamber and between each fabric layer to maintain the appropriate temperature. The drying chamber has heaters on the interior walls and between each of the fabric layers moving through the drying chamber. In the coating chamber, fresh solution is continually pumped above the top fabric layer, below the bottom fabric layer and between each layer of fabric. The pH of the exiting fluid is adjusted to the operating value and recycled through the coating chamber. Although the residence times of each pass are slightly different, residence time does not affect the

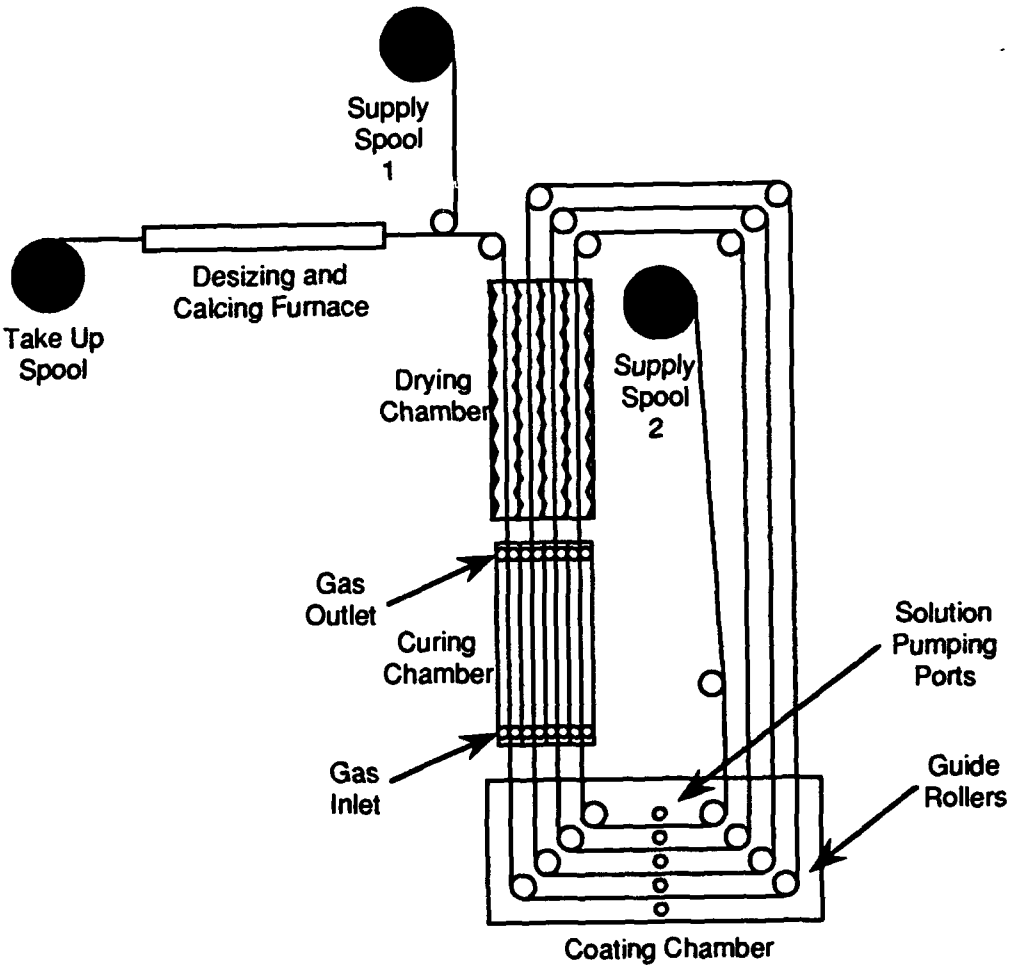


**Figure 54..** Conceptual design of liquid-phase continuous fabric coater.

coating thickness or quality unless it is so short that all the air trapped in the weave is not displaced.

## BN LIQUID PHASE COATINGS

Several polymeric and molecular precursors were experimentally evaluated. One polymeric and one molecular precursor were found to produce good coatings on Nicalon fabric and tows. The polymer precursor selected was polyborazylene. For molecular precursors, a simple dip coating process with ß-trichloroborazine solutions was the best overall system when evaluated with regard to coating quality, ease of processing, and safety. Both of these precursors have the advantage that no curing gas is needed in the coating zone, so protection of the coating bath from curing gases and water is greatly simplified. However, the polyborazylene is extremely sensitive to water contamination.

Polymers tested were Dietmar Seyferth's decaborane based precursor. One to five weight percent solutions of the decaborane based polymer in dimethylformamide (DMF) and hexamethylphosphoramide (HMPA) were used. A scanning electron micrograph of a coating on Nicalon from the decaborane polymer system is illustrated in Figure 55. The fiber tows were dipped 3 times in a 1 weight percent solution of the polymer in HMPA and heated to 300°C for 3 minutes between dips. The polymer was calcined by heating to 1000°C for 2.5 hours in a flowing ammonia atmosphere. The tracking parallel to the fibers is evident on all of the fibers. The coatings are also exceptionally thin. Higher weight percent solutions or more dips to increase the thickness leads to more tracking and agglomerates on the fibers.

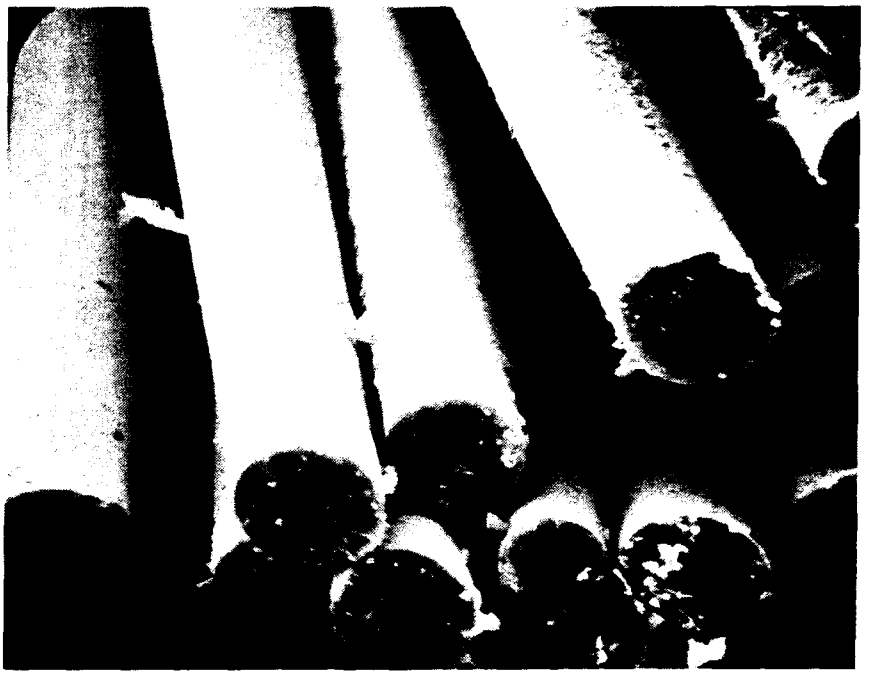

Figure 55. Scanning electron micrograph of BN-coated Nicalon derived from decarborane polymeric precursor (1000X).

Figure 56. Scanning electron micrograph of BN-coated Nicalon derived from polyborazylene precursor (4.5KX).

Larry Sneddon's polyborazylene precursor was also used to coat Nicalon. Coatings from the polyborazylene were made by dip coating in 0.5 to 1.5 weight percent solutions in dry glyme. A SEM of a fiber from Nicalon fabric coated using the polyborazine precursor is shown in Figure 56. This fabric was dip coated 3 times in a 1.5 weight percent solution and dried at 90°C between dips. The fabric was then heated to 1000°C in argon to convert the polymer to BN. Typically, coated fabric from 1.5 weight percent solutions exhibited a large amount of bridging and tracking. However, the bridging and tracking could be reduced by using a less concentrated solution and more dips.

While there are numerous boron/nitrogen containing compounds, two primary hurdles must be overcome in the development of liquid phase monomer precursors for BN coatings. First, if the precursor contains significant amounts of carbon, then carbon contamination of the BN is likely. Second, the compound must have a low vapor pressure during the pyrolysis to convert it to BN. In addition to these criteria, a precursor without potentially toxic vapor release was preferred to minimize the added safety requirements on the coater design. Although Larry Sneddon's group at the University of Pennsylvania had some success with the dibromoborane-dimethyl sulfide complex, it was not included in our initial study because of safety considerations. Three compounds were utilized in our study: ß-trichloroborazine, borane-tert-butylamine complex, and boric acid. The borane-tert-butylamine complex has the advantage that it does not react with water and in fact is soluble in water to some extent. The ß-trichloroborazine has a higher boron and nitrogen content and does not contain carbon. The boric acid has the advantage of easy processing, but the disadvantage of difficult conversion to BN.

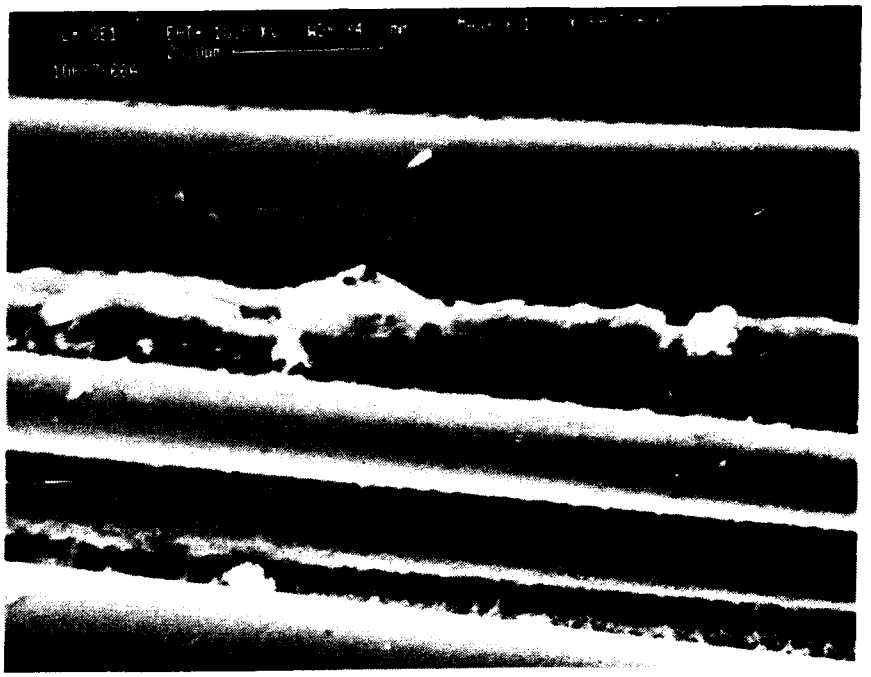

Figure 57. Scanning electron micrograph of Nicalon coated using the borane-tert-butylamine complex (1000X).

Coatings derived from the borane-tert-butylamine complex were attempted using standard dip coating and in-situ curing. One to twenty weight percent solutions of the compound in water, tetra- hydrofuran, toluene, xylene, glyme, pyridine, and methanol were tested. The results were disappointing because energy dispersive X-ray (EDX) analysis has shown little or no boron in most of the coatings. The coatings seem to the primarily silicon pulled from the fibers and bound with oxygen and nitrogen. A SEM of a Nicalon tow coated from a 10 weight percent solution in pyridine is shown in Figure 57. The fibers were coated by dipping 4 times in a 20 weight percent solution in methanol and drying for 5 minutes at 220°C between each dip. The coatings were pyrolyzed in flowing ammonia at 1050°C for two hours. Although not representative of our high-quality coatings, this micrograph is exemplary of the potential problems with all coatings. Obviously there is coating material between the fibers, but EDX analysis of the coating, shown in Figure 58, reveals no boron, little to no carbon, and plenty of nitrogen and oxygen. The higher energy EDX analysis revealed a large amount of silicon in the coating. Thus, the borane-tert-butylamine complex is not a good precursor for BN coatings.

Coatings derived from ß-trichloroborazine were fabricated by using in-situ curing, reaction bonding and dip coating. In each case, the precursor coated fiber was pyrolyzed in ammonia at 1000°C for 30 minutes. The in-situ curing process involves infiltrating the tow with a solution of ß-trichlorborazine and curing the wet tow with ammonia to cause a low molecular weight amino borazine polymer to precipitate onto the fibers. Reaction bonding involves first putting down a thin coating with free amine groups either by in-situ curing or by dip coating, drying and curing. The coating is then allowed to react with ß-trichloroborazine in solution, the excess solution is rinsed off, the rinse solvent is dried, and the newly added ß-trichloroborazine is cured and dried again. The coating growth is not limited to monoatomic layers because

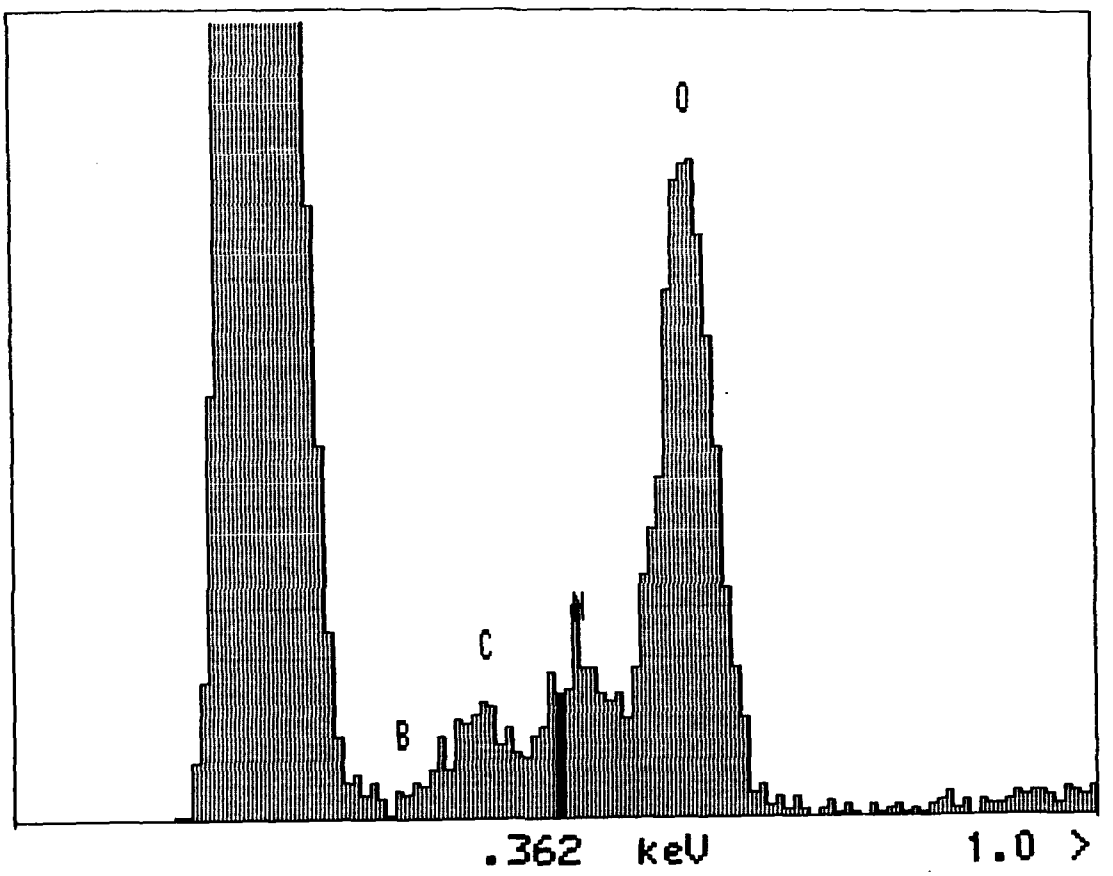


Figure 58. Low energy EDX analysis of coating shown in Figure 24.

adsorbed ammonia is allowed to remain providing more reactant on the fiber than just the surface aminoborazine groups. The simple dip coating process involves dipping in a ß-trichloroborazine solution and drying and pyrolyzing at 300°C to 500°C in an inert atmosphere between dips.

The quality of the coatings from the three methods with the ß-trichloroborazine precursor were similar. The dip coating process significantly reduces design complications because no ammonia is utilized near the coating chamber. The exclusion of ammonia and safety considerations give the ß-trichloroborazine process an advantage over the dibromoborane-dimethylsulfide complex process. Therefore, the ß-trichloroborazine dip coating process was chosen as the monomer precursor process.

Nicalon fibers were continuously coated with yttrium and zirconium oxide using an in-situ curing technique. The yttria coatings were derived from yttrium nitrate and the zirconia coatings were made from zirconyl nitrate. Both are relatively easy to work with and moderately stable, two conditions which are important for continuous coating.

The affect of the pH of the coating solution on the quality of the final coating was investigated. A Markson pH meter was inserted into the coating solution through a hole in the top of the coating box and the pH was continuously monitored throughout the coating runs to control the stability and uniformity of the coating solution during coating. This was necessary because during coating the ammonia from the curing zone wicks down the fibers and into the solution box. As the coater was run, the pH of the solution increased and eventually a precipitate formed in the solution. To prevent this occurrence, the solution was simultaneously pumped in and out of the solution box using a dual, reversible peristaltic pump. The pH of the solution going into the coating box was adjusted to a desired pH using dilute nitric acid. The

solution coming out of the coating box was collected in a separate reservoir. When the supply of solution was depleted, the pH of the solution in the reservoir was adjusted and the pump was reversed so the solution in the reservoir became the supply solution. The flow of the solution going into the coating box, approximately 100ml/min, was used to mix the solution.

## YTTRIUM OXIDE COATINGS

The quality of the yttrium oxide coatings was determined to be dependent not only on the concentration of the coating solutions but also on the pH of the solution. Previous work had shown that coating solution concentrations around 0.05M resulted in uniform, smooth, thin coatings. An increase in concentration to 0.1M led to thicker but highly tracked and rough coatings. By adjusting and maintaining the solution pH above 3.7, the pH of the 0.05M solution as prepared, the thicknesses of the coatings were increased. Continuous coating runs were performed with the solution pH ranging from 4 to 6. Increasing the pH of the solution led to an increase of coating thickness. Figure 59 shows Nicalon fibers continuously coated eight times with yttria using in-situ curing. The coated fibers in the top panel of Figure 59 were coated in a 0.05M yttrium nitrate solution with a pH of 3.7, which is the pH of the solution after preparation. The coated fibers in the bottom panel of Figure 59 were also coated with a 0.05M solution but the pH was adjusted to 6. Both sets of coated fibers were smooth with only a small amount of tracking. EDX, shows the presence of yttrium on all of the fibers examined.

Figure 60 is an end on view of a yttria coated fiber continuously coated eight times with 0.05M solution of pH 6. Measuring from micrographs, the coating thicknesses ranged from 170 to 270 nm. The resolution of SEM was too low to distinguish the coating prepared from the 0.05M solution at pH 3.7

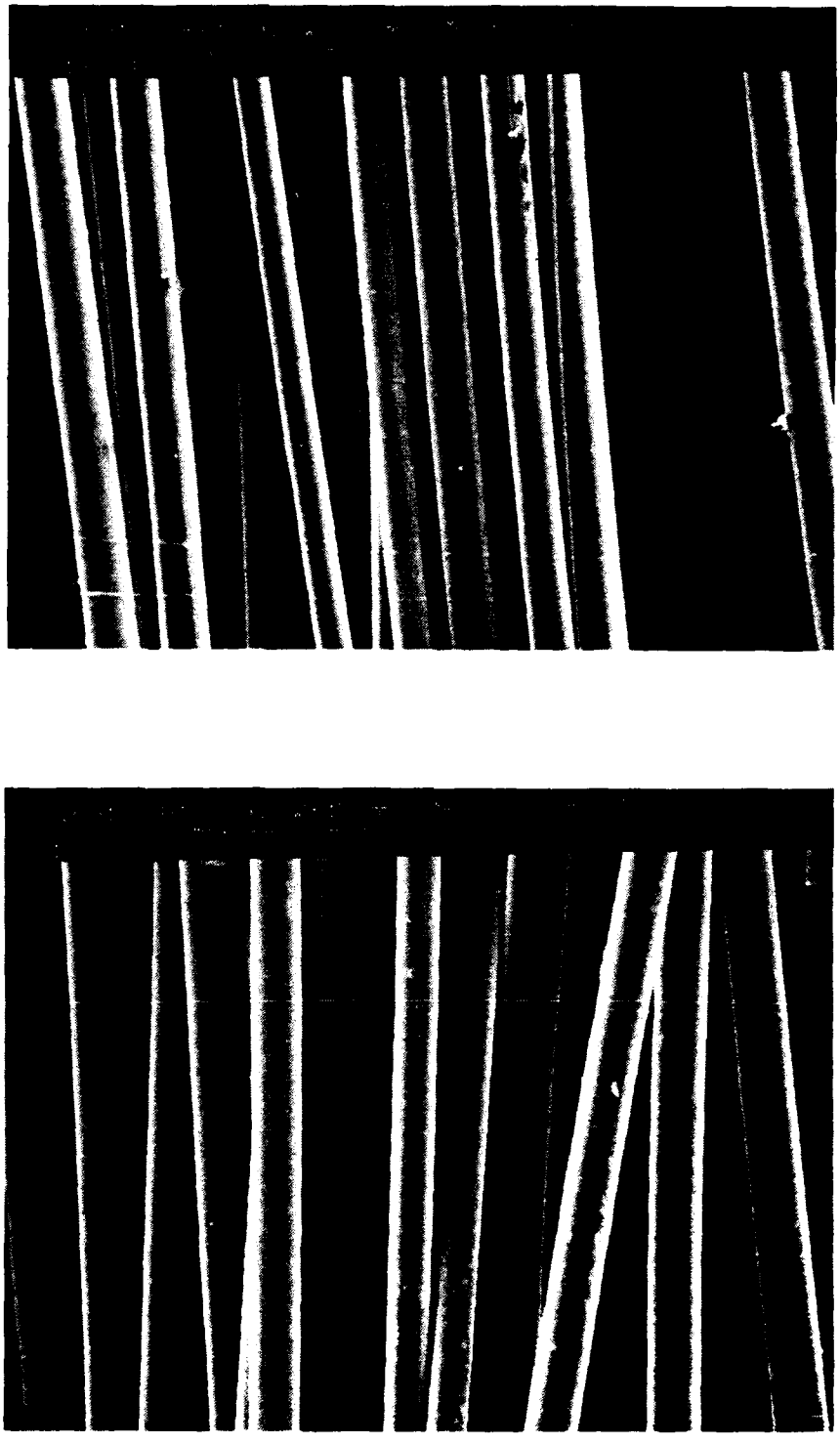

Figure 59. Scanning electron micrographs of continuously coated yttrium oxide on Nicalon. Top panel 0.05M solution, pH 3.7. Bottom panel 0.05M solution, pH 6.

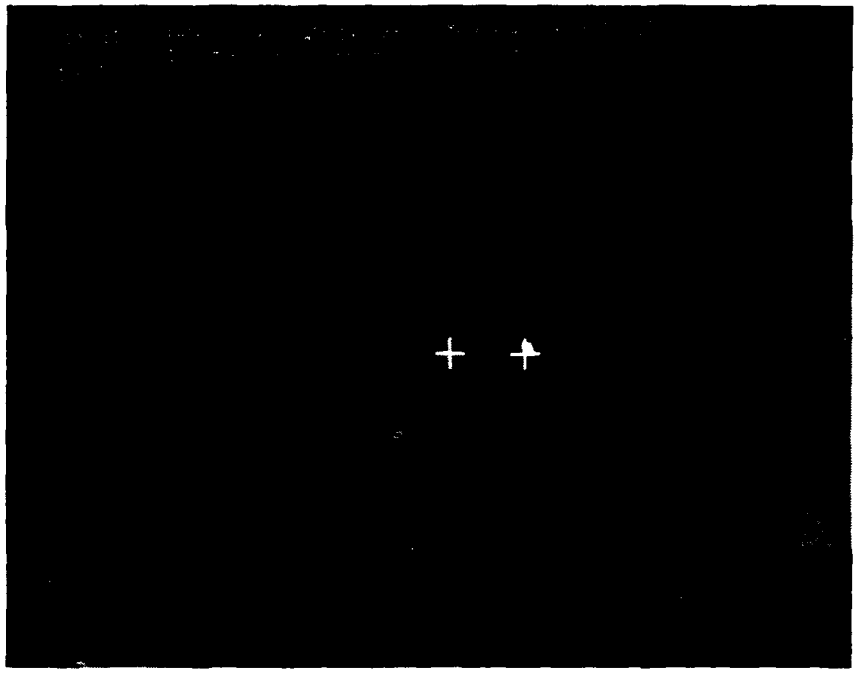

Figure 60. Scanning electron micrograph of continuously coated yttrium oxide on Nicalon from 0.05M solution adjusted to pH 6.

Figure 61 shows coated fiber of a continuous coating run which lasted for 9 hours with a coating rate of 4 m/hr. The pH was maintained at 5. These coatings are smooth with very little tracking but there is a slight amount of debris on the surface. The coating thicknesses ranged from 120 to 300 nm. Figure 61 (lower panel) is a micrograph showing the coating thickness of a yttria coated fiber.

## ZIRCONIUM OXIDE COATINGS

Adjusting the pH for the zirconia coating solutions was not necessary since the affect of the ammonia appears to be negligible due to the low pH of the starting solutions. Figure 62 (top panel) is a micrograph of continuously zirconia coated Nicalon fiber which passed through the coating solution eight times. The coatings are smooth but have a small amount of tracking. EDX verified the existence of zirconium on all of the fibers examined. Measuring from Figure 62 (bottom panel), a micrograph of a zirconia coated Nicalon fiber looking end on, the average coating thickness is about 300 nm. These fibers represent the end of a run in which Nicalon fiber was continuously coated with zirconia for 19 hours at a rate of 6 m/hr producing about 114 meters of coated fiber.

## SOLUTION COATING OF BORON NITRIDE

Nicalon fibers were dipped multiple times into various concentrations of polyboraxylene dissolved in either sodium dried glyme, sodium dried toluene or sodium dried tetrahydrofuran. These fibers were dipped and dried in a glove box. They were subsequently calcined in either ammonia or argon for 1 hour at 1000°C under vacuum. In all cases, EDX showed a substantial amount of oxygen present. The same result was obtained when carbon fibers were substituted for the Nicalon, indicating the oxygen did not originate from the substrate fiber.

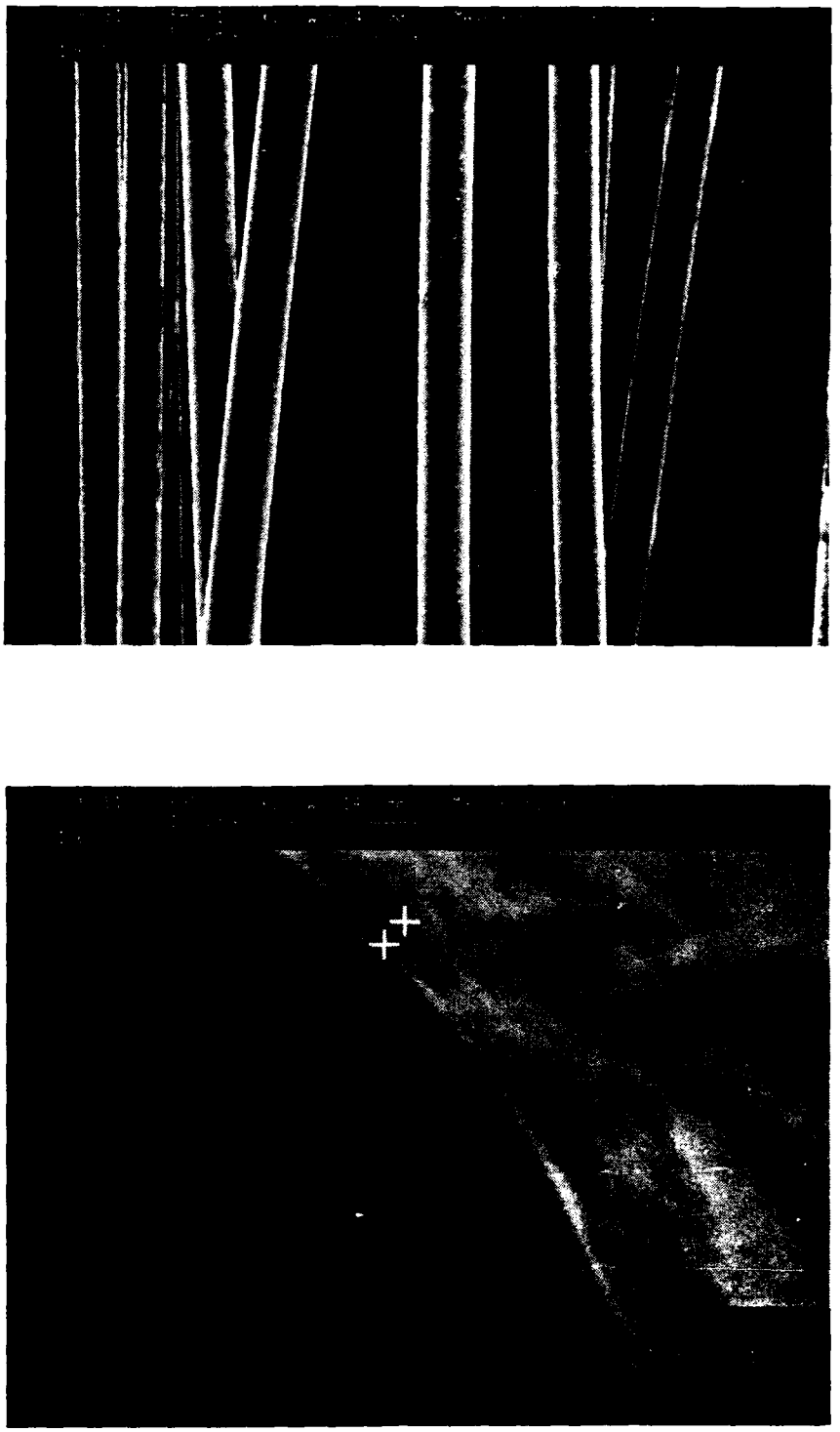

Figure 61. Scanning electron micrographs of continuously coated yttrium oxide on Nicalon from 0.05M solution adjusted to pH 5. Top panel: side view. Bottom panel: end view.

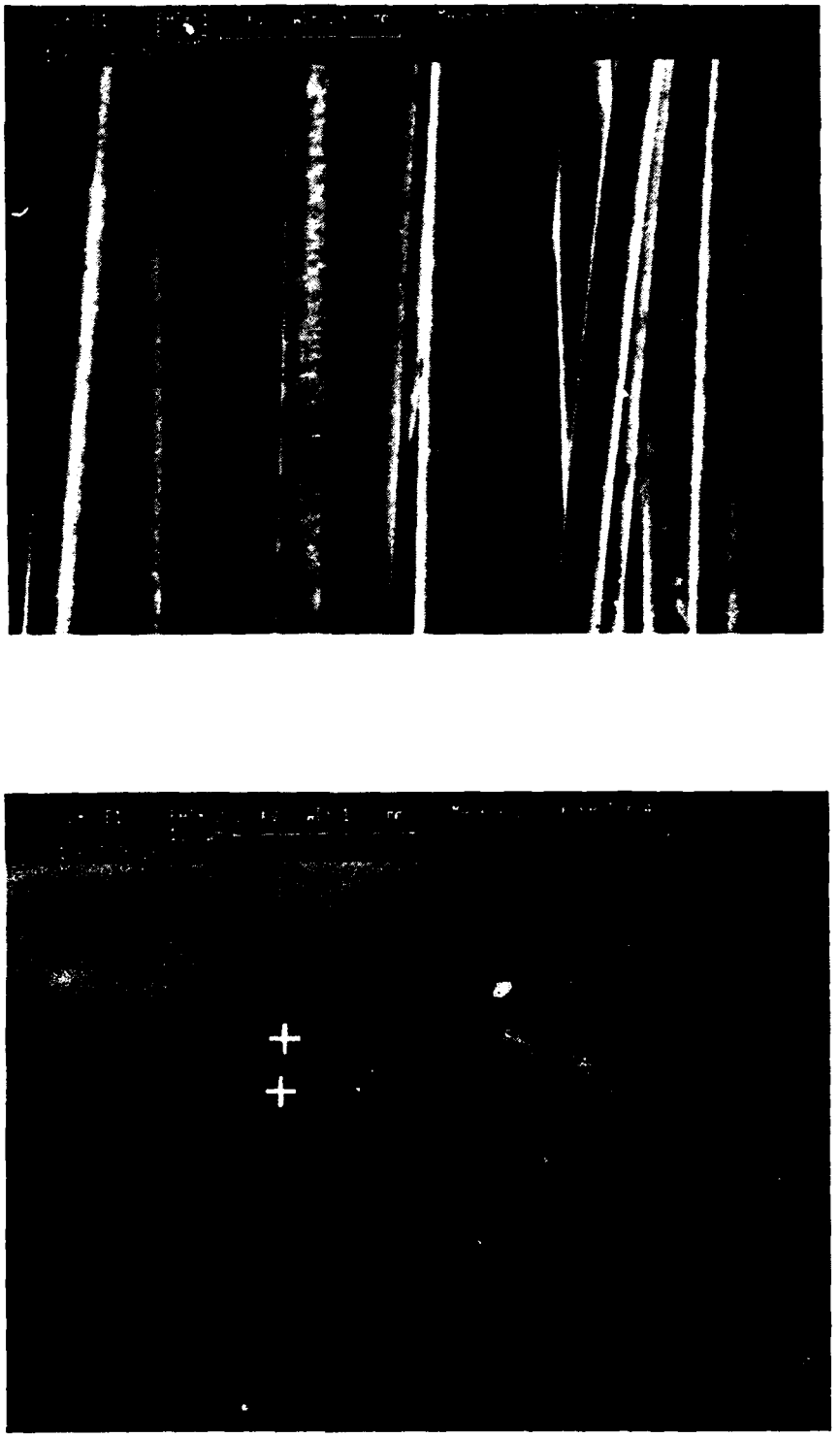

Figure 62. Scanning electron micrographs of continuously coated zirconium oxide on Nicalon from 0.04M solution adjusted to pH 1.8. Top panel: side view. Bottom panel: end view.

Other attempts to solution coat boron nitride onto Nicalon were made using beta-trichloroborazine in chlorobenzene. Multiple dips of the fibers into the solution with a drying step in between each dip were performed in the glove box. The coated fibers were calcined at 1000°C for 1 hour in high purity argon. Again EDX showed a large amount of oxygen present in the coatings.

## TASK 2-3 COMPOSITE FABRICATION AND EVALUATION

Coated fiber tows were infiltrated with $Si_3N_4$ matrix by chemical vapor deposition in order to investigate fiber matrix interactions. Fibers for this study included Nicalon, HPZ and T-300. Coatings included BN, SiC and a dual coating of BN and $Si_3N_4$.

The aim of this study was to investigate the behavior of the coated fibers in a silicon nitride matrix, in regards to strength and fiber pull-out, which is an indication of toughness. Three point bend tests were performed on specimens that were cut from these tows. These tests do not conform to standard test conditions but were performed only in order to compare these materials with each other. The strength values in Table 10 have to be viewed in this context. After the 3-point bend tests, the fracture surfaces of the samples were examined by SEM in order to investigate any fiber pull-out. Table 10 summarizes the results of these investigations.

TABLE 10. Flexural strength and pull-out of different fiber/coating combinations with a silicon nitride matrix.

| FIBER | COATING | MATRIX | STRENGTH (MPa) | PULL OUT |
|---|---|---|---|---|
| Nicalon | BN | $Si_3N_4$ | 737 | bi modal |
| Nicalon | $BN/Si_xN_y$ | $Si_3N_4$ | 786 | little |
| Nicalon | SiC | $Si_3N_4$ | none | none |
| T-300 | BN | $Si_3N_4$ | 504 | extensive |
| HPZ | BN | $Si_3N_4$ | none | little |
| HPZ | SiC | $Si_3N_4$ | none | none |
| HPZ | $BN/Si_xN_y$ | $Si_3N_4$ | none | none |

Of the tested materials only three show promising strength. The T-300 with a BN coating in a $Si_3N_4$ matrix shows less strength than the Nicalon coated with BN or with a dual coating of $BN/Si_3N_4$ in the same matrix, but displays greater pull-out, which is an indication of higher toughness. The other materials, as can be seen in Table 10, show little strength and little pull-out. Figures 63 through 66 show some fracture surfaces of the above materials.

This method provides an efficient way to survey fiber/coating/matrix interactions and to screen potential candidate systems experimentally before composite coupons or panels are fabricated. For the samples exhibiting no strength the failure mode was consistently with little or no fiber pull-out, indicating a strong fiber matrix bond. Additionally, fiber strength may have been compromised during the processing step in making some of these samples.

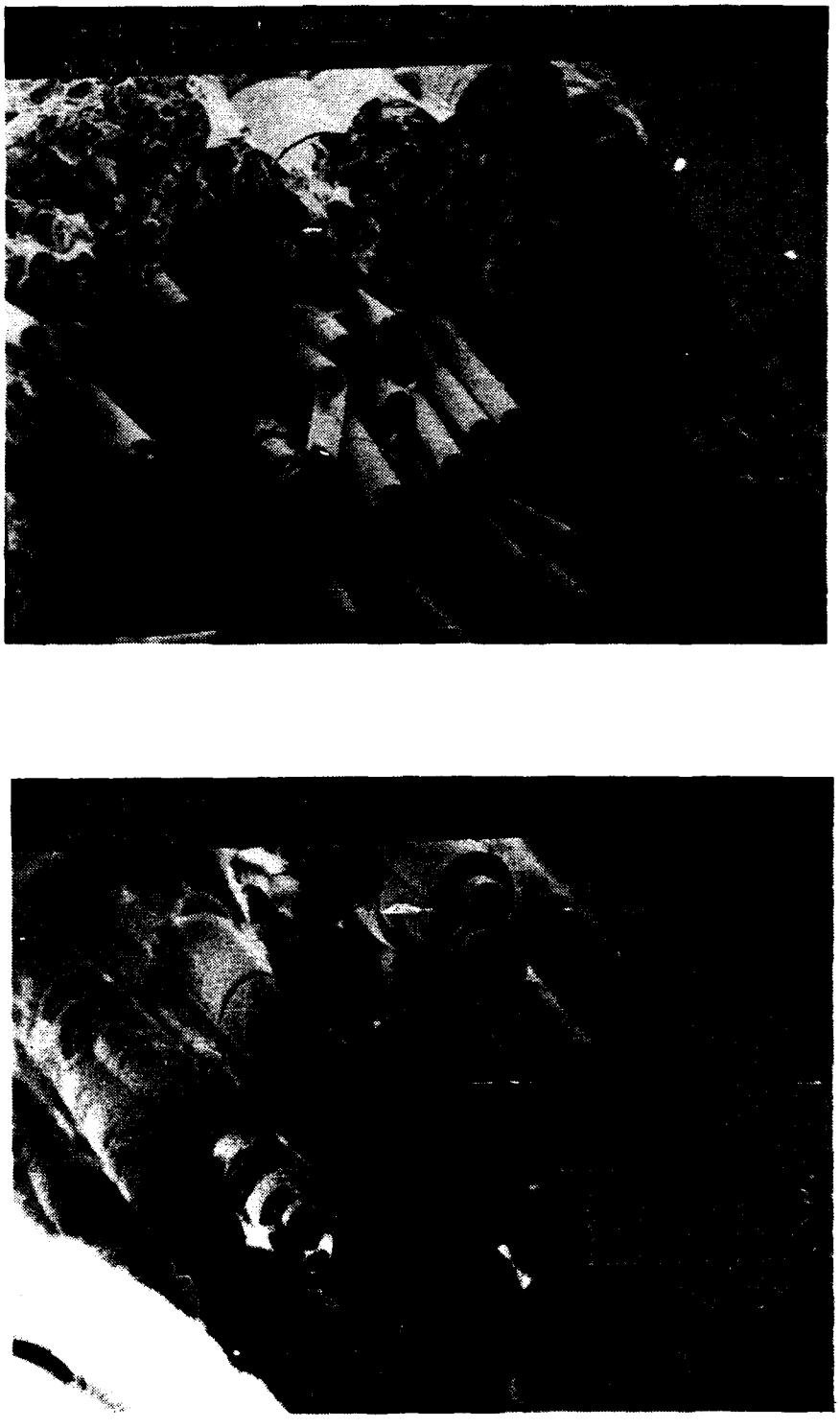

Figure 63. Scanning electron micrographs of fracture surfaces of $Si_3N_4$ infiltrated tows. Top panel: BN coated Nicalon. Bottom panel: Nicalon with dual coating of $BN/Si_xN_y$.

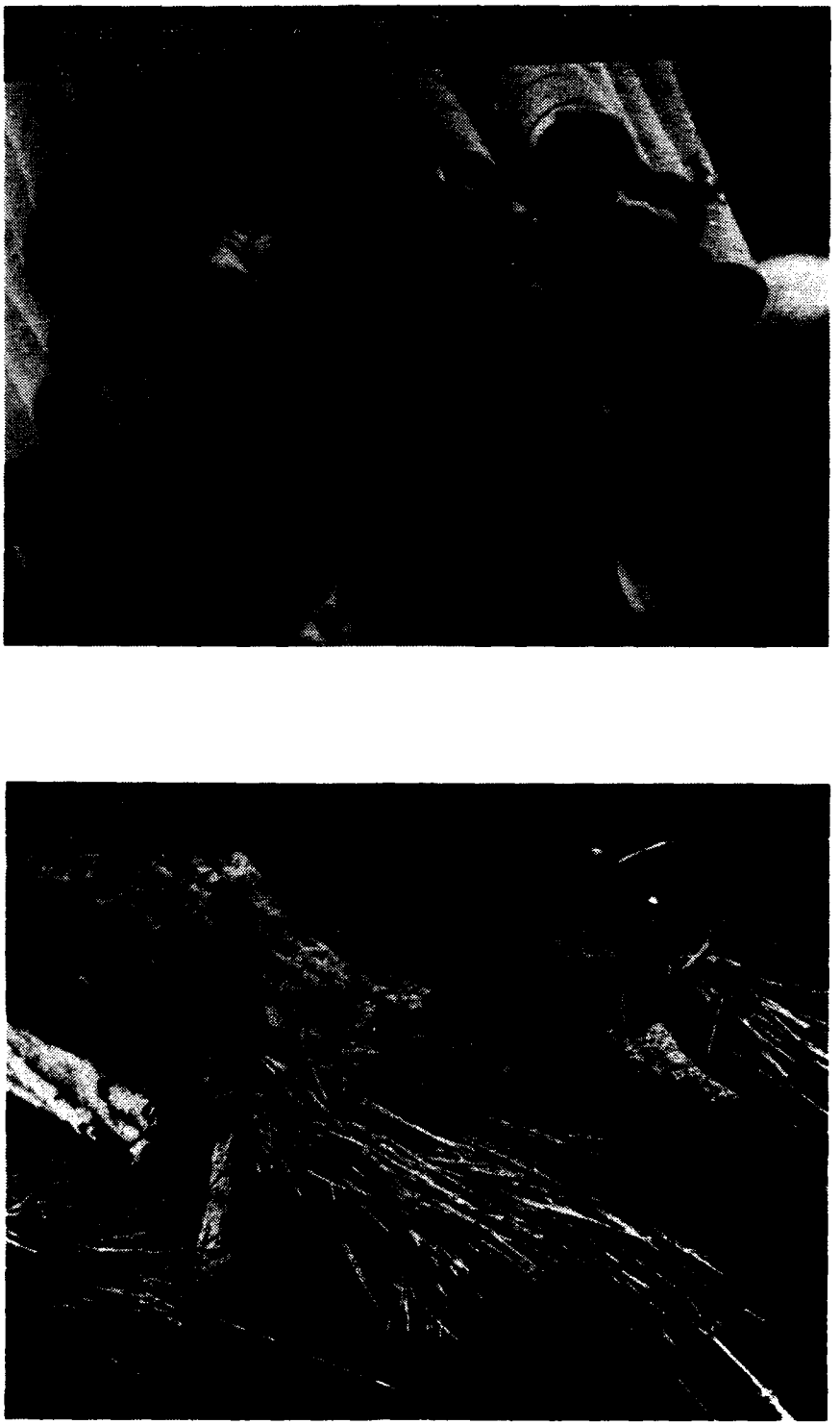

Figure 64. Scanning electron micrographs of fracture surfaces of $Si_3N_4$ infiltrated tows. Top panel: SiC coated Nicalon. Bottom panel: BN coated carbon fiber (T-300).

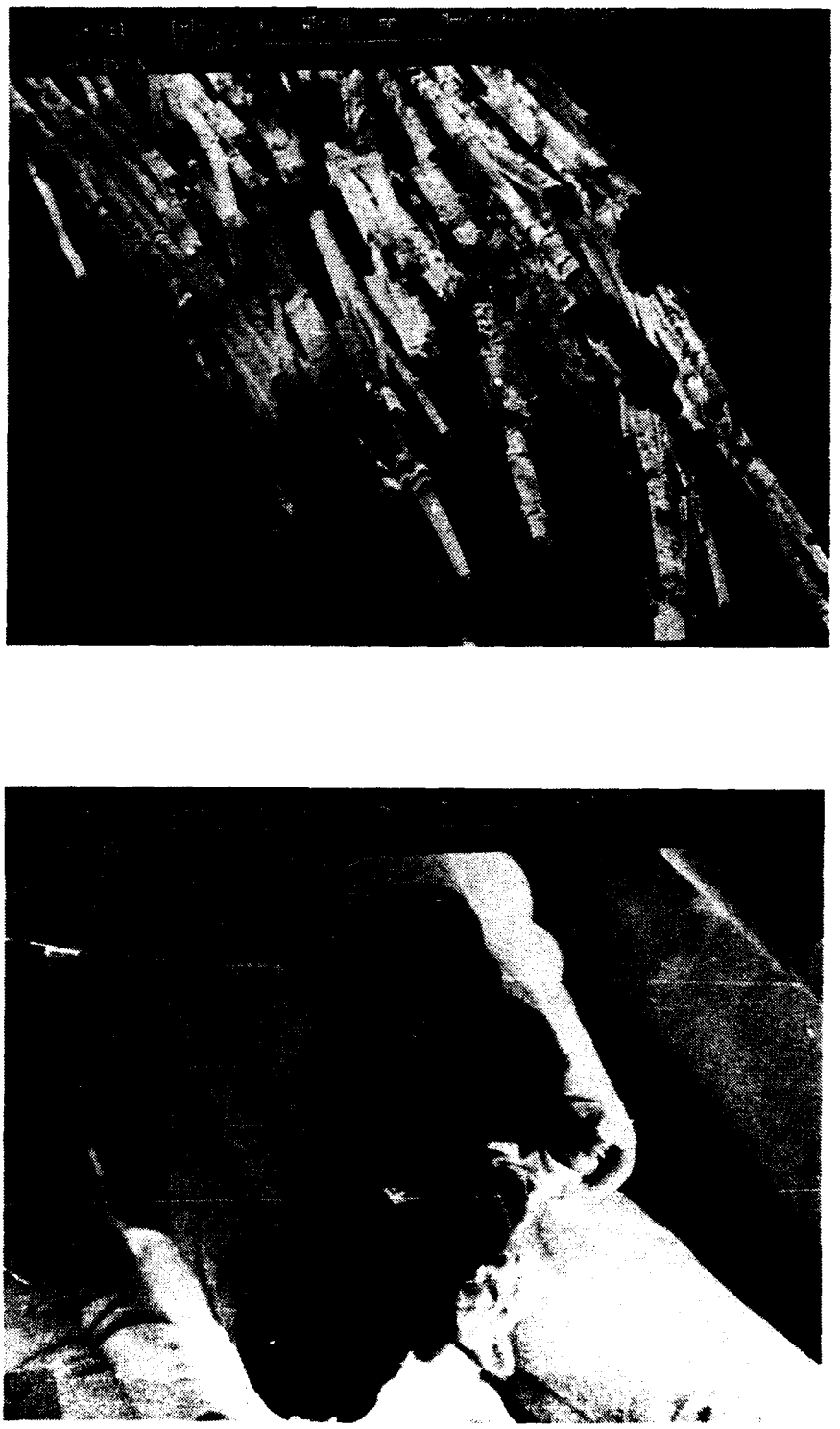

Figure 65. Scanning electron micrographs of fracture surfaces of $Si_3N_4$ infiltrated tows. BN coated HPZ.

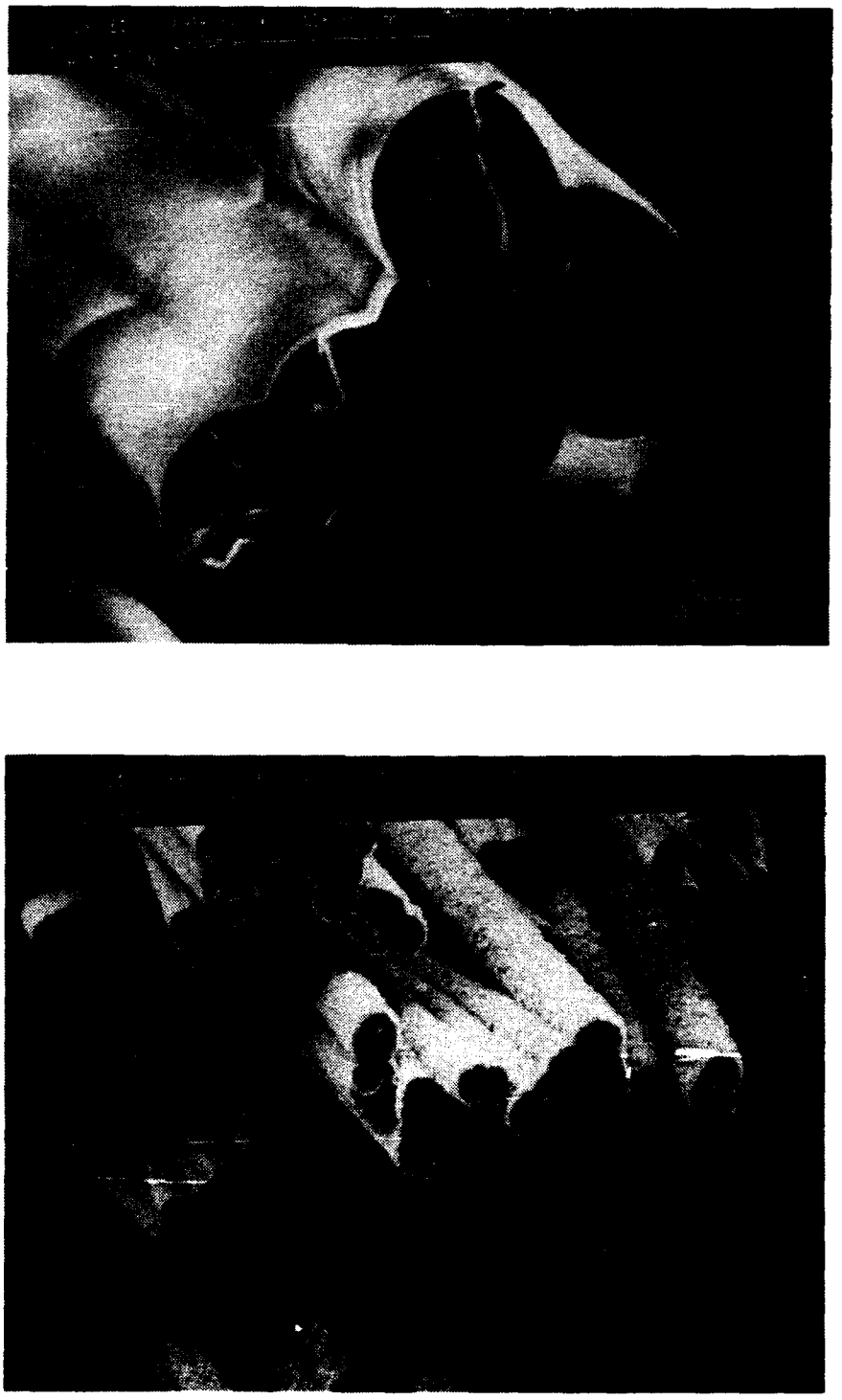

Figure 66. Scanning electron micrographs of fracture surfaces of $Si_3N_4$ infiltrated tows. Top panel: SiC coated HPZ. Bottom panel: HPZ with dual coating of $BN/Si_xN_y$.

Composite coupons were made from Nicalon cloth, which had been previously coated and then chemical vapor infiltrated with silicon nitride. The coupons were composed of six layers of cloth. The coated strips of cloth were made into preforms by binding the layers together with polystyrene. Preforms made in this manner have the advantage that fiber volume fraction can be more accurately controlled. These preforms were then cut into squares each 4 cm x 4 cm. The thickness of the coupons was influenced by the thickness of the coating on the fibers and ranged from 2.8 mm to 3.8 mm. In addition to the coupons made with CVD coated Nicalon there were four coupons made form Nicalon coated from liquid precursors, and one sample made from Nicalon with no coating.

Composite infiltration was performed using the 33 cm I.D. coater, (Figure 67) designed at GA for that purpose. The coater can be used for chemical vapor infiltration in a variety of formats such as isothermal, forced flow, thermal gradient, or thermal gradient with forced flow. For making the composites described here, a thermal gradient with forced flow was used. The polystyrene binder was thermally removed and the samples were radiantly heated from above and cooled from below. The coating gases were forced through the layers of cloth. As the reactant gases pass through the thermal gradient a series of reactions takes place which results in the deposit being formed at the hot surface. As the process continues, the deposition front moves downward through the preform raising the local temperature. The deposition of $Si_3N_4$ is achieved by reacting $SiCl_4$ vapor with $NH_3$ vapor at 750°C and a pressure of 13 kPa.

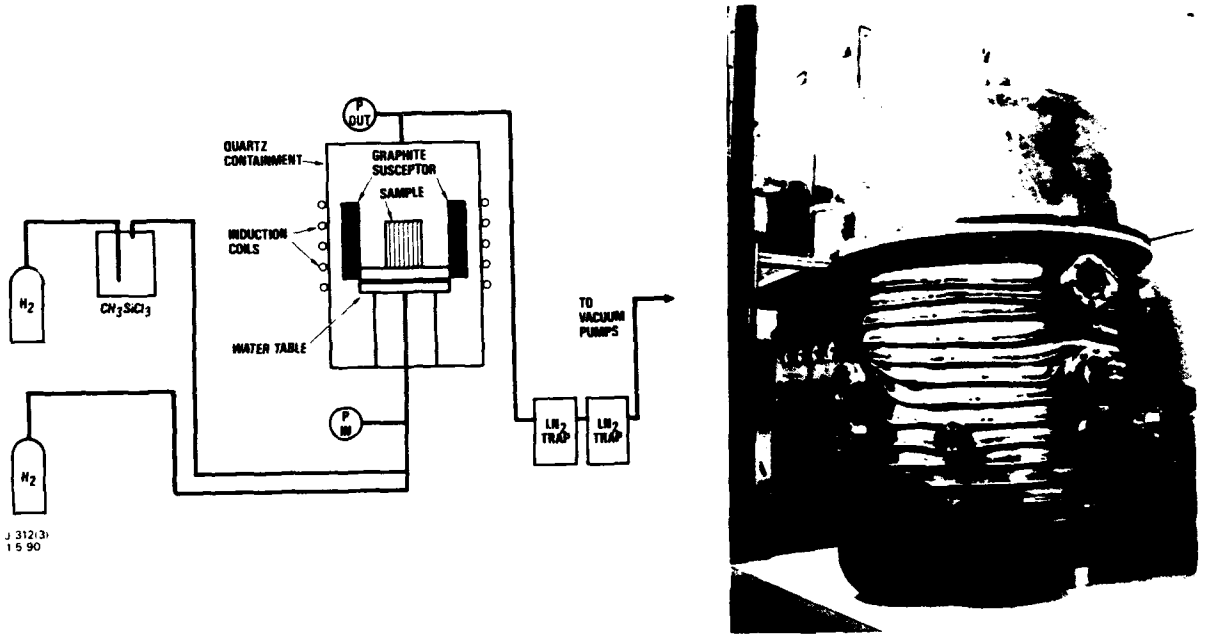


Figure 67. - Forced flow thermal gradient CVI apparatus

## COMPOSITE TESTING

The composite coupons were carefully removed from the graphite fixture, taking care to avoid prying the coupons which may weaken them. Each coupon was sectioned into six (6) strips using a diamond bladed sectioning saw. Each strip was approximately 1/6$^{th}$ of the total area, but some variance was unavoidable. The widths ranged from 5.3 mm to 7.3 mm with most being around 6 mm.

3-point bend tests were performed on the composite pieces. The test apparatus is shown in Figure 68 just at the point of initial failure. In Figure 69, the crosshead was allowed to continue pushing through the sample to demonstrate the toughness of this composite. The composite, shown in Figure 69, is the one in which the cloth was coated with the dual BN.

The 3-point bend test was performed on three samples from each coupon. Figure 70 shows the average flexural strengths for the samples tested. The high temperature BN composite showed the highest strength with an average strength of 212 MPa. The dual coating BN composite also exhibited good strength with an average of 132 MPa. The titanium diboride coated Nicalon composite shows some improvement over the uncoated Nicalon composite. The remainder of the samples were weak and failed in a brittle fashion.

Figure 71 shows an optical micrograph of two of the broken samples, magnified 8X. The sample made from the dual BN coated Nicalon is on the top (flexural strength, 132 MPa), and the sample made from the high temperature BN coated Nicalon is below (Flexural strength, 212 MPa). While both show the fiber pullout which is characteristic of tough composites, the degree of pullout in the bottom sample helps to explain the difference in strength between them.

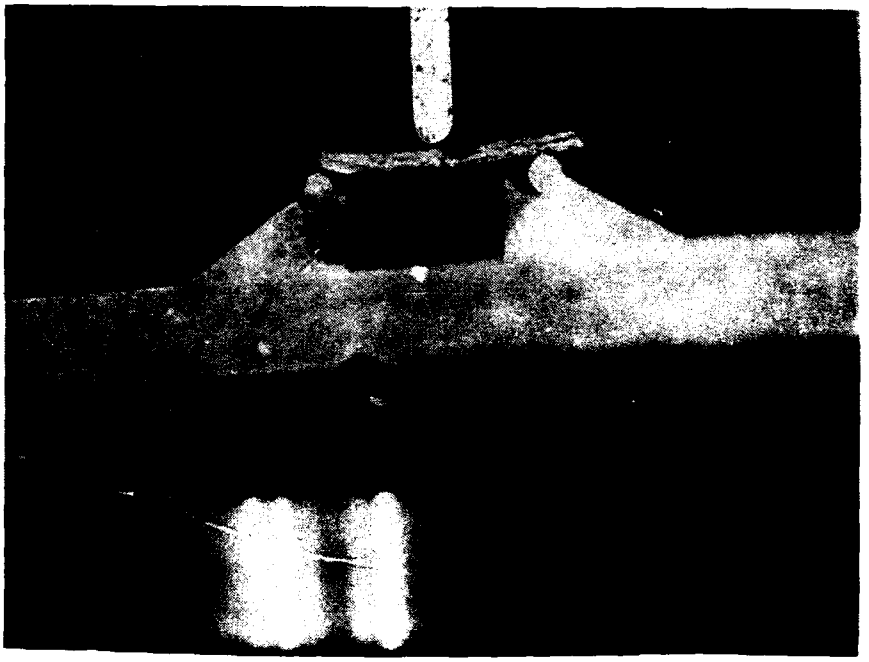

Figure 68. Initial point of failure for composite specimen in three-point bend test.

Figure 69. Continued crosshead travel demonstrates toughness of this composite. Composite is made from Nicalon CG with dual BN coating in $Si_3N_4$ matrix.

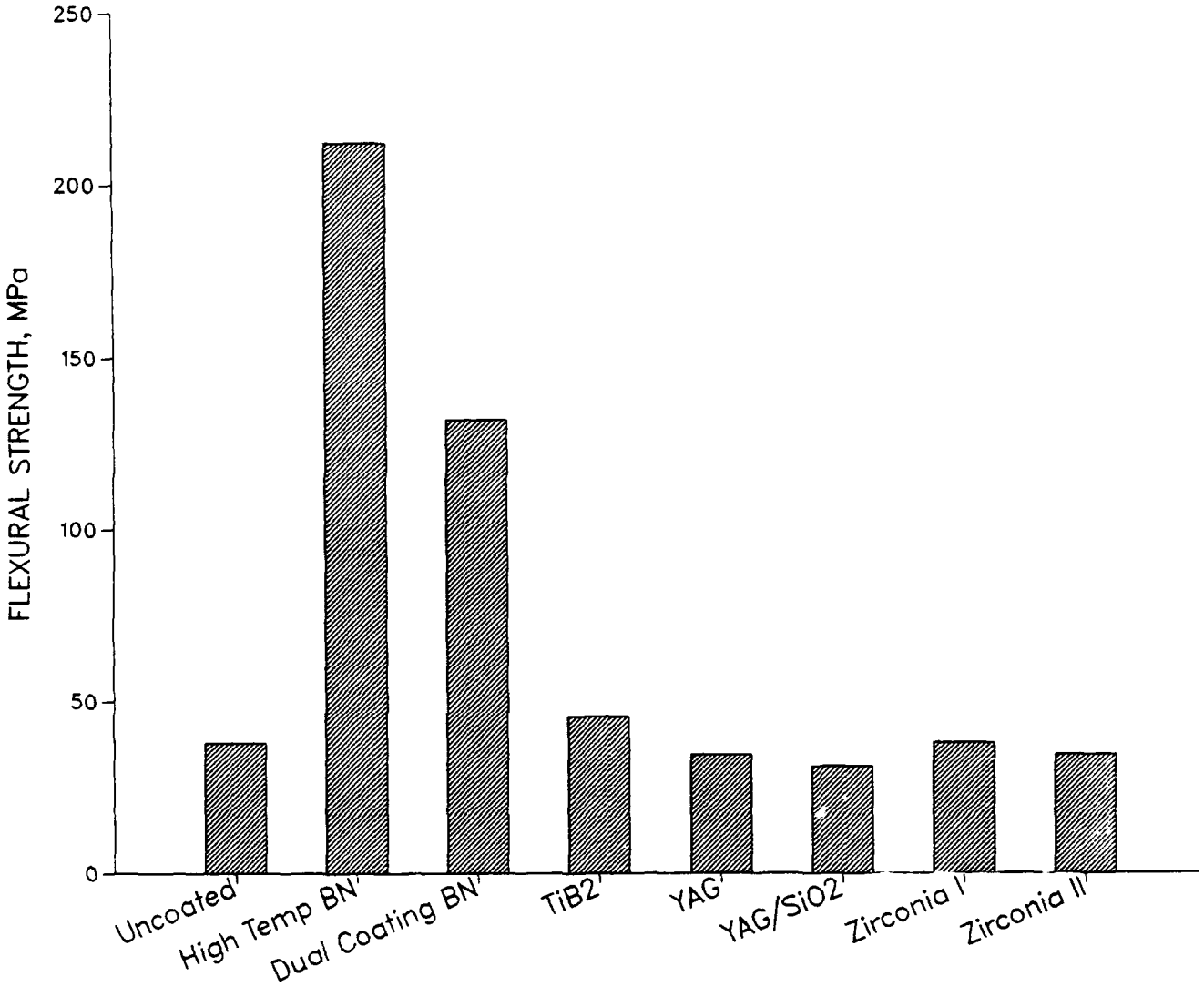


**Figure 70. Summary of three-point bend flexural strengths for various fiber coating on Nicalon CG in $Si_3N_4$ matrix.**

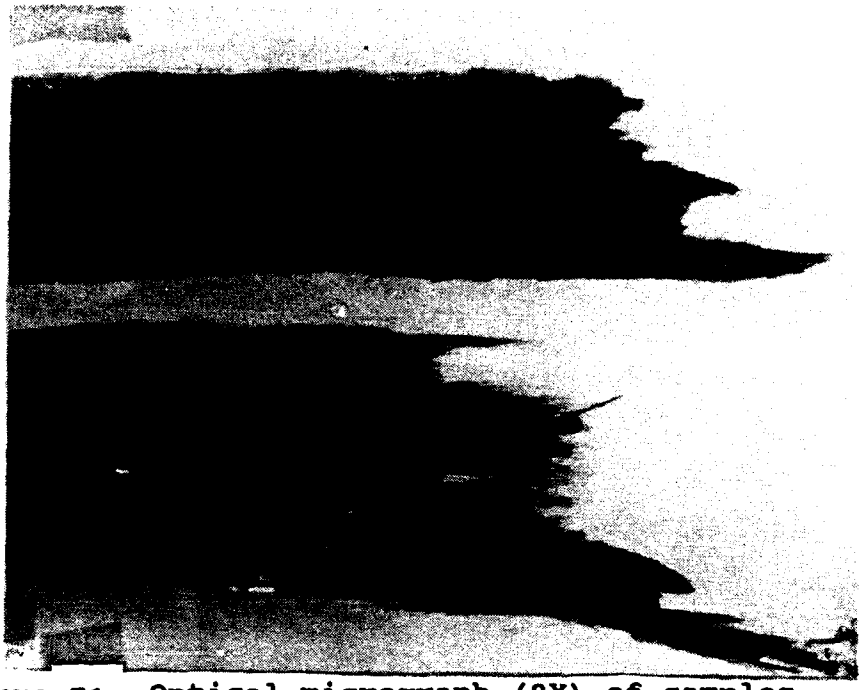

Figure 71. Optical micrograph (8X) of samples loaded to failure. Both are Nicalon CG in $Si_3N_4$ matrix. Top sample made with dual BN coating. Bottom sample made with high-temperature BN coating.

Figure 72. Scanning electron micrograph (2000X) showing fracture surface of composite made from Nicalon cloth coated with high-temperature BN.

## FIBER COATING OPTIMIZATION

The high temperature BN coated Nicalon composite exhibited the greatest flexural strength for this set of tests. Not immediately clear is, whether the difference in strengths seen between the high temperature BN and the dual BN coated Nicalon composites is due to the difference in the chemistry of the BN or some other parameter, such as coating thickness. The variation in coating thickness is readily apparent since the high temperature BN was on the order of 3000 nm to 4000 nm thick while the dual BN was approximately 750 nm thick. However, examination of the fracture surfaces for the two interface coatings (Figures 72 and 73) reveals that the crack deflection occurred at the fiber/coating interface. Figure 74 is a good example of fiber/coating separation.

If equal or perhaps greater strength in the composite can be obtained by a thinner coating, this would enhance not just the mechanical properties, but would speed processing as well. In order to address this concern, additional composites were made with different fiber coating thicknesses. Four coupons were made with high temperature BN coatings targeting thicknesses of 100, 500, 1000, and 4000 nm on Nicalon NVR. Actual thicknesses achieved were 120 nm, 550 nm, 1070 nm, and 5600 nm. Scanning electron micrographs of these coated fibers are shown in Figures 75, 76, 77 and 78, respectively. Two more coupons targeting 500 nm and 1000 nm thick coatings of high temperature BN on HPZ were also made. One coupon of Nicalon HVR with 1000 nm thick coating of low temperature BN was made. Additional coupons made from Nicalon CG with a pyrolytic carbon coating and from uncoated carbon cloth were tested.

The infiltration was repeated as described previously with $Si_3N_4$. The coupons were sectioned as described previously and also tested using a 3-point bend test. These results are shown in Figure 79.

Figure 73. Scanning electron micrograph (2000X) showing fracture surface of composite made from Nicalon cloth coated with dual BN.

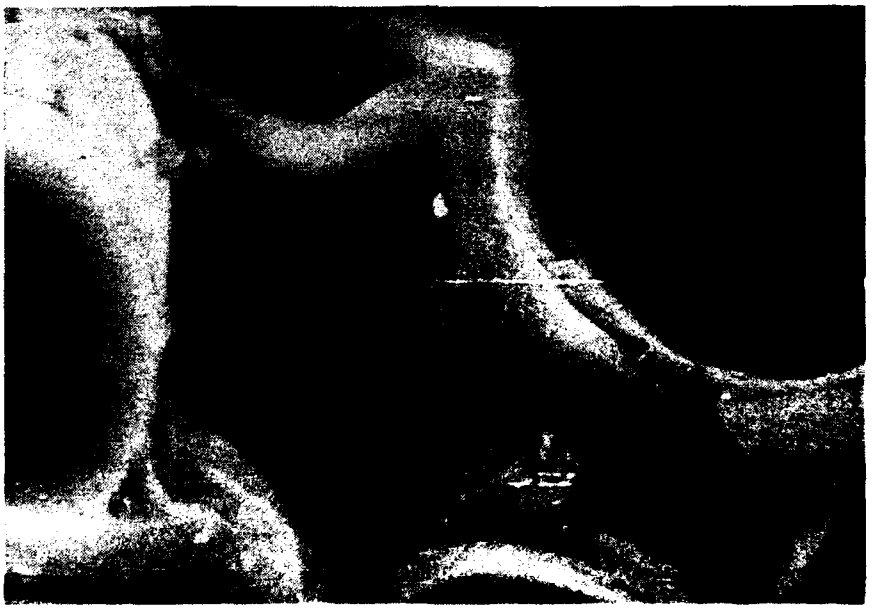

Figure 74. Scanning electron micrograph (4000X) of fracture surface of composite made from dual BN coated Nicalon. Fiber/coating separation is apparent.

Figure 75. Scanning electron micrograph (20,000X) of high temperature BN on Nicalon HVR. $BCl_3 + NH_3$; 1000°C; 1 min. coating. Coating thickness = 120 nm.

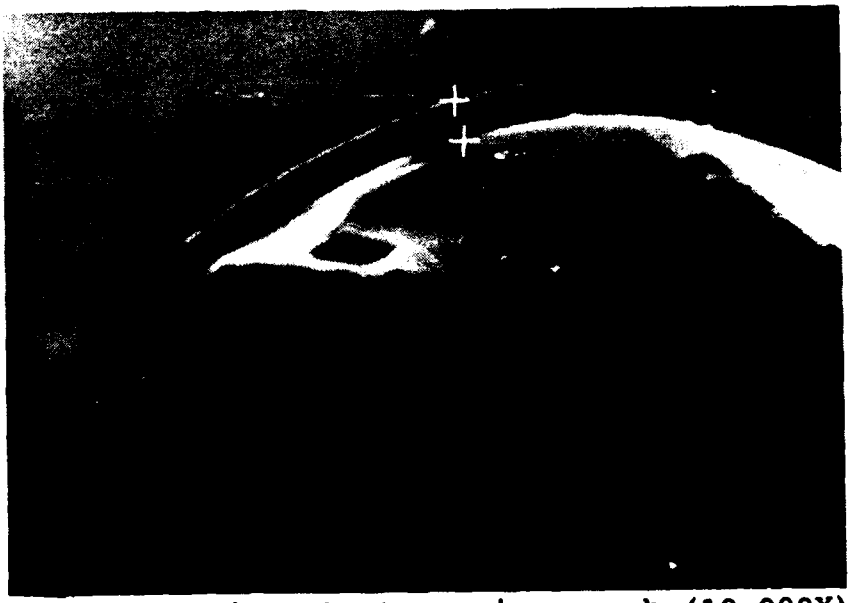

Figure 76. Scanning electron micrograph (10,000X) of high temperature BN on Nicalon HVR. $BCl_3 + NH_3$; 1000°C; 2 min coating. Coating thickness = 550 nm.

Figure 77. Scanning electron micrograph (10,000X) of high temperature BN on Nicalon HVR. $BCl_3$ + $NH_3$; 1000°C; 5 min coating. Coating thickness = 1000 nm.

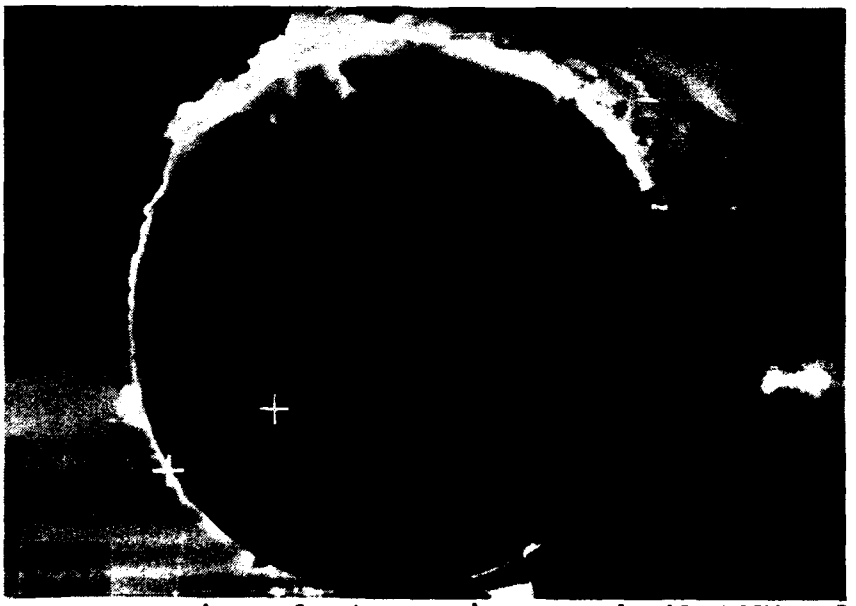

Figure 78. Scanning electron micrograph (3000X) of high temperature BN on Nicalon HVR. $BCl_3$ + $NH_3$; 1000°C; 20 min coating. Coating thickness = 5600 nm.

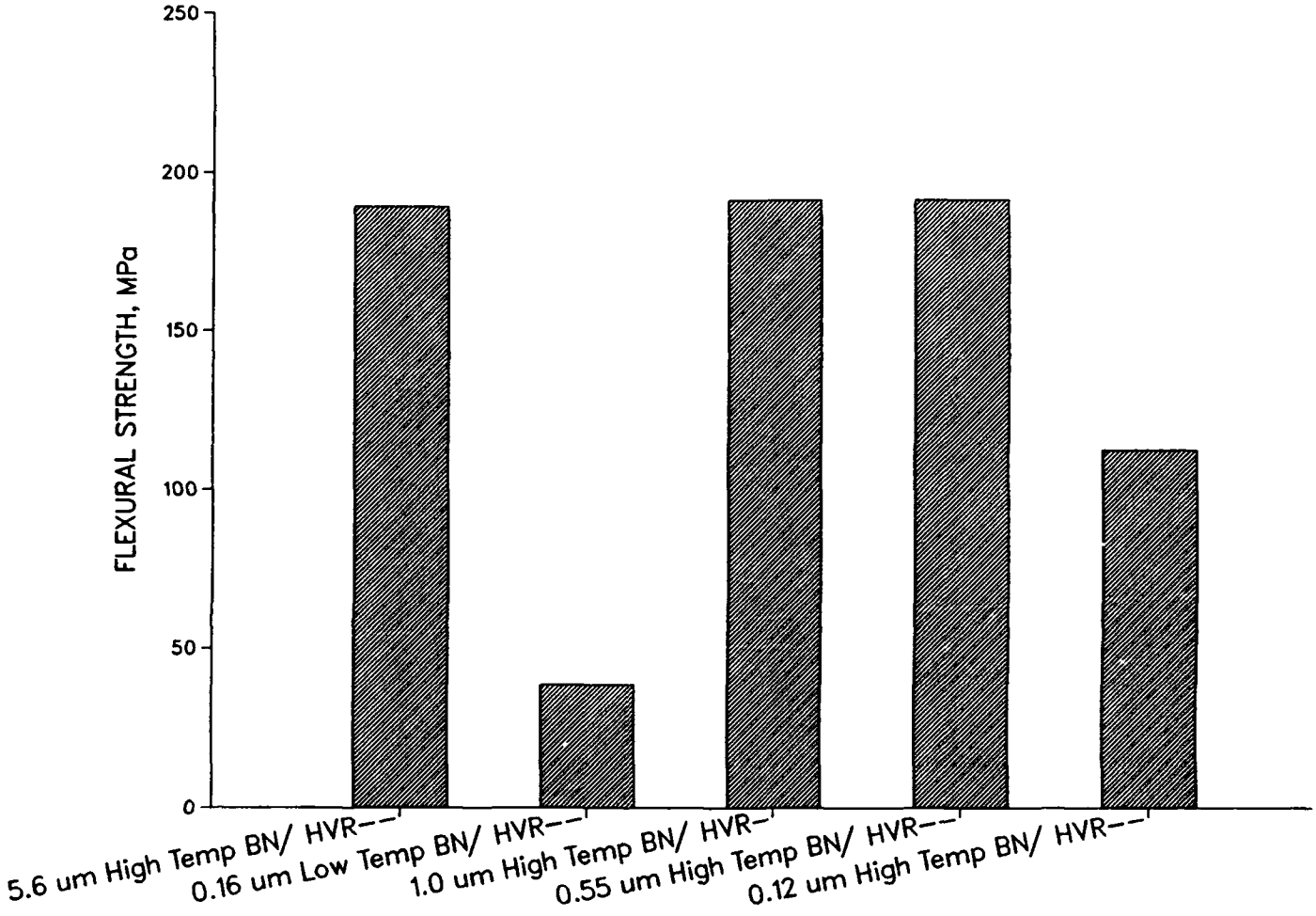


**Figure 79. Results of 3-point bend test for interface coatings and fibers in $Si_3N_4$ matrix composites.**

This figure illustrates that for the high temperature BN the composite strength is independent of fiber coating thickness for thicknesses greater than 500 nm. However, there is a significant reduction in strength when the coating thickness is reduced to 120 nm. Also, when comparing the 160 nm thick low temperature BN with the 120 nm thick high temperature BN, there is a distinct contrast between the effectiveness of the two coatings.

## INTERFACIAL PROPERTIES OF COMPOSITE COUPONS

When a crack occurs in the matrix of a ceramic matrix composite (CMC) due to tensile stress, the crack tip propagates and approaches a fiber. If the interfacial bond strength between the matrix and fiber is properly controlled the crack tip deflects at the fiber due to the higher Young's modulus of the fiber. Thus energy dissipation takes place and the crack tip energy is reduced. If the crack tip possesses enough energy, it continues to proceed through the matrix until the next fiber matrix interface where further energy dissipation takes place. When the crack tip energy is reduced below a critical level the crack comes to a standstill. Behind the crack tip the intact fibers act as connecting bridges between the two fracture surfaces and resist crack opening and crack propagation. Figure 80 is a scanning electron micrograph of a polished composite section of high-temperature BN coated Nicalon in $Si_3N_4$ matrix. The crack deflection at the BN coating is very apparent. The crack deflection occurred mainly at the fiber/coating interface and partially in the matrix/coating interface. The granular-like appearance of the sample is an artifact of the polishing procedure.

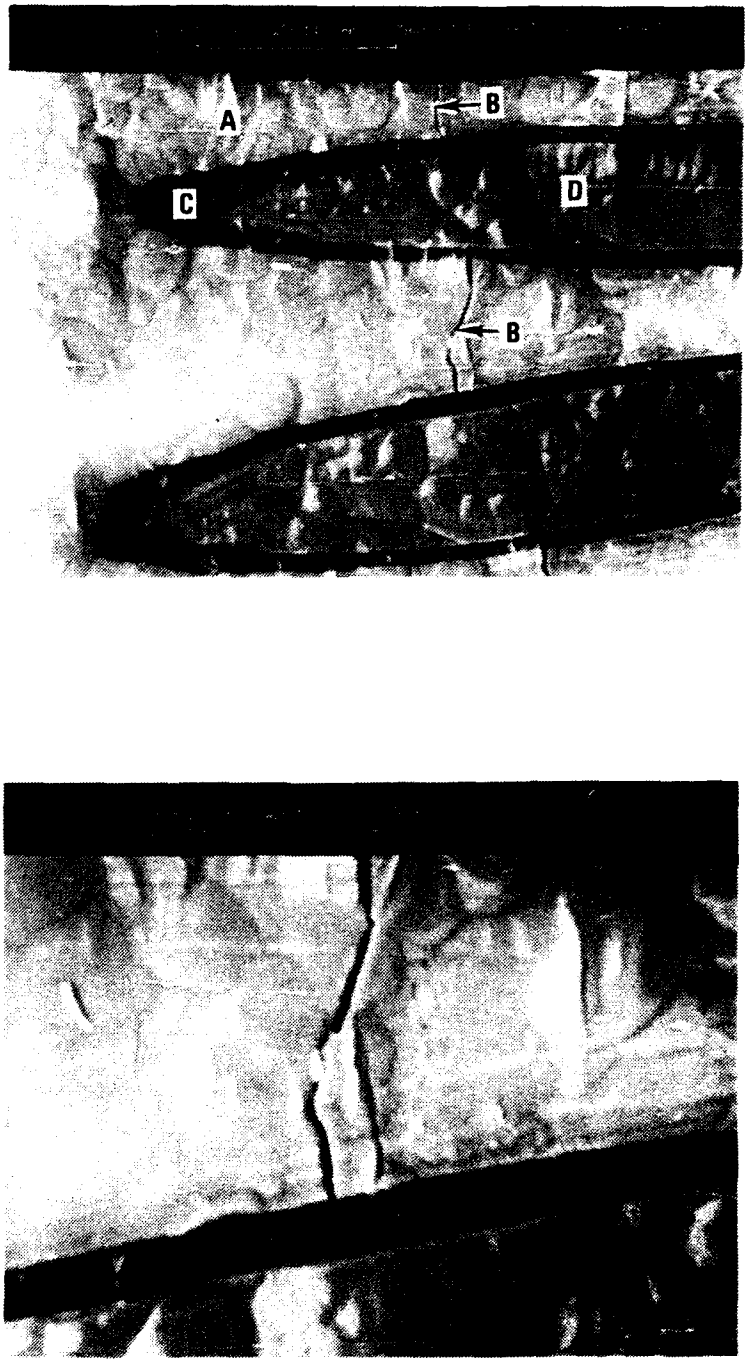


**Figure 80.** Scanning electron micrographs of polished BN-coated Nicalon in $Si_3N_4$ matrix showing crack deflection at interface. Upper panel 1.5 KX. Lower panel 4.0KX. A, $Si_3N_4$ matrix; B, crack; C, BN coating; D, Nicalon fiber.

## TRANSMISSION ELECTRON MICROSCOPE INVESTIGATIONS

Specimens of two previously produced and tested composite materials were prepared from Nicalon fibers coated with a boron nitride coating by CVD and infiltrated with silicon nitride matrix by chemical vapor infiltration. The difference between the two materials was the type of boron nitride coating. The first one, called high temperature boron nitride, shows a hexagonal structure and was produced from boron trichlororide and ammonia at 900°C. The second one, called low temperature boron nitride, was produced from diborane and ammonia at 500°C and was amorphous.

The three-point bend tests resulted in different flexural strength values for the two materials. The material with the high temperature boron nitride yielded a strength of about 215 MPa, while the low temperature BN gave a value of 135 MPa. Investigations by SEM have shown differences regarding the degree of fiber pull-out. The high temperature BN, in accordance with the high strength shows a large amount of pull-out. The low temperature BN in contrast shows less pull-out. Since the two materials were manufactured under the same conditions except for the coatings, and show a significant difference in strength and fiber pull-out it is of interest to know what the differences of the coatings and the interfaces with the Nicalon fiber and the $Si_3N_4$ matrix are. The investigation was performed on a Phillips Transmission Electron Microscope. Observations on the coatings and the interfaces indicate a thin reaction zone between the Nicalon fiber and the high temperature boron nitride (Figure 81). No reaction zone was observed between coating and matrix. Also, no reaction zone was observed in the material with the low temperature boron nitride coating (Figure 82). Observations at the fiber/coating and coating/matrix interfaces by SEM showed that crack deflection and crack branching takes place mostly in the fiber/coating interface (Figure 80) resulting in

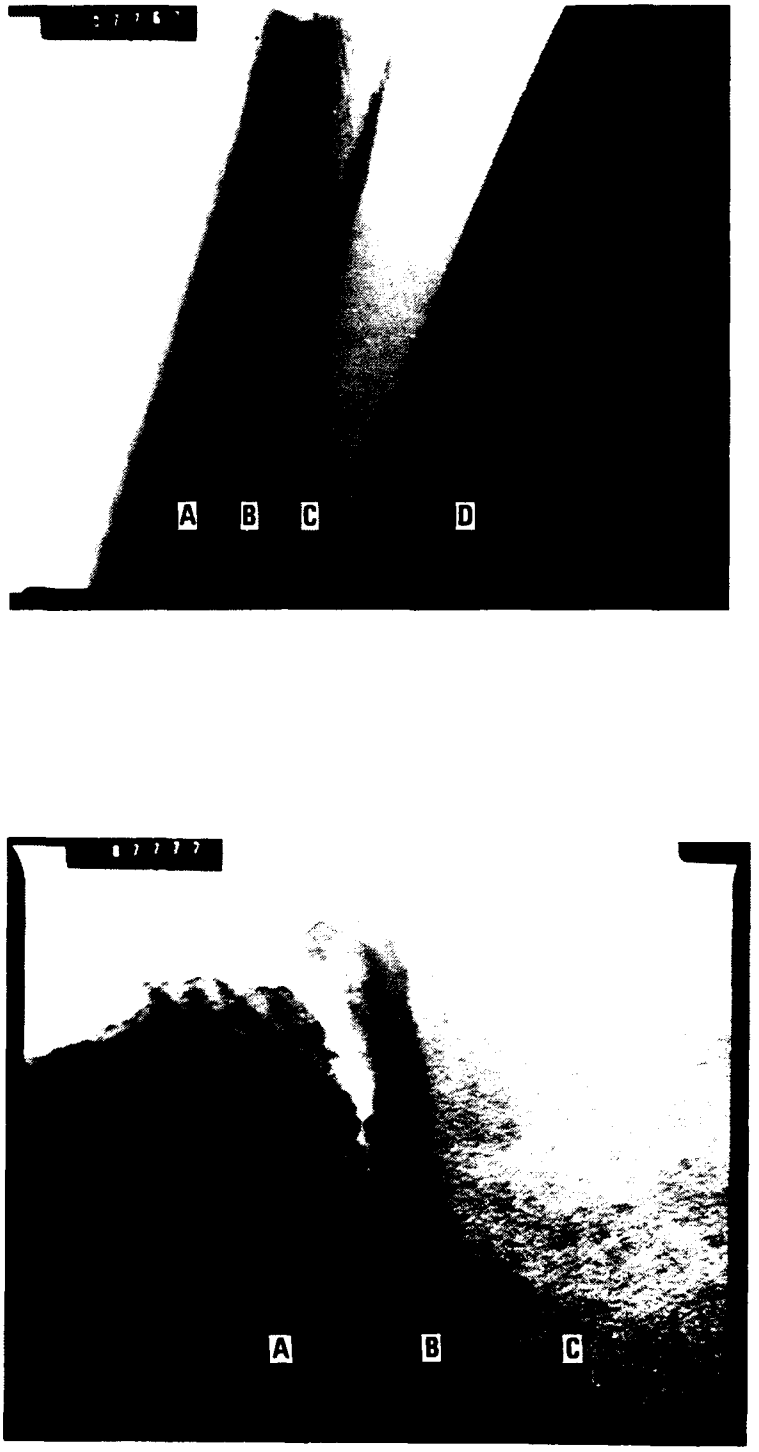


Figure 81. Transmission electron micrographs of high-temperature BN coating on Nicalon in $Si_3N_4$ matrix composite. Top panel: 54 KX. Bottom: 100 KX. A, $Si_3N_4$ matrix, B, Reaction zone; C, BN coating; D, Nicalon fiber.

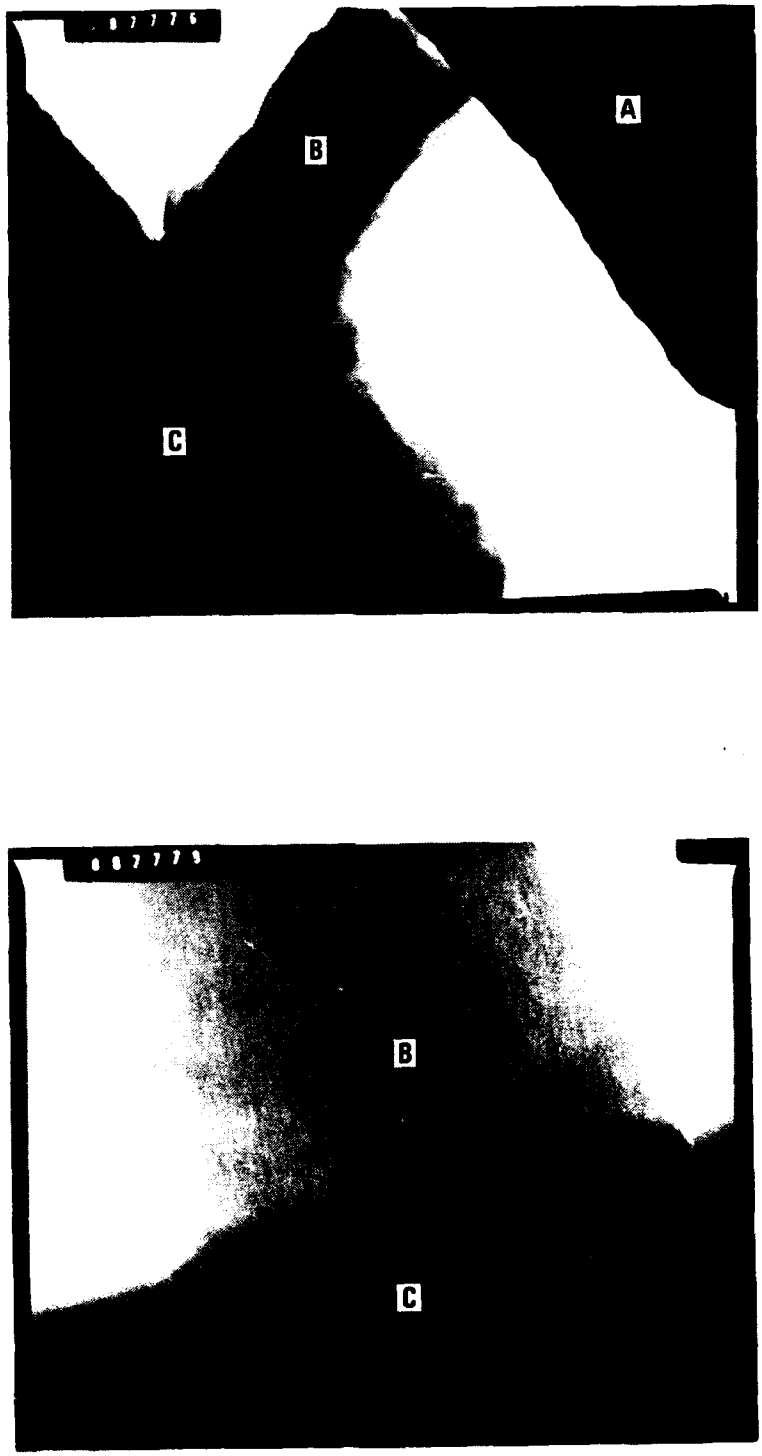


Figure 82. Transmission electron micrographs of low-temperature BN coating on Nicalon in $Si_3N_4$ matrix composite. Top panel: 54 KX. Bottom panel: 222KX. A, $Si_3N_4$ matrix; B, BN coating. C, Nicalon fiber.

a large amount of fiber pull-out. It could be assumed that the reaction zone between matrix and coating is stronger than either of those regions. This reaction zone may not cause primary crack deflection, but could contribute to a reduction of the stress intensity factor of the crack. Further investigation of this phenomena is required to draw a more concrete conclusion. However, this interface is strong enough to transfer a high load and to result in a high flexural strength.

## SUMMARY AND CONCLUSIONS

A wide variety of effective fiber and fabric coating methods were developed to coat oxides, nitrides and carbides on multifilament ceramic fibers. Table 11 summarizes the various coatings and methods developed in this program.

Three liquid-phase processes were studied: traditional dip coating, in-situ curing, and reaction bonding. Traditional dip coating is simple and results in good uniformity, but obtaining smooth adherent coatings without bridging or fiber degradation is difficult. In-situ curing sacrifices some quality of uniformity and smoothness to obtain adherent coatings with little bridging or fiber degradation. Reaction bonding is more complex requiring more passes through the coater for a given coating thickness, but the coating properties are excellent. For oxide coatings one of these liquid phase methods is the preferred choice.

The vapor phase coatings generally resulted in smooth continuous coatings with good stoichiometry control and good penetration into the tow. CVD is the preferred method for applying nitride and carbide coatings. The CVD equipment is more complex than the liquid-phase coating equipment and consequently is more expensive. It should be possible to scale up both liquid and gas phase processes to high through put rates without sacrificing quality.

TABLE 11

## SUMMARY OF COATINGS AND COATING METHODS ON CERAMIC FIBERS

| FIBER | COATING | METHOD |
|---|---|---|
| NICALON | $Al_2O_3$, $Y_2O_3$ | SOL-GEL |
| | MgO, YAG, $HfO_2$ | SOL-GEL |
| | $MgAl_2O_4$, $ZrO_2$ | SOL-GEL |
| | SiC, $Si_3N_4$, BN | POLYMER |
| | BN, SiC | CVD |
| | BN/SiC | CVD |
| | $BN/Si_3N_4$ | CVD |
| NEXTEL 480 | $Al_2O_3$, $Y_2O_3$ | SOL-GEL |
| | SiC, $Si_3N_4$ | POLYMER |
| | BN | CVD |
| | $BN/Si_3N_4$ | CVD |
| FP-PRD-166 | $Y_2O_3$ | SOL-GEL |
| | SiC, $Si_3N_4$ | POLYMER |
| | BN, SiC | CVD |
| | $Si_3N_4$ | PACVD |
| HPZ | BN, SiC | CVD |
| | BN | POLYMER |

Small scale production capabilities were established. Throughput rates of up to 50 m/hr were achieved with present equipment. With improved design this rate could be increased significantly to make fiber coating economically more attractive. High quality coatings for filament winding and other specialty applications will require coating of fiber tows. To dramatically increase throughput and reduce cost, continuous fabric coating will have to be developed. A small scale fabric coater was designed and constructed to demonstrate the principles of coating fabric continuously.

The ability to produce multilayer coatings for controlling not only the mechanical properties, but also the electrical or thermal properties was demonstrated. Coated fibers were incorporated into silicon nitride ceramic matrix composites. Boron nitride coated Nicalon exhibited substantial improvement in strength and toughness over uncoated fiber and several other coatings. These results demonstrate the requirement of tailoring the coating chemistry to the fiber/matrix system. Most importantly, it demonstrates the great improvements in composite properties achievable through effective fiber coating.

## REFERENCES


1. Sawyer, L.C., M. Jamieson, Duane Brikowski, M.I. Haider, and R. T. Chen, J. Am. Ceram. Soc., 70, 798 (1987).

2. Dow Corning new product information report for Dow Corning X9-6371 HPZ ceramic fiber.

3. Lipowitz, J., H. A. Freeman, R. T. Che, and E.R. Prack, Adv. Ceram. Mat. 2, 121 (1987).

4. Yeheskel, O., M.L. Balmer, and D.C. Cranmer, Ceram. Eng. Sci. Proc. 9, 687 (1988).

5. Johnson, D.D., A.R. Holtz, and M.F. Grether, Ceram. Eng. Sci. Proc. 8, 744 (1987).

6. Mah, T., et al., J. Mater. Sci. 19, 1191 (1984).

7. Lipowitz, J., et al, Adv. Ceram. Mater. 2, 121 (1987).

8. Sawyer, L. C., et al., J. Am. Ceram. Soc. 70, 798 (1987).

9. Yeheskel, O., et al., Ceram. Eng. Sci. Proc. 9, 687 (1988).

10. Johnson, D.D., et al, Ceram. Eng. Sci Proc. 8, 744 (1987).

11. Luthra, K.L., J. Am. Ceram. Soc., 69, C-231 (1986).

12. Johnson, S.M., et al., J. Am. Ceram. Soc. 71, C132 (1988).

13. Jaskowiak, M. H., and J. A. DiCarlo, J. Am. Ceram. Soc. 72, 192 (1989).

14. JANAF Thermochemical Tables, D. R. Stull and H. Prophet (eds.), U.S. Government Printing Office, Washington, D.C., 1971.

15. Levin, E.M., and H.F. McMurdie, Phase Diagram for Chemists, Supplements, American Ceramic Society, 1975.

16. Meara, C.O., et al., "Phase Relationships in the System $SiO_2$-$Y_2O_3$-$Al_2O_3$" in High Tech Ceramics, P. Vincenzini (ed.), Elsevier Science Publishes B. V., Amsterdam, 1987, p. 265.

17. Bondar, A., and F. Y. Galakhov, Izv. Akad. Nauk. SSSR, Ser. Khim. 7, 1325 (1963).

18. Jack, K. H., "SiAlON Hardmetal Materials," in Science of Hard Materials, E.A. Almond et al. (eds), Adam Hilger Ltd., Boston, 1986, p. 363.

19. Bathie, W.W., Fundamental of Gas Turbines, John Wiley and Sons, 1984.

20. Maeda, M., et al., J. Mater. Sci., 23, 3933 (1988).

21. Luthra, K.L., and H. D. Park, J. Amer. Ceram. Soc. 73, 1014 (1990).

22. Osendi, M.I., J. Mater. Sci. 25, 3561 (1990).

23. Singhal, S.C., "Oxidation of Sialon-Based Structural Ceramics," in Fracture Mechanics of Ceramics, Proceedings of Symposium, Pennsylvania State University, 1973, R.C. Bradt et al. (eds.), Plenun Press, N.Y., 1974, p. 697.

24. Maeda, M., et al., J. Mater. Sci. Ltrs. 24, 2120 (1989).

25. Luthra, K.L., and H.D. Park, Air Force Report No. AFWAL-TR-89-4009, April 1989.

26. Mazdiyasni, K.S., C.T. Lynch, and J.S. Smith, Inorg. Chem., 5, 342 (1966).

27. Mazdiyasni, K.S. and L.M. Brown, J. Am. Ceram. Soc., 53, 43-45 (1970).

28. Rees, W., and D. Seyferth, Ceram. Eng. Sci. Proc., 10, 837 (1989).

29. Adams, A., and C. Capio, J. Electrochem. Soc., 127, 399 (1980).

30. Murarka, S.P., C.C. Chang, D.N. K. Wang, and T.E. Smith, J. Electrochem. Soc. 126, 1951 (1979).